

**Biofilm Formation and Quorum Sensing in  
*Pseudomonas fluorescens* Pf0-1**

Emily Bordeleau, B.Sc. Hon.

Biotechnology

Submitted in partial fulfillment of the requirements for the degree of Master of Science

Faculty of Mathematics and Science, Brock University  
St. Catharines, Ontario  
December, 2016

© Emily Bordeleau, 2016

## **Abstract**

A bacterial biofilm is a community of microorganisms adhering to a surface, exhibiting biochemical and phenotypic differences from their planktonic counterparts. The transition from a free-floating to sessile cell type has been shown to be, in part, mediated by high intracellular levels of the nucleotide second messenger c-di-GMP. It is suggested that one of the environmental cues for biofilm formation, recognized by members of the c-di-GMP network, is local cell density. In areas of high cell density, cells can communicate through a system called quorum sensing. In gram negative bacteria, acyl-homoserine lactone (AHL) molecules are excreted into the surrounding medium and recognized by cells in close proximity. It is hypothesized that upon recognizing AHLs through c-di-GMP signaling, gene expression is altered leading to a sessile lifestyle. Thus, the long-term goal of this research is to provide evidence for the link between c-di-GMP and quorum sensing-mediated mechanisms in biofilm formation in *Pseudomonas fluorescens* Pf0-1.

The first objective towards this goal was to identify the AHLs utilized by *P. fluorescens* Pf0-1 in quorum sensing mechanisms. Through gas-chromatography mass-spectrometry (GC-MS), two AHLs were identified in the supernatant of *P. fluorescens* Pf0-1; *N*-butyryl-HSL and *N*-decanoyl-HSL. Subsequent work will focus on the identification of AHLs with longer acyl-chain and varying levels of acyl chain oxidation.

The second objective towards this goal was to utilize the 96-well static microtiter plate biofilm assay as a platform for studying the relationships between c-di-GMP and AHL-mediated mechanisms in biofilm formation. As a protocol for 96-well static biofilm assays that was previously successful was no longer reproducible, different microtiter plate surfaces were surveyed for their ability to support *P. fluorescens* Pf0-1 biofilm and to investigate potential factors that could interfere with development on the abiotic surface. Throughout the troubleshooting process, biofilm assay experiments carried out in microtiter plates with the same type of surface chemistry,

but from different manufacturers and batches, resulted in variable quantities of biofilm. This observation then inspired the production of a surface that would create more favorable interactions with bacterial cells and offer increased points of attachment to further promote biofilm formation. In this new platform, microtiter plates are pre-treated by abrasive forces such as sandblasting and drilling before biofilm assays, which gives robust biofilm formation that will allow for future investigation into connections between c-di-GMP and AHL-controlled mechanisms of biofilm formation in *P. fluorescens* Pf0-1.

## **Acknowledgements**

I would first like to extend my sincerest thanks to my supervisor, Dr. Tony Yan, for his support and encouragement throughout this process. Ever since the beginning of my undergraduate studies, he has assisted me in building a stronger skill set in chemistry. With this expanded understanding of chemistry, I have been able to better apply the fundamentals of chemistry to biological systems.

I would like to thank the committee members; internal examiners Dr. Atkinson and Dr. Després as well as external examiner Dr. Logan. I greatly appreciate the time they have given to this process. Thank you to the mass spectrometry technologist Liqun Qiu for her guidance in the GC-MS work and Steve Crumbs for his help in the modification of microtiter plates.

To all the members of Dr. Yan's group, both past and present, I thank you for all the support and good times over the past few years. I would like to thank the members of Dr. Atkinson's group as well, as they too have helped me to develop into the researcher I am today.

A huge thanks to my friends and family for all the love and support throughout my academic career. Lastly, but certainly not least, a special thanks to my husband Keith Slappendel. Despite the countless hours I would spend in the lab, he was always there supporting me. He has always helped me to stay positive and focused with my research even as we planned a wedding. I would like to thank him for his patience over the past year, I wouldn't be where I am without him.

## Table of contents

Abstract.....	ii
Acknowledgements.....	iv
List of figures.....	viii
List of tables.....	xi
List of abbreviations.....	xi
Chapter 1: Literature review .....	1
1.1. Stages of biofilm development .....	1
1.1.1. Initial attachment .....	1
1.1.2. Microcolony formation .....	3
1.1.3. Maturation: physiological characteristics .....	4
1.1.4. Dispersal .....	5
1.2. Antimicrobial tolerance in biofilms .....	5
1.2.1. The protective barrier: extracellular matrix .....	6
1.2.2. Altered microenvironments.....	7
1.2.3. Persister cells .....	7
1.3. The role of the nucleotide second messenger c-di-GMP in biofilm formation.....	8
1.3.1. C-di-GMP synthesis and degradation .....	8
1.3.2. Mechanisms of c-di-GMP signaling .....	9
1.4. Quorum sensing .....	10
1.4.1. Introduction to quorum sensing in gram negative bacteria .....	10
1.4.2. Acyl-homoserine lactone quorum sensing in <i>P. aeruginosa</i> .....	12
1.5. Model microorganism of study: <i>P. fluorescens</i> .....	14
1.5.1. Acyl-homoserine lactone based quorum sensing networks in <i>P. fluorescens</i> .....	14
1.5.2. Biofilm formation in <i>P. fluorescens</i> Pf0-1 .....	15
1.6. Connecting c-di-GMP to quorum sensing systems in gram negative bacteria .....	16
Chapter 2: Identification of acyl-homoserine lactones produced by <i>P. fluorescens</i> Pf0-1 .....	18
2.1. Introduction and objectives.....	18
2.2. Methods and materials .....	21
2.2.1. Bacterial strains and growth conditions .....	21
2.2.2. LB-Miller (LB) media.....	21
2.2.3. UV/ <i>vis</i> Spectrophotometric measurements .....	21
2.2.4. Extraction of acyl-homoserine lactones from <i>P. fluorescens</i> Pf0-1 cultures .....	21
2.2.5. Acyl-homoserine lactones storage conditions.....	22

2.2.6. GC-MS analysis of acyl-homoserine lactone standards and bacterial culture extracts.....	22
2.3. Results.....	24
2.3.1 GC chromatogram and EI-MS fragmentation library of HSL standards .....	24
2.3.2. GC-MS analysis of <i>P. fluorescens</i> Pf0-1 culture supernatant extracts .....	25
2.3.3. GC-MS analysis of <i>P. fluorescens</i> Pf0-1 culture supernatant extracts spiked with 0.1 ng/μL of standard AHL.....	29
2.4. Concluding remarks and future works .....	39
Chapter 3: Troubleshooting biofilm formation in <i>P. fluorescens</i> Pf0-1 .....	40
3.1. Introduction and objectives.....	40
3.2. Methods and materials .....	42
3.2.1. Bacterial strains and growth conditions .....	42
3.2.2. LB-Miller (LB) media.....	42
3.2.3. Minimal (M63) media.....	42
3.2.3.1. Preparation of M63 used for methods sections 3.2.6.1 through to 3.2.6.4.....	43
3.2.3.2. Preparation of M63 used for methods section 3.2.6.5.....	43
3.2.3.3. Preparation of M63 used for methods section 3.2.6.6.....	43
3.2.4. UV/ <i>vis</i> Spectrophotometric measurements.....	44
3.2.5. Statistical analysis .....	44
3.2.6. Static biofilm assay and quantification .....	44
3.2.6.1. Preliminary analysis of biofilm formation across different brands of microtiter plates .....	44
3.2.6.2. Secondary screening of microtiter plates: biofilm formation across different surface treatments of polystyrene.....	45
3.2.6.3. Biofilm formation on an untreated Corning (No. 351172) polystyrene microtiter plate .....	45
3.2.6.4. Effect of carbon source on the quantity of biofilm produced on a Corning polystyrene microtiter plates (No. 351172).....	46
3.2.6.5. Quantitative analysis of biofilm formed on non-treated polypropylene surface from two different manufacturers.....	60
3.2.6.6. Quantitative analysis of biofilm formed on Corning No. 351172 microtiter plates after abrasive treatment .....	60
3.2.8. Abrasive treatment of microtiter plates.....	60
3.2.9. Drill press modification of microtiter plates .....	48
3.2.10. Scanning electron microscopy (SEM) .....	48
3.3 Results.....	50
3.3.1. Preliminary analysis of biofilm formation across different brands of microtiter plates .....	50

3.3.2. Secondary screening of microtiter plates: biofilm formation across different surface treatments of polystyrene.....	52
3.3.3. Biofilm formation on a Corning (No. 351172) microtiter plate untreated polystyrene surface.....	54
3.3.4. Effect of carbon source on the quantity of biofilm produced on a medium binding crystal grade polystyrene surface .....	56
3.3.5. Quantitative analysis of biofilm formed on non-treated polypropylene surface from two different manufacturers.....	59
3.3.6. Qualitative analysis of topographical changes in polystyrene surfaces post abrasive treatment with 80-grit aluminum oxide.....	65
3.4. Concluding remarks and future works .....	75
Chapter 4: Literature cited .....	90
Appendix.....	84

## List of figures

Figure 1.1. Developmental stages of biofilm formation and defining characteristics.....	1
Figure 1.2. Enzymatic synthesis and degradation of c-di-GMP.....	9
Figure 1.3. Generalized overview of Lux protein family quorum sensing network.....	11
Figure 1.4. Acyl-homoserine lactones produced by <i>P. aeruginosa</i> .....	13
Figure 1.5. Phosphate dependent c-di-GMP regulation for biofilm formation in <i>P. fluorescens</i> Pf0-1.....	16
Figure 2.1. Fragmentation pattern of the radical ion at m/z 199 ( <b>4</b> ) for <i>N</i> -hexanoyl-HSL to produce the most abundant radical ion at of m/z 143 ( <b>5</b> and <b>6</b> ).....	19
Figure 2.2. Structures of marker fragment ions at m/z of 125 ( <b>7</b> ), 143 ( <b>8</b> ) and 156 ( <b>9</b> ).....	20
Figure 2.3. High-resolution MID spectra of <i>N</i> -hexanoyl-HSL standard.....	25
Figure 2.4. EIC for m/z fragment ion of 143 in chloroform extract of <i>P. fluorescens</i> Pf0-1 supernatant....	26
Figure 2.5. Acyl-homoserine lactones under investigation by GC-MS for their presence in <i>P. fluorescens</i> supernatant.....	27
Figure 2.6. High-resolution MID spectra of possible <i>N</i> -butyryl-HSL found in the chloroform extract of <i>P. fluorescens</i> Pf0-1 supernatant.....	28
Figure 2.7. High-resolution MID spectra of possible <i>N</i> -decanoyl-HSL found in the chloroform extract of <i>P. fluorescens</i> Pf0-1 supernatant.....	28
Figure 2.8. High-resolution MID spectra of possible <i>N</i> -heptanoyl-HSL found in the chloroform extract of <i>P. fluorescens</i> Pf0-1 supernatant.....	29
Figure 2.9. EIC for m/z fragment ion of 143 in AHL-spiked chloroform extract of <i>P. fluorescens</i> Pf0-1 supernatant from 4.97 – 7.03 min.....	30
Figure 2.10. EIC for m/z fragment ion of 143 in AHL-spiked chloroform extract of <i>P. fluorescens</i> Pf0-1 supernatant from 4.97 – 12.99 min.....	31
Figure 2.11. High-resolution MID spectra for AHL-spiked chloroform extract of <i>P. fluorescens</i> Pf0-1 supernatant at retention time frame of 5.74 – 5.82 min.....	32
Figure 2.12. High-res MID spectra for AHL-spiked chloroform extract of <i>P. fluorescens</i> Pf0-1 supernatant at retention time frame of 10.63 – 10.66 min.....	33
Figure 2.13. High-res MID spectra for AHL-spiked chloroform extract of <i>P. fluorescens</i> Pf0-1 supernatant at retention time frame of 8.38 – 8.52 min.....	34
Figure 2.14. EIC for m/z fragment ion of (A) 125 and (B) 143 in chloroform extract of <i>P. fluorescens</i> Pf0-1 supernatant after oven program adjustment. Supernatant extract dissolved in HPLC grade MeOH. Temperature ramp was decreased to 2.5 °C/min.....	35

Figure 2.15 EIC for $m/z$ fragment ion of (A) 125 and (B) 143 in chloroform extract of <i>P. fluorescens</i> Pf0-1 supernatant dissolved in HPLC grade MeOH and spiked with 0.1 ng/ $\mu$ L of <i>N</i> -heptanoyl-HSL. Temperature ramp was decreased to 2.5 °C/min .....	36
Figure 2.16. High-resolution MID spectrum for chloroform extract of <i>P. fluorescens</i> Pf0-1 supernatant at retention time of 15.62 min for the chromatogram in Fig. 2.14A. EI-SIM mode was performed for $m/z$ fragment ions of 125, 143 and 156.....	37
Figure 2.17. High-resolution MID spectra for AHL-spiked chloroform extract of <i>P. fluorescens</i> Pf0-1 supernatant. EI-SIM mode was performed for $m/z$ fragment ions of 125, 143 and 156. (A) Retention time of 15.62 min for the chromatogram in Fig. 2.15A. (B) Retention time of 15.63 min for the chromatogram in Fig. 2.15B.....	38
Figure 3.1. Crystal violet stained <i>P. fluorescens</i> Pf0-1 on a non-treated polystyrene surface.....	41
Figure 3.2. Drill bit used to modify microtiter plate wells.....	48
Figure 3.3. Initial qualitative analysis of microtiter plates that support <i>P. fluorescens</i> Pf0-1 biofilm formation.....	51
Figure 3.4. Quantitative analysis of <i>P. fluorescens</i> Pf0-1 biofilm formation during secondary screening of microtiter plates.....	54
Figure 3.5. Biofilm formation in two individual Corning microtiter plates No. 351172.....	55
Figure 3.6. Quantitative analysis of the effects the carbon source has on biofilm formation in <i>P. fluorescens</i> Pf0-1 No. 1.....	57
Figure 3.7. Qualitative analysis of the effects the carbon source has on biofilm formation in <i>P. fluorescens</i> Pf0-1.....	57
Figure 3.8. Quantitative analysis of the effects the carbon source has on biofilm formation in <i>P. fluorescens</i> Pf0-1 No. 2.....	58
Figure 3.9. Comparison of biofilm formed by <i>P. fluorescens</i> Pf0-1 cultures using glucose as the carbon source, either filter- or autoclave sterilized.....	59
Figure 3.10. Initial comparison of Norgen polypropylene plate and ThermoFisher Scientific Plate for quantity of <i>P. fluorescens</i> Pf0-1 biofilm formed.....	61
Figure 3.11. Norgen and ThermoFisher Scientific microtiter plate comparison biofilm assay No. 1.....	62
Figure 3.12. Norgen and ThermoFisher Scientific microtiter plate comparison biofilm assay No. 2.....	63
Figure 3.13. Norgen and ThermoFisher Scientific microtiter plate comparison biofilm assay No. 3.....	64
Figure 3.14. Comparison of polystyrene surface post abrasive treatment to the unmodified polystyrene surface using SEM. 15.0 kV used for SEM analysis at a magnification of 500x.....	66
Figure 3.15. SEM analysis of polystyrene post abrasive treatment at 2.0 kV and 1000x magnification.....	67

Figure 3.16. Comparison of <i>P. fluorescens</i> Pf0-1 biofilm formed on an unmodified polystyrene plate and a polystyrene plate post abrasive treatment.....	68
Figure 3.17. Photograph of sand-treated microtiter plate.....	69
Figure 3.18. Quantitative comparison No. 1 of <i>P. fluorescens</i> Pf0-1 biofilm formed on unmodified and sandblasted polystyrene on the same plate.....	69
Figure 3.19. Quantitative comparison No. 2 of <i>P. fluorescens</i> Pf0-1 biofilm formed on unmodified and sandblasted polystyrene.....	70
Figure 3.20. Quantitative comparison No. 3 of <i>P. fluorescens</i> Pf0-1 biofilm formed on unmodified and sandblasted polystyrene.....	71
Figure 3.21. Quantitative comparison No. 4: <i>P. fluorescens</i> Pf0-1 biofilm formed on unmodified and drill-modified polystyrene plate No.1.....	73
Figure 3.22. Quantitative comparison No. 4: <i>P. fluorescens</i> Pf0-1 biofilm formed on unmodified and drill-modified polystyrene plate No.2.....	73
Figure 3.23. Quantitative comparison No. 4: <i>P. fluorescens</i> Pf0-1 biofilm formed on unmodified and sandblasted polystyrene plate No.1.....	74
Figure 3.24. Quantitative comparison No. 4: <i>P. fluorescens</i> Pf0-1 biofilm formed on unmodified and sandblasted polystyrene plate No.2.....	74
Figure A-1. TIC for standard AHLs; <i>N</i> -hexanoyl-HSL, <i>N</i> -heptanoyl-HSL and <i>N</i> -decanoyl-HSL.....	84
Figure A-2. TIC for standard AHL <i>N</i> -butyryl-HSL.....	84
Figure A-3. High-res MID spectra of <i>N</i> -heptanoyl-HSL standard.....	85
Figure A-4. High-res MID spectra of <i>N</i> -decanoyl-HSL standard.....	85
Figure A-5. High-res MID spectra of <i>N</i> -butyryl-HSL standard.....	86
Figure A-6. TIC for spiked chloroform extract of <i>P. fluorescens</i> Pf0-1 supernatant.....	86
Figure A-7. EIC for m/z fragment ion of 143 in chloroform extract of <i>P. fluorescens</i> Pf0-1 supernatant ....	87
Figure A-8. TIC for 0.1 ng/μL standard spiked chloroform extract of <i>P. fluorescens</i> Pf0-1 supernatant.....	87
Figure A-9. EIC for m/z fragment ion of 143 in 0.1 ng/μL standard spiked chloroform extract of <i>P. fluorescens</i> Pf0-1 supernatant.....	88
Figure A-10. EIC for m/z fragment ion of 143 in 1 ng/μL standard spiked chloroform extract of <i>P. fluorescens</i> Pf0-1 supernatant.....	88

## List of tables

Table 2.1. Acyl-homoserine lactones under investigation.....	24
Table 2.2. Retention time comparison between AHL standards and peaks observed in the <i>P. fluorescens</i> Pf0-1 extract sample chromatogram.....	27
Table 3.1. Product information for preliminary screening of microtiter plates.....	51
Table 3.2. Product information for secondary screening of microtiter plates.....	53
Table 3.3. Product information for microtiter plates purchased from Corning.....	55
Table 3.4. Product information for polypropylene plates tested.....	60

## List of abbreviations

**5'pGpG**: linear form of bis-(3'-5')-cyclic dimeric GMP

**ACN**: acetonitrile

**AFM**: atomic force microscopy

**AHL**: acyl-homoserine lactone

**aphA**: gene encoding a transcription factor involved in *Vibrio cholerae* c-di-GMP signaling

**aprA**: gene encoding virulence factor alkaline protease

**BLUF**: Blue Light FAD

**BSE**: back-scattered electrons

**Ca<sup>2+</sup>**: calcium ion

**c-di-GMP**: bis-(3'-5')-cyclic dimeric GMP

**CSLM**: confocal laser scanning microscopy

**D/NxSxxG**: conserved sequence motif in PilZ domain of c-di-GMP effector proteins

**DGC**: diguanylate cyclase

**EAL**: domain found within the active site of phosphodiesterases required for c-di-GMP degradation

**eDNA**: extracellular DNA

**ESI-MS**: electron ionization spray-mass spectrometry

**EI**: electron ionization

**EI-SIM-MS**: electron ionization-mass spectrometry in the selected ion monitoring mode

**Fe<sup>2+</sup>**: ferrous ion

**FeSO<sub>4</sub>·7H<sub>2</sub>O**: ferrous sulfate

**GC**: gas chromatography

**GC-MS**: gas chromatography-mass spectrometry

**GGDEF**: domain found within the active site of diguanylate cyclases required for c-di-GMP synthesis

**GMP**: guanosine-5'-monophosphate

**GTP**: guanosine-5'-triphosphate

**hapR**: gene involved in quorum sensing network of *Vibrio cholerae*

**HD-GYP**: less commonly found domain within the active site of phosphodiesterases required for c-di-GMP degradation

**HdtS**: novel AHL synthase in *Pseudomonas fluorescens* F113

**HPLC**: high-performance liquid chromatography

**HSL:** homoserine lactone  
**KH<sub>2</sub>PO<sub>4</sub>:** potassium phosphate monobasic  
**KOH:** potassium hydroxide  
**LapA:** adhesion protein required for biofilm formation in *Pseudomonas fluorescens* Pf0-1  
**LapD:** inner membrane effector protein containing a degenerate EAL-domain  
**LapG:** protease  
**LasI:** autoinducer synthase responsible for the production of *N*-(3-oxododecanoyl)-HSL  
**LasR:** autoinducer receptor for *N*-(3-oxododecanoyl)-HSL  
*lasA:* gene encoding virulence factor elastase  
*lasB:* gene encoding virulence factor metalloprotease elastase  
**LB:** LB-Miller media, Miller's modification of nutrient rich Luria-Broth  
**LC-MS:** liquid chromatography-mass spectrometry  
**LuxI:** autoinducer synthase  
**LuxIR:** first major quorum sensing network observed across different bacterial species  
**LuxR:** autoinducer receptor  
**MALDI-TOF MS:** matrix assisted laser desorption ionization-time of flight mass spectrometry  
**Mg<sup>2+</sup>:** magnesium ion  
**MgSO<sub>4</sub>·7H<sub>2</sub>O:** magnesium sulfate heptahydrate  
**Mn<sup>2+</sup>:** manganese ion  
*mpuI-mpuR:* biosynthetic gene cluster for mupirocin  
**MRSA:** methicillin-resistant *Staphylococcus aureus*  
**MS:** mass spectrometry  
**MS<sup>2</sup>:** tandem mass spectrometry  
**MupIR:** LuxIR type quorum sensing network in *Pseudomonas fluorescens* strain NCIMB 10586  
**NaOH:** sodium hydroxide  
**(NH<sub>4</sub>)<sub>2</sub>SO<sub>4</sub>:** ammonium sulfate  
**Ni<sup>2+</sup>:** nickel ion  
**PAS:** oxygen sensing domain  
**PcoIR:** LuxIR type quorum sensing system in *Pseudomonas fluorescens* 2P24  
**PDE:** phosphodiesterase  
**PilZ:** a common c-di-GMP binding domain in receptor proteins  
**PleD:** a response regulator for cell cycle initiation and cell differentiation from a swarmer cell into a stalked cell in *Caulobacter crescentus*  
**pppGpG:** diguanosine triphosphate  
**PTFE:** polytetrafluoroethylene  
**R<sub>a</sub>:** average roughness measurement  
**R<sub>q</sub>:** root mean square roughness measurement  
**RapA:** phosphodiesterase  
**REC:** phosphorylation receiver domains  
**RhII:** autoinducer synthase responsible for the production of *N*-butyryl-HSL  
**RhIR:** autoinducer receptor for *N*-butyryl-HSL  
*rhIAB:* gene cluster that controls the biosynthesis of rhamnolipid  
**RpfR:** phosphodiesterase  
**RxxD:** c-di-GMP feedback inhibition motif found in diguanylate cyclases

**RxxxR**: conserved sequence motif in PilZ domain of c-di-GMP effector proteins  
**SAM**: S-adenosylmethionine  
**SE**: secondary electrons  
**SEM**: scanning electron microscopy  
**toxA**: gene encoding virulence factor exotoxin A  
**UV**: ultraviolet  
**vpsT**: gene encoding a transcription factor involved in *Vibrio cholerae* c-di-GMP signaling  
**Zn<sup>2+</sup>**: zinc ion

## Chapter 1: Literature review

### 1.1. Stages of biofilm development

Bacterial biofilms are the adhesion of cells to a living or non-living surface, connected by a self-made matrix of polysaccharides, DNA, and proteins. Within this extracellular matrix is a complex network of channels that allows for the delivery of essential nutrients and molecules for communication. The transition from a planktonic to sessile lifestyle creates a physiologically and genetically diverse population that has increased antimicrobial tolerance and ability to evade the host's defence system. (Bjarnsholt, Jensen, Moser, & Høiby, 2010) Stages involved in this transition are depicted below in Figure 1.1.

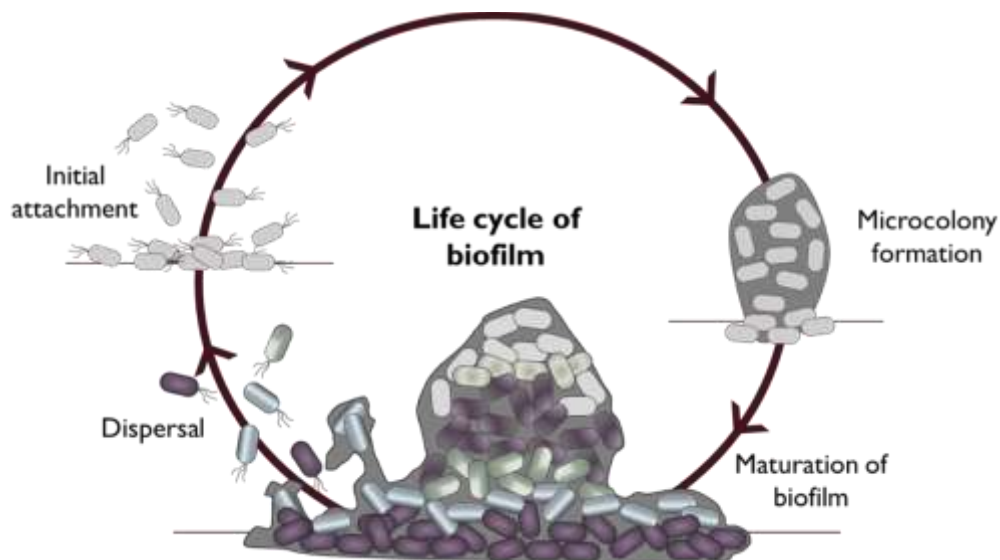


Figure 1.1. Developmental stages of biofilm formation and defining characteristics. Single cells or clusters irreversibly attach to a surface and begin forming microcolonies. A mature biofilm forms, consisting of multiple genetically different subpopulations of cells (heterogeneity depicted by each subpopulation represented by a different colour). Final life stage of biofilms is the seeding dispersal. This stage involves the release of single cells or clusters from the mature biofilm for seeding of new biofilms in the environment.

#### 1.1.1. Initial attachment

Physicochemical forces, such as Van der Waals and electrostatic interactions, facilitate initial reversible interactions between bacterial cells and a surface. These interactions remain reversible and are dependent on the bacterial cells' ability to overcome repulsive forces from the

bacterial cell surface, environmental factors and the physicochemical properties of the surface. (Berne, Ducret, Hardy, & Brun, 2015; Song, Koo, & Ren, 2015)

Bacterial cells that can utilize different types of pili and flagella have a competitive advantage when overcoming repulsive forces encountered at a surface. For example, the negative charge from the bacterial cell envelope can generate an electrostatic repulsion. To overcome this barrier, motile bacteria can utilize flagella as propellers to direct the cells while hydrophobic domains on the pili can facilitate favourable non-specific interactions with a surface. (Donlan, 2002; Tolker-Nielsen, 2015; Tuson & Weibel, 2013) Alongside the use of flagella and pili, there are also nonfimbrial adhesions and polysaccharide adhesions that bacteria can produce to permanently attach onto a surface. The production of these adhesions is regulated mainly through the signaling network of bis-(3'-5')-cyclic dimeric GMP (c-di-GMP) in response to changes in the environment (i.e. pH, nutrient levels, oxygen availability, temperature). (Donlan, 2002; Tolker-Nielsen, 2015; Van Houdt & Michiels, 2010) High levels of this intracellular nucleotide second messenger will trigger the production of various adhesions and extracellular matrix components to hold cells together on a surface. (Tolker-Nielsen, 2015)

There are also several surface physicochemical properties that influence cell-surface interactions; surface charge differences, hydrophobicity, hydrodynamics and surface roughness. Literature agrees that an increase in surface roughness promotes bacterial adhesion. These surfaces provide increased points of attachment for cell positioning and protection from shear forces. (Donlan, 2002; Song *et al.*, 2015) Bacterial adhesion studies commonly define roughness as an  $R_a$  (average roughness) and  $R_q$  (root mean square roughness) value. (Crawford, Webb, Truong, Hasan, & Ivanova, 2012; Mei, Busscher, van der Mei, & Ren, 2011; Song *et al.*, 2015; Verran *et al.*, 2014) These parameters measure roughness in relation to the amplitude of peaks and valleys

on a surface. It is important to note that these parameters do not consider three-dimensional structures or their spatial orientation that can further influence bacteria adhesion. (Crawford *et al.*, 2012; Song *et al.*, 2015) Surfaces exhibiting the same chemical properties can result in bacterial adhesion profile differences based on the topographical properties of the surfaces. The topography of a surface, both on a micro- and nanoscale, has been shown to dictate the expression of different adhesive proteins necessary for bacterial attachment. (Hsu, Fang, Borca-Tasciuc, Worobo, & Moraru, 2013; Mitik-Dineva *et al.*, 2009; Wu, Zitelli, TenHuisen, Yu, & Libera, 2011) For example, a study performed on *Escherichia coli*, *Pseudomonas aeruginosa* and *Staphylococcus aureus* showed that all displayed different responses (metabolic activity, cell morphologies) to surfaces of nanoscale roughness (as measured by  $R_a$  and  $R_q$  values). (Mitik-Dineva *et al.*, 2009) Therefore, it is difficult to predict the response bacterial cells will have once the properties of the bacterial cells and other environmental factors such as ionic strength of the media, temperature and nutrient levels are considered. (Donlan, 2002)

### **1.1.2. Microcolony formation**

Once the appropriate conditions are met, bacterial cells are irreversibly bound and microcolonies will begin to form. The proximity of cells results in the exchange of signaling molecules called autoinducers, which are an important mediator in the quorum sensing communication system. This system allows the coordination of cellular activities and cell organization on the surface during microcolony development. Different signaling mechanisms continue to be activated in order to reduce motility and further trigger the production of extracellular matrix components that will trap nutrients required to sustain the growing biofilm. (Roilides, Simitsopoulou, Katragkou, & Walsh, 2015) The bacterial species forming the biofilm, in conjunction with the nutrients provided, will affect the resulting architecture and organization of cells in the microcolonies. (Tolker-Nielsen, 2015)

There are several mechanisms through which biofilm formation can occur and they cannot be grouped under a single set of genes. The maturation of biofilm is based on adaptive responses to changes in the environment where bacteria are required to alter their adhesiveness and motility when needed. (Tolker-Nielsen, 2015)

### **1.1.3. Maturation: physiological characteristics**

The bacterial communication via quorum sensing remains an important factor during maturation to maintain the structural integrity of the biofilm and support cell growth. Complex structures within the biofilm are formed and subpopulations are created leading to a genetically diverse and mature heterogeneous biofilm. (Franklin, Chang, Akiyama, & Bothner, 2015; Roilides *et al.*, 2015)

As a biofilm grows in thickness, chemical gradients are created as nutrients and oxygen diffuse into the biofilm at varying rates and are utilized. Different regions of the biofilm are then exposed to unique microenvironments with varying access to nutrients and accumulation of waste products that could alter the pH of the immediate surroundings. As a result, the physiological state of cells will vary greatly as gene expression is altered to adapt to their local microenvironment. (Franklin *et al.*, 2015) The genetic variability will then lead to multiple subpopulations of cells differing in both metabolic and reproductive activity. (Kaplan, 2010)

The proximity of cells within a biofilm allows for horizontal gene transfer to occur at a much greater rate than that between free-floating cells in a liquid culture. The protein expression levels within a biofilm can also differ as much as 70% from the planktonic cells of the same strain of bacterial species. (Costerton, 2007) For example, in a study performed by Sauer *et al.*, the authors utilized a combination of approaches, such as *in situ* reporter gene analysis, 2-D gel electrophoresis and MALDI-TOF MS, to demonstrate the development of multiple phenotypes in *P. aeruginosa* biofilms. Changes in the protein expression profiles were observed throughout

various stages in biofilm development for several metabolic pathways, such as carbon catabolism, amino acid metabolism and cofactor biosynthesis. In comparison to planktonic cells, more than 50 % of all the proteins were upregulated within the first six days of biofilm development. The authors also found that the protein profiles for *P. aeruginosa* PAO-1 and *P. putida* ATCC 39168 planktonic cells had more in common than planktonic cultures of *P. aeruginosa* to six-day old *P. aeruginosa* biofilms. (Sauer, Camper, Ehrlich, Costerton, & Davies, 2002)

Genetic variation is further induced due to mutations such as single nucleotide polymorphisms or chromosomal rearrangements. Variants will form subpopulation within a biofilm when chosen through natural selection. Lastly, stochastic gene expression allows for neighbouring cells existing in very similar environments to express the same set of genes at different levels. As a result, this behavior promotes the division of labour among cells, increasing biofilm complexity. (Franklin *et al.*, 2015; Stewart & Franklin, 2008)

#### **1.1.4. Dispersal**

The last stage of biofilm development is the release of cells from the mature colonies to colonize other areas of the environment. The dispersal process can occur at any time, in response to changes in the environment or self produced signals, and result in complete dissociation of the biofilm. (Barraud, Kjelleberg, & Rice, 2015; Kaplan, 2010) Many of the mechanisms involved in cell-detachment are regulated by the second messenger c-di-GMP. (Tolker-Nielsen, 2015)

#### **1.2. Antimicrobial tolerance in biofilms**

The formation of a biofilm provides the bacteria with a unique defence mechanism against a number of stresses such as the innate immune defences and antibiotics. (Penesyan, Gillings, & Paulsen, 2015; Roilides *et al.*, 2015) In addition to the physical barrier, the protection that biofilms provide also originates from the heterogeneity of subpopulations as well as the communication

and coordination of cellular activities between cells. The heterogeneity within a biofilm results in antibiotic resistance up to 1000 times higher than that observed in planktonic cells of the same strain. (Penesyan *et al.*, 2015) There are several cooperative mechanisms that biofilms use in order to increase their tolerance to antibiotics as elaborated in the sections below.

### **1.2.1. The protective barrier: extracellular matrix**

The first barrier encountered by antimicrobials is the complex network of the extracellular matrix. The thickness of the matrix is capable of limiting the diffusion of antibiotics to the deeper layers of the biofilm and contains components such as polysaccharides, proteins and extracellular DNA (eDNA), that is capable of acting as a chelator. (Penesyan *et al.*, 2015; Stewart, 2015) In terms of protection against the innate immune defences, the matrix acts as a shield for the biofilm cells against inflammatory assault by phagocytes as well. A bacterial infection in the human body is easily targeted by the innate immune system when cells are exposed and freely floating throughout the bloodstream. However, issues arise if bacteria find the opportunity to colonize either tissues or the surface of an implanted medical device. When phagocytes attempt to degrade the biofilm, degradative enzymes are released, but are incapable of breaking down the matrix structure. Instead, damage to the surrounding tissues occur. (Costerton, Stewart, & Greenberg, 1999) An example of this form of protection is seen in chronic *P. aeruginosa* infections in the lungs of cystic fibrosis patients in response to polymorphonuclear leukocytes (PMNs). (Bjarnsholt *et al.*, 2005; Costerton *et al.*, 1999) In order to protect itself from surrounding PMNs, *P. aeruginosa* produces the exopolysaccharide alginate to scavenge radical oxygen species and through quorum sensing mechanisms produces rhamnolipids as a shield. (Alhede *et al.*, 2009; Bjarnsholt *et al.*, 2010; Jensen *et al.*, 2007; Kaplan, 2010; Leid *et al.*, 2005)

### **1.2.2. Altered microenvironments**

The next obstacle antibiotics face when encountering a biofilm community is the altered physiological state found within the different biofilm subpopulations. The diversity of metabolic activity present in the biofilm disables the mechanism of action for some antibiotics whose targets are key components of cellular processes. (Stewart, 2015) An example of this process was demonstrated in *P. aeruginosa* biofilms in a study conducted by Pamp *et al.* Upon treating the biofilm with three different types of antibiotics, the authors found that different areas of the biofilm were affected. The antibiotics ciprofloxacin and tetracycline targeted cells in the upper layers of the biofilm due to their increased metabolic activity. Cells that resided in the base of the biofilm were targeted by the antibiotic colistin due to their decreased metabolic activity. The lack of targeting by colistin to cells in the upper layers of biofilm were due to those cells expressing genes *pmrHFIJKLM* and *mexAB-oprM*. The *pmr* operon mediates lipopolysaccharide modification to reduce interaction with this drug while the *mex* operon facilitates the transport of the antibiotic out of the cell through an efflux pump. These systems are not turned on in cells with a lower metabolic rate and thus render the base of the biofilm more susceptible to colistin. The three antibiotics were only found to be effective when administered as a combined treatment regimen. (Pamp, Gjermansen, Johansen, & Tolker-Nielsen, 2008)

### **1.2.3. Persister cells**

There are cells that reside in the base of a biofilm that play a key role in antimicrobial tolerance, particularly the development of chronic infections. The subpopulation of cells called persisters are found in bacteria of many different genera. (Wood, Knabel, & Kwan, 2013) Persisters were first characterized in a study performed by Bigger in 1944 while studying antibiotic resistance in *Staphylococcus pyogenes*. (Bigger, 1994) Upon administering penicillin to a population of bacterial cells, the author found a group of cells had survived without having to

undergo any genetic changes. This group of cells also exhibited growth delays upon transfer to a nutrient-rich media. These cells are termed to be metabolically dormant, exhibiting rates of metabolic activity that is so low that there are virtually no targets available for antibiotics. It is this population of cells that is responsible for rebuilding the biofilm once the upper layers have been destroyed and antibiotic levels are diminished, resulting in a persistent chronic infection. (Wood *et al.*, 2013) A more recent study performed in cultures of *Escherichia coli* demonstrated how extracellular stresses, such as antibiotics, could trigger the formation of the persister cell type. The authors found an absence of protein synthesis within the persister population providing further validation of these cells' metabolic dormancy. (Wood *et al.*, 2013)

### **1.3. The role of the nucleotide second messenger c-di-GMP in biofilm formation**

#### **1.3.1. C-di-GMP synthesis and degradation**

C-di-GMP was first identified in 1987 by researchers studying cellulose synthesis regulation in *Gluconacetobacter xylinus*. (Ross *et al.*, 1987) Researchers demonstrated c-di-GMP was capable of allosterically activating the enzyme as well as the steps involved in c-di-GMP synthesis and degradation. The biosynthesis of the intracellular signaling molecule c-di-GMP begins from two equivalents of guanosine-5'-triphosphate (GTP) and proceeds through a diguanosine triphosphate intermediate pppGpG. (Tal *et al.*, 1998) The reaction is catalyzed by diguanylate cyclases (DGC) whose active site contains a critical GGDEF domain characterized by conserved GGDEF or GGEEF amino acid motifs. This domain was first described by Gregory Hecht and Austin Newton in 1995 while studying the sequence of the response regulator PleD in *Caulobacter crescentus*. (Hecht & Newton, 1995; Römling, Galperin, & Gomelsky, 2013) These enzymes can also possess an inhibitory binding site characterized by an RxxD motif to allow for product feedback inhibition. The degradation of c-di-GMP is then catalyzed by phosphodiesterases (PDE) which contain either an EAL or, less commonly, HD-GYP domain. (Kalia *et al.*, 2013) The

EAL-containing PDE hydrolyzes c-di-GMP into 5'-pGpG where the PDE containing a HD-GYP domain hydrolyzes c-di-GMP directly into 2 GMP through a 5'-pGpG intermediate. (Ryan *et al.*, 2006) Both types of PDEs require  $Mg^{2+}$  or  $Mn^{2+}$  as cofactors and are inhibited  $Ca^{2+}$ ,  $Ni^{2+}$ ,  $Fe^{2+}$  and  $Zn^{2+}$  ions. (Kalia *et al.*, 2013)

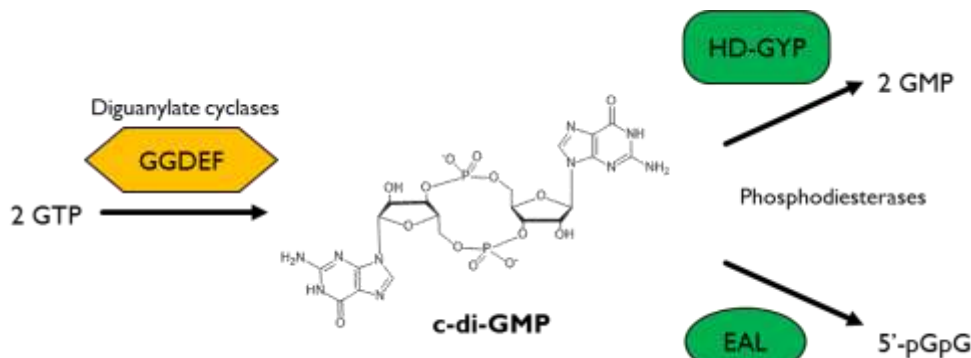


Figure 1.2. Enzymatic synthesis and degradation of c-di-GMP

### 1.3.2. Mechanisms of c-di-GMP signaling

The nucleotide second messenger c-di-GMP is involved in regulating several cellular processes such as cell differentiation, motility, virulence as well as the initiation and dispersal stages of biofilm formation. Through various transmembrane sensor proteins containing c-di-GMP binding domains, bacteria can respond to environmental changes by altering the intracellular levels of c-di-GMP to induce the appropriate biological response such as biofilm formation. (Kalia *et al.*, 2013) Examples of sensory input domains include sensors for Blue Light FAD (BLUF) (Gomelsky & Klug, 2002), phosphorylation receiver domains (REC) (Kalia *et al.*, 2013) and oxygen sensing (PAS). (B. L. Taylor & Zhulin, 1999)

Depending on the environmental cue, intracellular pools of c-di-GMP will be increased and thus initiate the production of components required for the production of a biofilm, or levels of c-di-GMP will decrease in order to initiate dispersal and thus favouring a free-floating cell state. (Ha & O'Toole, 2015) In order to regulate the cycle of biofilm formation c-di-GMP can bind to five major types of receptors, PilZ domain containing effector proteins, transcriptional regulators,

degenerate GGDEF or EAL proteins and riboswitches. (Kalia *et al.*, 2013) Effector proteins containing PilZ domains are one of the major types of effectors found among different bacterial species, first being implicated as an important c-di-GMP receptor during sequence analysis of cellulose synthases. (Amikam & Galperin, 2006) These effector proteins are characterized by the following two conserved motifs, RxxxR and D/NxSxxG, where x refers to any amino acid. Within the RxxxR motif resides a seven-residue loop that undergoes a conformational change upon binding c-di-GMP. This structural change allows the protein to participate in different protein-protein interactions required for biofilm development. (Kalia *et al.*, 2013; Ryjenkov, Simm, Römling, & Gomelsky, 2006)

#### **1.4. Quorum sensing**

##### **1.4.1. Introduction to quorum sensing in gram negative bacteria**

The chemical signaling system of quorum sensing allows bacteria to coordinate their behaviors in environments of high cell density. Through the synthesis, secretion and subsequent detection of molecules called autoinducers, bacteria are able to communicate with their neighbours or identify their competitors and alter their gene expression accordingly. (Papenfort & Bassler, 2016) The quorum sensing network is also capable of responding to environmental inputs such as nutrient availability, pH and temperature. (Hagen, 2015; Hense, Müller, Kuttler, & Hartmann, 2012) Information from both of these factors are integrated into a push-pull regulatory system that determines the phenotypic outcome. (Hense *et al.*, 2012)

Quorum sensing is commonly recognized for its role in the bioluminescence of *Vibrio harveyi* (Anetzberger, Pirch, & Jung, 2009; Engebrecht, Nealson, & Silverman, 1983) as well as virulence and biofilm development for *P. aeruginosa*. (Allesen-Holm *et al.*, 2006; Hentzer *et al.*, 2002; Hoffman *et al.*, 2009; Winson *et al.*, 1995) More recently, the quorum sensing system in

*Serratia* sp. ATCC39006 (Patterson *et al.*, 2016) as well as *P. aeruginosa* PA14 (Høyland-Kroghsbo *et al.*, 2016), has been shown to regulate CRISPR-Cas systems.

The major class of autoinducers utilized by gram negative bacteria are the acyl-homoserine lactones (AHLs). The core structure of these molecules is characterized by a homoserine lactone (HSL) moiety connected through an amide bond to an acyl chain that can range from four to eighteen carbons in length. These molecules can be differentiated further by varying levels of oxidation at the 3'-position of the acyl chain and extent of saturation throughout the R-group. (Brameyer, Bode, & Heermann, 2015; Papenfort & Bassler, 2016)

The first major type of synthases observed across different bacterial species are from the LuxI family. These enzymes link the lactone moiety derived from the substrate *S*-adenosylmethionine (SAM), with the acyl chain component originating from fatty acid biosynthesis intermediates. (Brameyer *et al.*, 2015; Papenfort & Bassler, 2016)

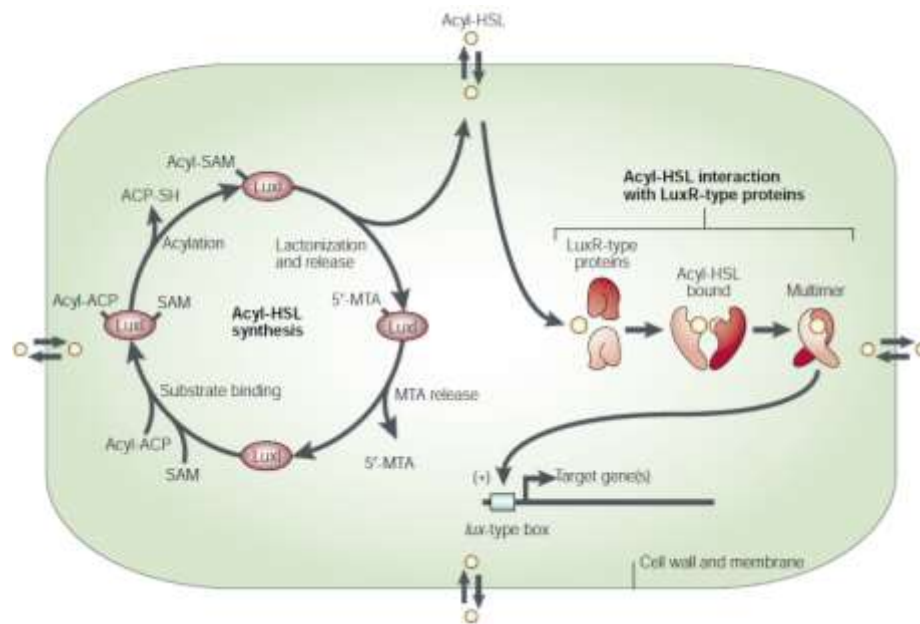


Figure 1.3. Generalized overview of Lux protein family quorum sensing network. Reprinted by permission from Macmillan Publishers Ltd: Nature Reviews Molecular Cell Biology (Fuqua & Greenberg, 2002), © (2002) Image was originally modified from Fuqua, Parsek & Greenberg, 2001.

Once AHLs are produced, they are capable of freely diffusing through the cell membrane (Brameyer *et al.*, 2015; Papenfort & Bassler, 2016) as well as through active transport mechanisms. (Pearson, Van Delden, & Iglewski, 1999) Changes in the concentration of LuxI-derived AHLs in response to the local cell density are recognized by partner LuxR-type receptors that reside in the cytoplasm. The LuxR receptors when unbound to an AHL are unable to fold properly and are thus degraded. Once the appropriate AHL binds to the amino-terminal binding domain of a LuxR, the protein is stabilized by dimerization. The LuxR-AHL complex can then bind to DNA through the protein's carboxyl terminal DNA-binding domain and regulate gene expression required for group behavior. (Papenfort & Bassler, 2016) There are also a class of LuxR receptors that do not have a partner LuxI synthase and thus called LuxR-solo transcription factors. (Brameyer *et al.*, 2015; Fuqua & Greenberg, 2002) These transcription factors can respond to both AHLs produced endogenously by non-LuxI synthases or exogenously produced AHLs by neighbouring bacteria. (Papenfort & Bassler, 2016; Patel *et al.*, 2013) LuxR solo are unique in that they can also bind non-AHL molecules produced endogenously or exogenously, such as small molecules from plants. (Hartmann, Rothballer, Hense, & Schröder, 2015; Patel *et al.*, 2013; Schikora, Schenk, & Hartmann, 2016; Venturi & Ahmer, 2015)

#### **1.4.2. Acyl-homoserine lactone quorum sensing in *P. aeruginosa***

*P. aeruginosa* is an opportunistic pathogen that uses quorum sensing networks in the regulation of genes for virulence factors (Jimenez *et al.*, 2012; Passador, Cook, Gambello, Rust, & Iglewski, 1993) and maturation of biofilm. (Allesen-Holm *et al.*, 2006; De Kievit, Gillis, Marx, Brown, & Iglewski, 2001) With respect to acyl-homoserine lactones, there are two LuxIR type systems that regulate 2-5 % of it's genes, LasR and LasI and RhIR and RhII. (Whiteley, Lee, & Greenberg, 1999)

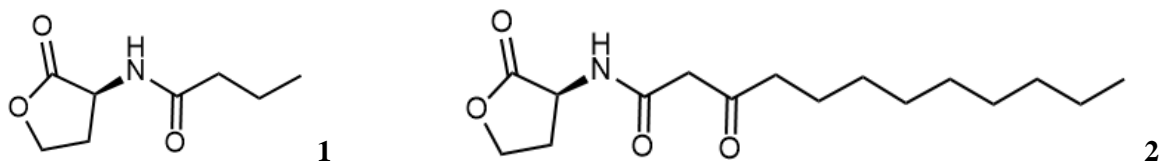


Figure 1.4. Acyl-homoserine lactones produced by *P. aeruginosa*. *N*-butryl-HSL **1** and *N*-(3-oxododecanoyl)-HSL **2**.

The acyl-HSL synthases LasI and RhII are responsible for the respective synthesis of *N*-(3-oxododecanoyl)-HSL and *N*-butryl-HSL. Once produced, the formation of complexes LasR – *N*-(3-oxododecanoyl)-HSL and RhIR – *N*-butryl-HSL then activates the expression of target genes through the binding to conserved *las-rhl* boxes within promoter regions. (Lee & Zhang, 2015; Papenfort & Bassler, 2016) Downstream of these promoters are also *lasI* and *rhII* genes, generating a positive feedback loop for each quorum sensing network. (Fuqua & Greenberg, 2002; Lee & Zhang, 2015; Papenfort & Bassler, 2016)

The first gene identified to be under control of LasR in *P. aeruginosa* was *lasB*, encoding the virulence factor metalloprotease elastase. (Gambello & Iglewski, 1991) The production of this enzyme is an integral part of pseudomonad infection due to the different virulent mechanisms it is responsible for. Elastase acts as a trigger inside the cell for biofilm formation, and destroys tissues at the infection site to release essential nutrients required for growth and manipulates the host's immune response. (Cathcart *et al.*, 2011) Subsequent studies then identified the LasR – acyl-HSL complex to be responsible for the regulation of several other genes encoded by virulence factors, including *aprA* (alkaline protease) (Gambello, Kaye, & Iglewski, 1993), *lasA* (elastase) (Toder, Gambello, & Iglewski, 1991) and *toxA* (exotoxin A). (Passador *et al.*, 1993) The RhIR-RhII system was first identified to control rhamnolipid synthesis through expression of the gene cluster *rhlAB* through the binding of *N*-butryl-HSL. (Ochsner & Reiser, 1995) The expression of *rhII* can also be induced by LasR, creating an additional layer of regulation for virulence factor gene activation when in different environments. (Papenfort & Bassler, 2016)

## **1.5. Model microorganism of study: *P. fluorescens***

The *P. fluorescens* species complex is a group of gram negative, rod shaped, motile bacteria capable of inhabiting a wide range of environments. The name “fluorescens” originates from their fluorescent behavior when viewed under UV light, resulting from the iron-chelating pigment pyoverdine. Members of the *P. fluorescens* species complex are an important source of secondary antimicrobial metabolites, and can be utilized as biocontrol agents as well as promoters of plant growth. Quorum sensing networks and biofilm forming properties are integral components for their roles in the environment. (Fazli *et al.*, 2014; Scales, Dickson, LiPuma, & Huffnagle, 2014; Silby, Winstanley, Godfrey, Levy, & Jackson, 2011)

### **1.5.1. Acyl-homoserine lactone based quorum sensing networks in *P. fluorescens***

Three homoserine lactone-based quorum sensing networks have been recognized in *P. fluorescens*. The first was the *mpuI-mpuR* system identified in *P. fluorescens* strain NCIMB 10586. This LuxIR type system regulates the biosynthesis of the polyketide antibiotic mupirocin. (El-Sayed *et al.*, 2003; El-Sayed, Hothersall, & Thomas, 2001) This antibiotic is an important combatant against methicillin-resistant *Staphylococcus aureus* (MRSA), with a mechanism of action in inhibiting isoleucyl-tRNA synthase. (El-Sayed *et al.*, 2003) The expression of the gene cluster through the MupIR quorum sensing system is regulated by binding of 3-oxodecanoyl-HSL (Figure 1.5). (Hothersall *et al.*, 2011)

The second system was identified in the biocontrol strain *P. fluorescens* F113. The only known components in this system known are the AHL synthase and the AHLs it produces. The novel AHL synthase, HdtS protein, is related to the lysophosphatidic acid acyltransferase family and can produce three AHLs, *N*-hexanoyl-HSL, *N*-(3-hydroxy-7-*cis*-tetradecenoyl)-HSL and *N*-decanoyl-HSL. (Kalia, 2015; Laue *et al.*, 2000)

Lastly is another biocontrol strain, *P. fluorescens* 2P24 and its LuxIR type quorum sensing, PcoIR. Through the synthesis of six AHLs, *P. fluorescens* 2P94 coordinates wheat root colonization, suppression of the take-all disease in wheat and antibiotic production. (Kwak & Weller, 2013; Wei & Zhang, 2006)

### **1.5.2. Biofilm formation in *P. fluorescens* Pf0-1**

The key component for biofilm formation in *P. fluorescens* Pf0-1 is the Bap protein, large adhesion protein A (LapA). This surface-associated protein facilitates the irreversible adhesion of cells to abiotic surfaces via the entire cell length, allowing the monolayer of cells to form. (Hinsa & O'Toole, 2006) The presence of both hydrophobic and hydrophilic domains on this protein allows *P. fluorescens* Pf0-1 to adhere to a wide variety of surfaces such as glass, quartz or plastics and thus colonize different environments. (Berne *et al.*, 2015)

The localization of LapA to the cell surface is mediated through phosphate levels within the environment that are sensed through the c-di-GMP signaling network. When high levels of phosphate are present, c-di-GMP synthesis is increased, allowing for its binding to the inner membrane effector protein called LapD via a degenerate EAL domain. (Hinsa & O'Toole, 2006; Newell, Boyd, Sondermann, & O'Toole, 2011) This protein then undergoes a conformational change allowing it to then sequester the protease activity of LapG. With this protease bound, it is unable to cleave the N-terminal domain of LapA that is bound to the outer membrane. Thus, the adhesion protein LapA can facilitate irreversible binding to a surface. However, once phosphate levels in the environment are depleted, the transcription of the PDE RapA is increased, decreasing intracellular levels of c-di-GMP. Without the nucleotide second messenger bound to LapD, the effector protein can no longer sequester LapG. This in turn leads to the cleavage of the N-terminus on LapA and subsequent release from the cell's surface. (Newell *et al.*, 2011)

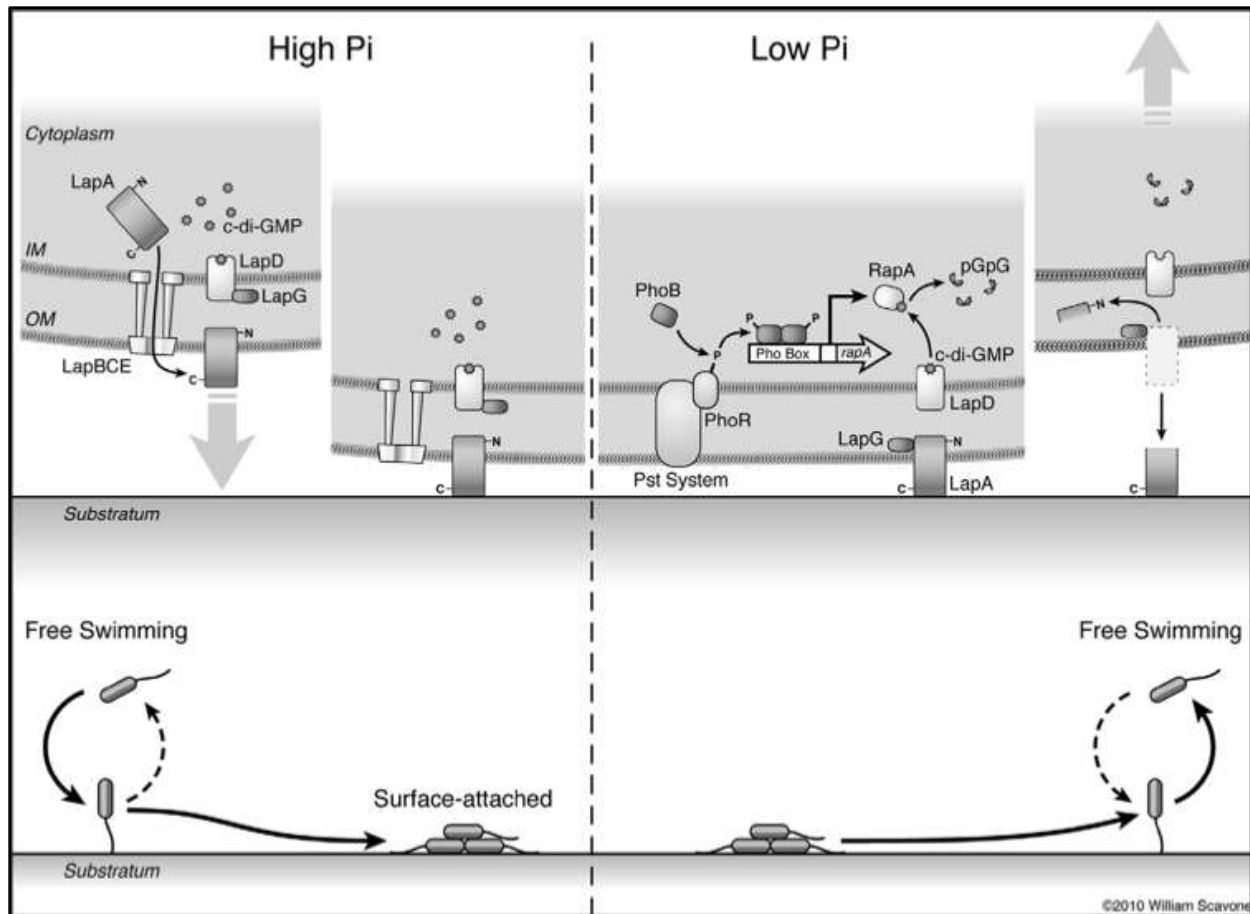


Figure 1.5. Phosphate dependent c-di-GMP regulation for biofilm formation in *P. fluorescens* Pf0-1. Image copied from Newell *et al.*, 2011 (open access).

## 1.6. Connecting c-di-GMP to quorum sensing systems in gram negative bacteria

The formation of biofilm, virulence factors and several other behaviors, have been shown to be mediated in part by intracellular levels of c-di-GMP as well as quorum sensing mechanisms in bacteria such as *P. fluorescens*, (Fazli *et al.*, 2014; Newell *et al.*, 2011; Newell, Monds, & O'Toole, 2009) *P. aeruginosa* (Fazli *et al.*, 2014; Ha & O'Toole, 2015) and *V. cholera*. (Tischler & Camilli, 2004; Waters, Lu, Rabinowitz, & Bassler, 2008) Identifying links between these networks has become more of interest to achieve a greater understanding of how bacteria respond to environmental cues and integrate this information into an overall signaling network. The connection between these two networks has been shown in several gram-negative bacteria such as *Vibrio parahaemolyticus*, *Xanthomonas campestris* and *V. cholerae*. (Srivastava & Waters, 2012)

In *Burkholderia cenocepacia*, the binding of the autoinducer *cis*-2-dodecenoic acid to GGDEF and EAL domain-containing protein RpfR induces phosphodiesterase activity to decrease intracellular levels in c-di-GMP. (Deng *et al.*, 2012; Papenfort & Bassler, 2016) Population density increases in *V. cholerae*, thus increasing autoinducer concentration, leads to downstream expression of *hapR*. The protein product of this gene then represses *vpsT* and *aphA* expression, which are transcription factors involved in c-di-GMP signaling. (Kalia *et al.*, 2013; Srivastava & Waters, 2012) Understanding where these networks overlap, could provide information about potential alternative drug targets for chronic infections regulated by these integrated complex mechanisms.

## Chapter 2: Identification of acyl-homoserine lactones produced by *P. fluorescens* Pf0-1

### 2.1. Introduction and objectives

The focus of this chapter was to identify the acyl-homoserine lactones (AHLs) that are involved in the quorum sensing network of *P. fluorescens* Pf0-1. Previous work in this laboratory has suggested the possible presence of the following three AHLs, *N*-butyryl-L-homoserine lactone, *N*-hexanoyl-L-homoserine lactone and *N*-octanoyl-L-homoserine lactone. (Bell, 2014) The evidence supporting the existence of these three AHLs was obtained through tandem mass spectrometry (MS<sup>2</sup>) and liquid-chromatography mass spectrometry (LC-MS). However, utilizing LC-MS alone to confirm the identity of these molecules can be extremely difficult. These molecules exist at low nanomolar (nM) concentrations causing their ion traces during LC-MS to become overshadowed due to background noise in the sample. (Cataldi, Bianco, Frommberger, & Schmitt-Kopplin, 2004; Zhai, Zhang, Shen, Zhou, & Liu, 2012) The ionization method used for LC-MS, electron ionization spray-mass spectrometry (ESI-MS), can also suffer from ion suppression, generating significant differences between the spectrum of a standard compound and the complex matrix of samples. (Cullum, Meng, Zavitsanos; 2004)

To increase the sensitivity and resolution of the analysis, gas-chromatography mass spectrometry (GC-MS) was used in the present study. GC is a suitable technique for volatile compounds such as lipids, flavonoids and esters. Since AHLs contain a cyclic ester moiety (lactone ring) as well as a long acyl chain component, they are compatible with GC-MS as well. (Agilent Technologies, 2009) GC-MS has been successfully used to identify AHLs in clinical samples of *P. aeruginosa* (Rani, Kumar, Malik, & Schmitt-Kopplin, 2011) as well as bacteria isolated from marine sponges. (M. W. Taylor *et al.*, 2004) The high resolution of GC also allows for a more effective separation for structurally similar molecules like AHLs. (Beškoski, Gojgić-Cvijović,

Jovančićević, & Vrvic, 2012; Cataldi *et al.*, 2004; Agilent Technologies, 2009) A DB-5ms column from Agilent was chosen because of its low stationary phase polarity, well suited for the varying acyl chain lengths in the AHLs to be analyzed. (Osorno, Castellanos, Ramos, & Arévalo, 2012)

The most common ionization source used for GC-MS analysis is electron ionization (EI). This robust and reproducible ionization source produces characteristic mass spectral fragmentation patterns without suffering from ion suppression. (Osorno *et al.*, 2012; Agilent Technologies, 2009)

The most abundant ion produced from EI fragmentation for AHLs is the ion at  $m/z$  of 143, resulting from a McLafferty rearrangement (Figure 2.1). This form of rearrangement is characteristic of carbonyl groups with a hydrogen atom in the  $\gamma$ -position. (Cataldi *et al.*, 2004; McLafferty, 1959; Osorno *et al.*, 2012; Rani *et al.*, 2011)

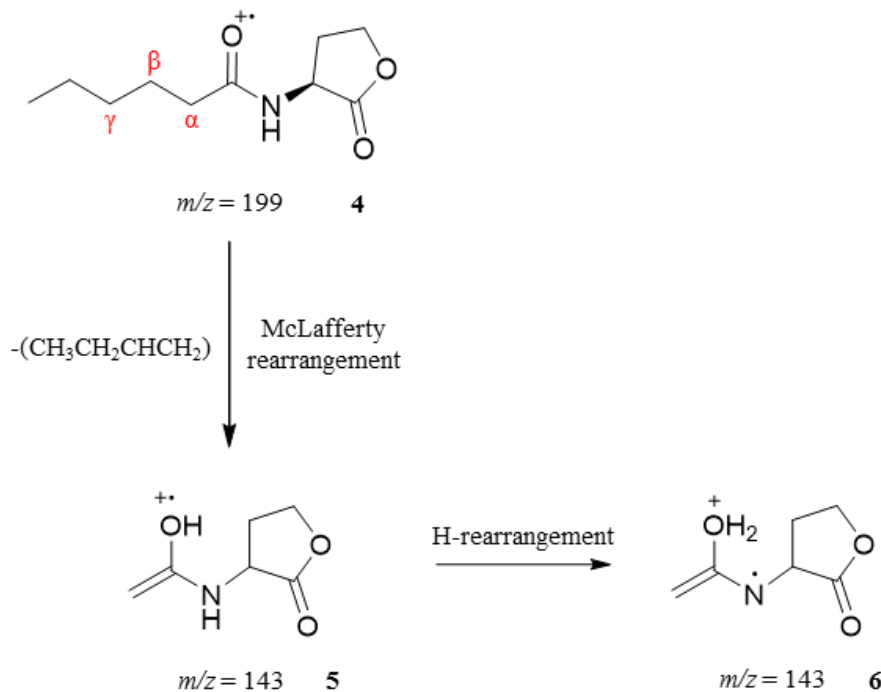


Figure 2.1. Fragmentation pattern of the radical ion at  $m/z$  199 (**4**) for *N*-hexanoyl-HSL to produce the most abundant radical ion at of  $m/z$  143 (**5** and **6**).

The  $m/z$  143 fragment radical cation **8**, along with two others **7** and **9**, all shown in Figure 2.2, were chosen as marker fragments when operating the mass detector in selected ion monitoring (SIM) mode for AHL standards. The EI fragmentation patterns and structures for the fragment

ions for *N*-hexanoyl-HSL have been previously predicted and suggested in a study performed by Cataldi *et al.* using the Mass Frontier 1.0 software from High Chem, Ltd. (Cataldi *et al.*, 2004)

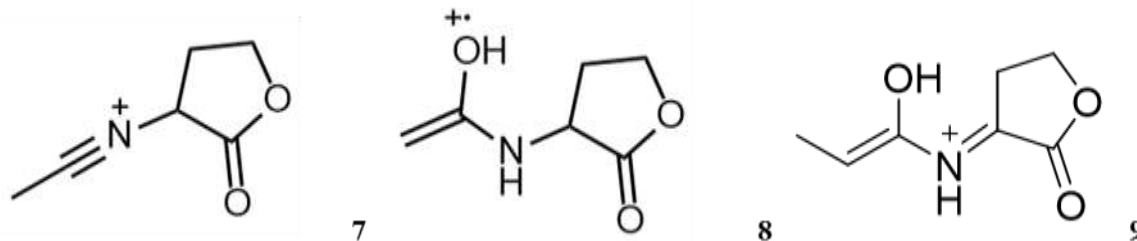


Figure 2.2. Structures of marker fragment ions at  $m/z$  of 125 **7**, 143 **8** and 156 **9**

Once the fragmentation patterns for each of the standards were identified, along with their retention times in the DB-5ms column, the same GC-MS protocol was used to identify matching chromatograms and EI-SIM mass spectra in *P. fluorescens* Pf0-1 culture supernatant extracts.

The following AHLs were investigated for their presence in *P. fluorescens* Pf0-1 culture, *N*-butyryl-L-homoserine lactone, *N*-hexanoyl-L-homoserine lactone, *N*-heptanoyl-L-homoserine lactone as well as *N*-decanoyl-L-homoserine lactone. GC-MS data of *N*-octanoyl-L-homoserine lactone standard could not be obtained at this writing due to technical issues with the GC-MS instrument. There was a sudden presence of both tailing and broadening of peaks in the chromatograms after the instrument was used to analyze derivatized samples from another GC-MS project. Residue from these derivatized samples, such as leftover derivatization reagent, within the liner or column reacted with the AHL standards. A new liner was not obtainable within the time frame of completing this project.

## **2.2. Methods and materials**

### **2.2.1. Bacterial strains and growth conditions**

The strains of *P. fluorescens* used in this study were provided by Professor George O'Toole at Dartmouth College. *P. fluorescens* wild-type strain Pf0-1 was stored as 15-25 % v/v glycerol stocks at -80 °C. Cultures were revived by streaking onto LB-Miller (LB) agar and then incubated statically at 30 °C. Overnight pre-cultures were then prepared in LB broth from single colonies of *P. fluorescens* Pf0-1 and incubated at 30 °C and 180 RPM until the required optical density for experimentation was reached.

### **2.2.2. LB-Miller (LB) media**

The following reagents were added to 950 mL of distilled water: 10.00 g bacto tryptone, 5.00 g yeast extract, 10.00 g NaCl. The pH was adjusted to  $7.00 \pm 0.10$  with NaOH and the final volume of the solution was adjusted to 1 L with distilled water. When preparing solid media, 15.00 g of agar was added after pH adjustment. Liquid media were sterilized by autoclaving at 121 °C with a 30 min sterilization cycle, then stored in the dark at room temperature until use.

### **2.2.3. UV/vis Spectrophotometric measurements**

Bacterial culture growth was monitored by UV spectrophotometric measurements at 600 nm and carried out on a ThermoScientific Genesys 10S UV-Vis spectrometer.

### **2.2.4. Extraction of acyl-homoserine lactones from *P. fluorescens* Pf0-1 cultures**

Overnight pre-cultures of *P. fluorescens* Pf0-1 were subcultured 1:100 into LB media. 250 mL Cultures were incubated at 30 °C at 180 RPM for sampling. At different phases of growth, 50 mL samples were taken from the growing culture and aliquoted into Falcon tubes. The samples were then centrifuged at 4700 RPM for 60 min or until a clear supernatant was generated. The supernatant was then pipetted into a new container and flash frozen in liquid nitrogen for

lyophilizing overnight using the Labcono FreeZone 4.5. The remaining pellet from lyophilisation was then reconstituted in 2 mL of distilled water and extracted with 500  $\mu$ L of chloroform at a 1:1 ratio. The mixture was inverted and swirled gently to mix the solution without generating emulsions. A total of three rounds of liquid-liquid extractions were performed before combining the organic extracts. Once the chloroform had been removed under a gentle stream of air, the final pellet was re-suspended into HPLC grade acetonitrile (ACN). The homogenous solution was then aliquoted into several smaller vials and solvent was again removed under a gentle stream of air. The dry material was stored at -20 °C until GC-MS analysis.

#### **2.2.5. Acyl-homoserine lactones storage conditions**

Acyl-homoserine lactone standards were purchased from Cayman chemicals as 1 mg or 5 mg dry weight stocks. For long-term storage, the AHLs were solubilized in HPLC grade ACN and volumes containing 100  $\mu$ g were aliquoted into vials. The solutions were then flash frozen for lyophilisation using the Labcono FreeZone 4 and the resulting pellet was stored in a -20 °C freezer.

#### **2.2.6. GC-MS analysis of acyl-homoserine lactone standards and bacterial culture extracts**

Analyses were performed on a ThermoFisher Scientific Trace 1310 Gas Chromatograph system connected to a DFS High Resolution Magnetic Sector Mass Spectrometer. An Agilent DB-5ms capillary column (Part No. 122-5532G) was used for sample separation, 0.25 mm (I.D.) and 30 m length, coated with 0.25  $\mu$ m film thickness of phenyl arylene polymer. Samples (1  $\mu$ L) were injected into the column at a split flow of 5 mL/min and a solvent delay of 4 min. The GC inlet and transfer line temperatures were set to 280 °C. The GC carrier gas used was pure helium at a flow rate of 1.00 mL/min. The GC oven temperature program is as follows: An initial temperature was set to hold at 150 °C for 3.00 min followed by an increase in temperature at a rate of 15.0 °C/min until a temperature of 275 °C was reached. The temperature was held at 275 °C for 2.00

min after which another temperature ramp was performed at 55 °C/min until a final temperature of 300 °C was reached. The oven program was later adjusted to separate the *N*-heptanoyl-HSL standard from a coeluting compound in the *P. fluorescens* Pf0-1 cell extracts. To achieve this separation, the temperature ramp was decreased from 15 °C/min to 2.5 °C/min from 150 °C until a temperature of 190 °C was reached. The mass spectrometer was operated in selected ion monitoring (SIM) mode for  $m/z$  125, 143 and 156. The electron ionization (EI) source was set to 70 eV with an emission current of 1 mA and source temperature of 220 °C.

## 2.3. Results

### 2.3.1 GC chromatogram and EI-MS fragmentation library of HSL standards

Acyl-homoserine lactone standards were purchased from Cayman Chemicals to prepare the library of GC chromatograms and EI-SIM-MS spectra. Standard solutions were prepared in HPLC grade MeOH to a concentration of 0.1 ng/ $\mu$ L. The AHLs investigated for this study by GC-MS are summarized below in Table 2.1 with their respective retention times in gas-chromatography. Each of these compounds contains varying lengths of the R group acyl chain without further modifications, such as saturation or oxidation.

Table 2.1. Acyl-homoserine lactones under investigation

Acyl-homoserine lactone (AHL)	Acronym	Molecular ion [M] <sup>+</sup>	Retention time (min)
<i>N</i> -butyryl-L-homoserine lactone	<i>N</i> -butyryl-HSL	171	5.77
<i>N</i> -hexanoyl-L-homoserine lactone	<i>N</i> -hexanoyl-HSL	199	7.54
<i>N</i> -heptanoyl-L-homoserine lactone	<i>N</i> -heptanoyl-HSL	213	8.38
<i>N</i> -decanoyl-L-homoserine lactone	<i>N</i> -decanoyl-HSL	255	10.62

As observed in the multiple ion detection (MID) MS spectra for each of the standards studied, as highlighted in Figure 2.3 for *N*-hexanoyl-HSL, the most abundant fragment ion is at  $m/z$  of 143, accompanied by the lower intensity fragment ions at  $m/z$  of 125 and 156. The chromatograms and subsequent MID MS spectra for each standard studied can be found in the Appendix (Figures A1-A5). The relative peak ratios were then compared with MID MS spectra of cell extracts to identify AHLs of interest.

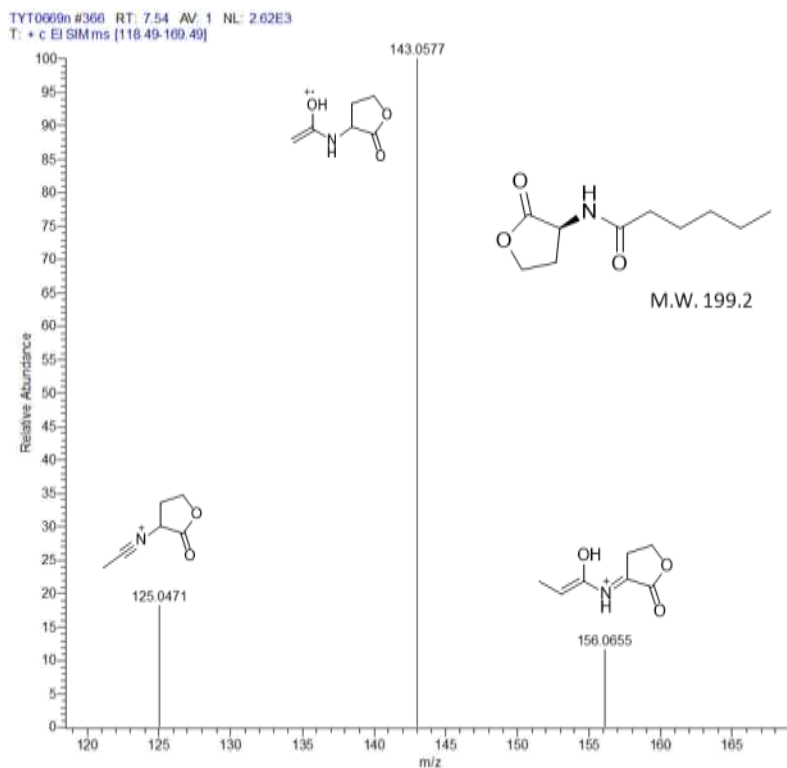


Figure 2.3. High-resolution MID spectra of *N*-hexanoyl-HSL standard. EI-SIM mode was performed for *m/z* fragment ions of 125, 143 and 156.

### 2.3.2. GC-MS analysis of *P. fluorescens* Pf0-1 culture supernatant extracts

The *P. fluorescens* Pf0-1 supernatant chloroform extract submitted for GC-MS analysis originated from a culture grown in LB broth to an O.D<sub>600</sub> of 1.382, representing late exponential growth for this bacterial species. The high cell density present in the medium at this point in the growth curve should generate an increased concentration of autoinducers in the surrounding environment. (Hagen, 2015) The resulting chromatograms were scanned for peaks that eluted near the retention times of the standard AHLs. The high-resolution MID spectrum for each suspect peak was then analyzed for fragmentation patterns characteristic of AHLs.

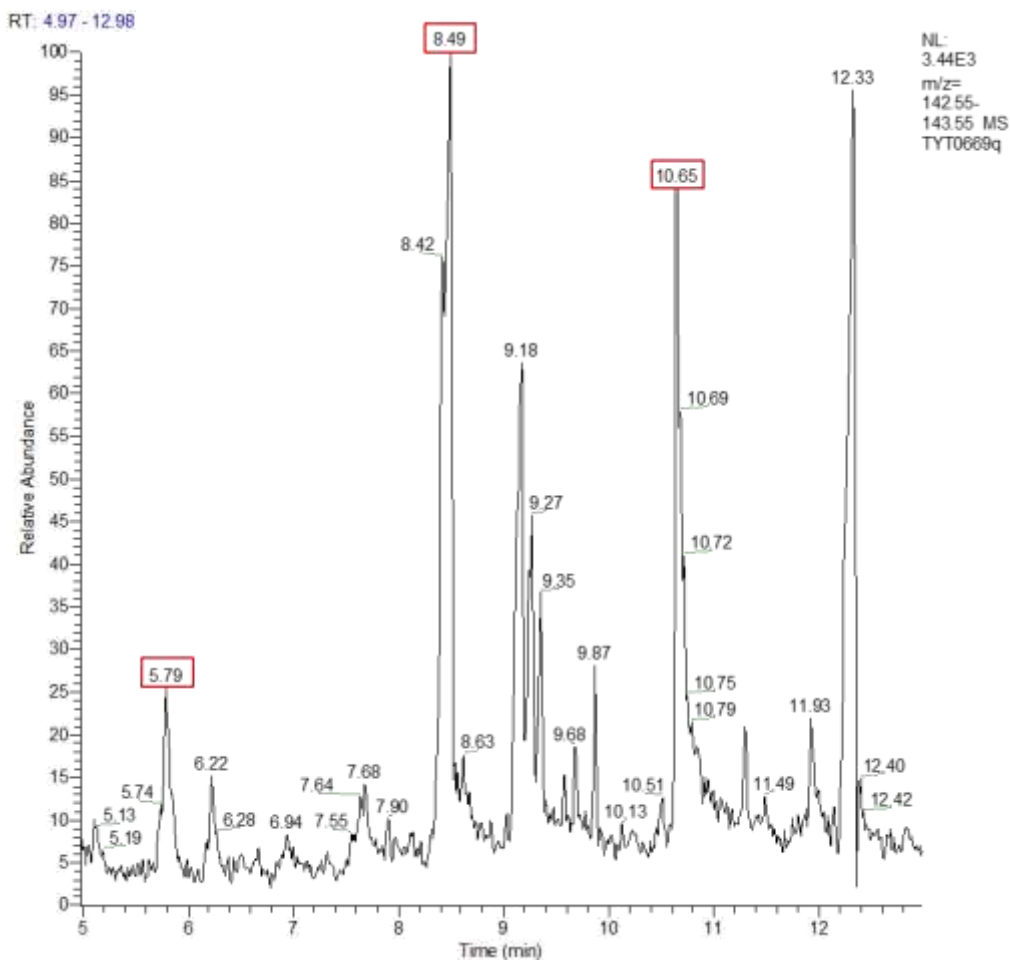


Figure 2.4. EIC for  $m/z$  fragment ion of 143 in chloroform extract of *P. fluorescens* Pf0-1 supernatant. Sample was dissolved in HPLC grade MeOH. Highlighted peaks correspond to retention times close to that of AHL standards.

The chromatogram in Figure 2.4 displays the extracted ion chromatogram (EIC) at an  $m/z$  of 143 for the supernatant extract. In this chromatogram, high intensity peaks were observed near the retention times of the standards for *N*-butyryl-HSL (5.79 min) and *N*-decanoyl-HSL (10.65 min). The slight shift in retention time for these two AHLs can be attributed to the complex matrix of the sample affecting their retention in the column. A much larger shift in retention time was observed for what could be potentially identified as *N*-heptanoyl-HSL eluting at 8.49 min, with an unknown compound co-eluting at 8.42 min. There was no major peak observed near the retention time of standard *N*-hexanoyl-HSL.

Table 2.2. Retention time comparison between AHL standards and peaks observed in the *P. fluorescens* Pf0-1 extract sample chromatogram.

Acyl-homoserine lactone (AHL)	Retention time (min) of AHL in MeOH	Retention time (min) of suspected AHL in supernatant extract
<i>N</i> -butyryl-HSL	5.77	5.79
<i>N</i> -hexanoyl-HSL	7.54	N/A <sup>a</sup>
<i>N</i> -heptanoyl-HSL	8.38	8.49
<i>N</i> -decanoyl-HSL	10.62	10.65

<sup>a</sup> Peak was not observed around the retention time of *N*-hexanoyl-HSL

Subsequent EI-SIM MS analysis of the supernatant extract produced MID spectra showing characteristic peak ratios for AHLs near the retention times of *N*-butyryl-HSL and *N*-decanoyl-HSL (Figures 2.6 and 2.7 respectively). The matching relative peak ratios for AHL *m/z* fragments 125, 143 and 156, at retention times close to standard AHL elution times, suggested the presence of these two compounds in the supernatant of *P. fluorescens* Pf0-1.

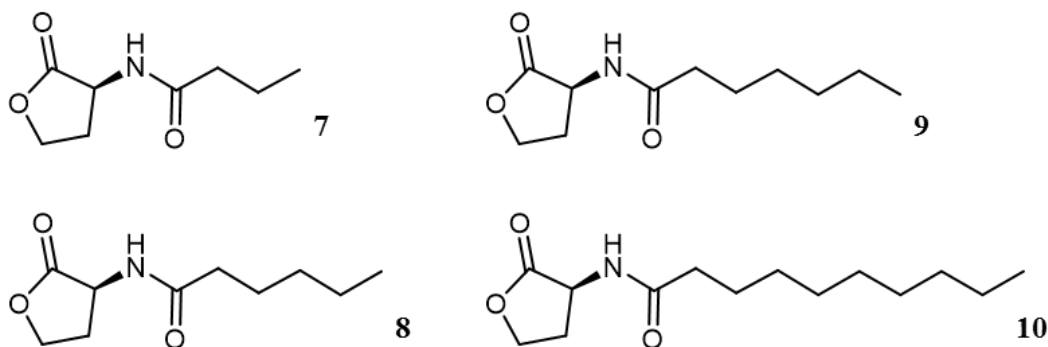


Figure 2.5. Acyl-homoserine lactones under investigation by GC-MS for their presence in *P. fluorescens* supernatant. *N*-butyryl-HSL **7** *N*-hexanoyl-HSL **8** *N*-heptanoyl-HSL **9** *N*-decanoyl-HSL **10**

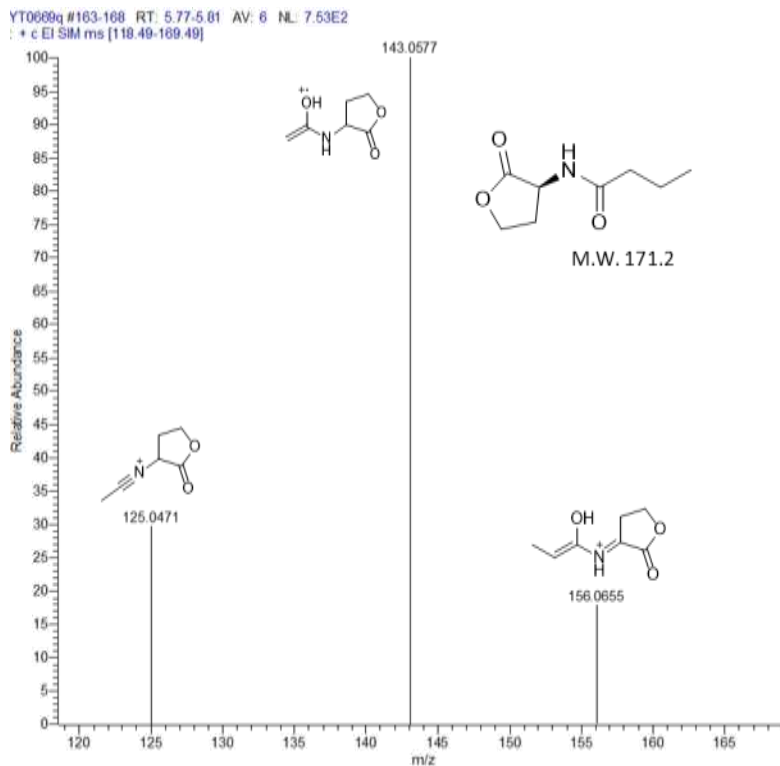


Figure 2.6. High-resolution MID spectra of possible *N*-butryl-HSL found in the chloroform extract of *P. fluorescens* Pf0-1 supernatant. EI-SIM mode was performed for *m/z* fragment ions of 125, 143 and 156.

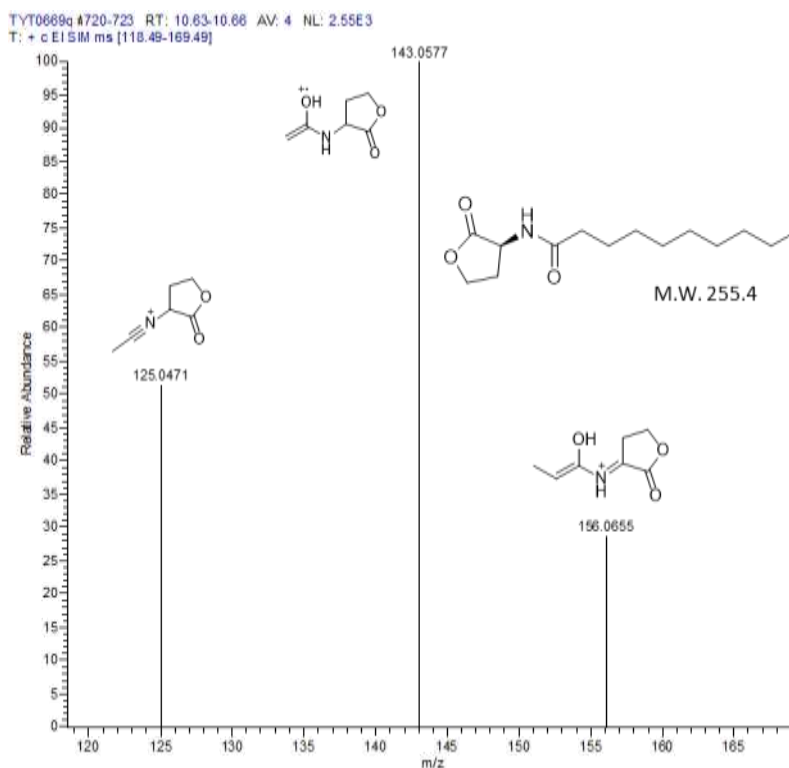


Figure 2.7. High-resolution MID spectra of possible *N*-decanoyl-HSL found in the chloroform extract of *P. fluorescens* Pf0-1 supernatant. EI-SIM mode was performed for *m/z* fragment ions of 125, 143 and 156.

Upon examination of the MID spectra for the retention time between 8.38 and 8.52 min, it was clear that the relative peak ratios did not correspond to those of AHLs (Figure 2.8). The peak of highest abundance was for a fragment ion  $m/z$  of 125 as opposed to the AHL characteristic  $m/z$  fragment ion of 143. Therefore, this data suggested the absence of *N*-heptanoyl-HSL in *P. fluorescens* culture supernatant.

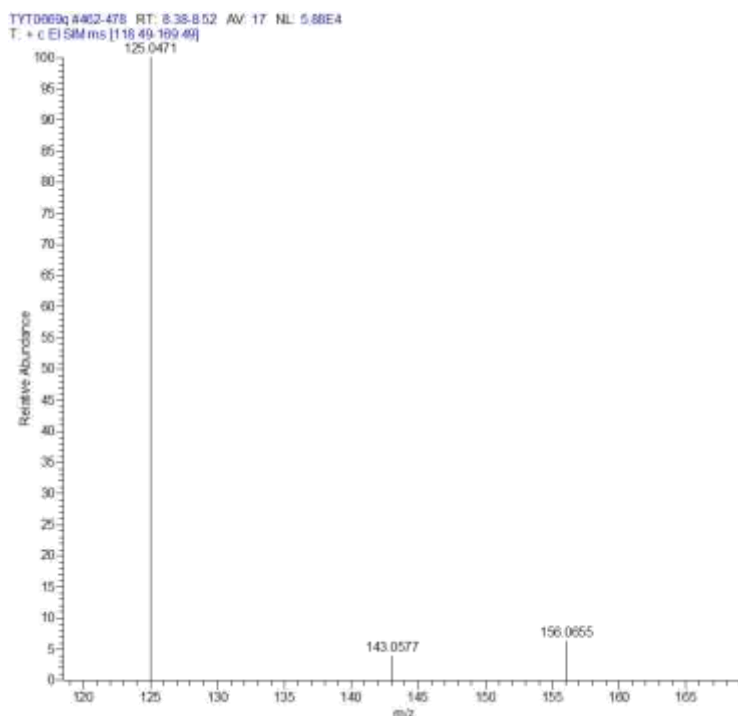


Figure 2.8. High-resolution MID spectra of possible *N*-heptanoyl-HSL found in the chloroform extract of *P. fluorescens* Pf0-1 supernatant. EI-SIM mode was performed for  $m/z$  fragment ions of 125, 143 and 156.

The suppression of the 143  $m/z$  ion was suspected to have potentially resulted from the co-eluting species at 8.42 min. These peaks were further investigated through spiking experiments to first confirm a shift in retention time for *N*-heptanoyl-HSL standard in the sample and second, determine if the peak observed at 8.49 min belonged to *N*-heptanoyl-HSL.

### 2.3.3. GC-MS analysis of *P. fluorescens* Pf0-1 culture supernatant extracts spiked with 0.1 ng/ $\mu$ L of standard AHL

To provide supporting evidence for the existence or absence of the AHLs under investigation, a series of spiking experiments were performed where the supernatant extract of *P.*

*fluorescens* Pf0-1 culture was spiked with 0.1 ng/μL of the standard AHLs in MeOH. The retention times of peaks with increased intensity due to the presence of the standard, along with corresponding high-resolution MID spectra generated from EI-SIM MS analysis, were compared to the data obtained from the standard AHLs.

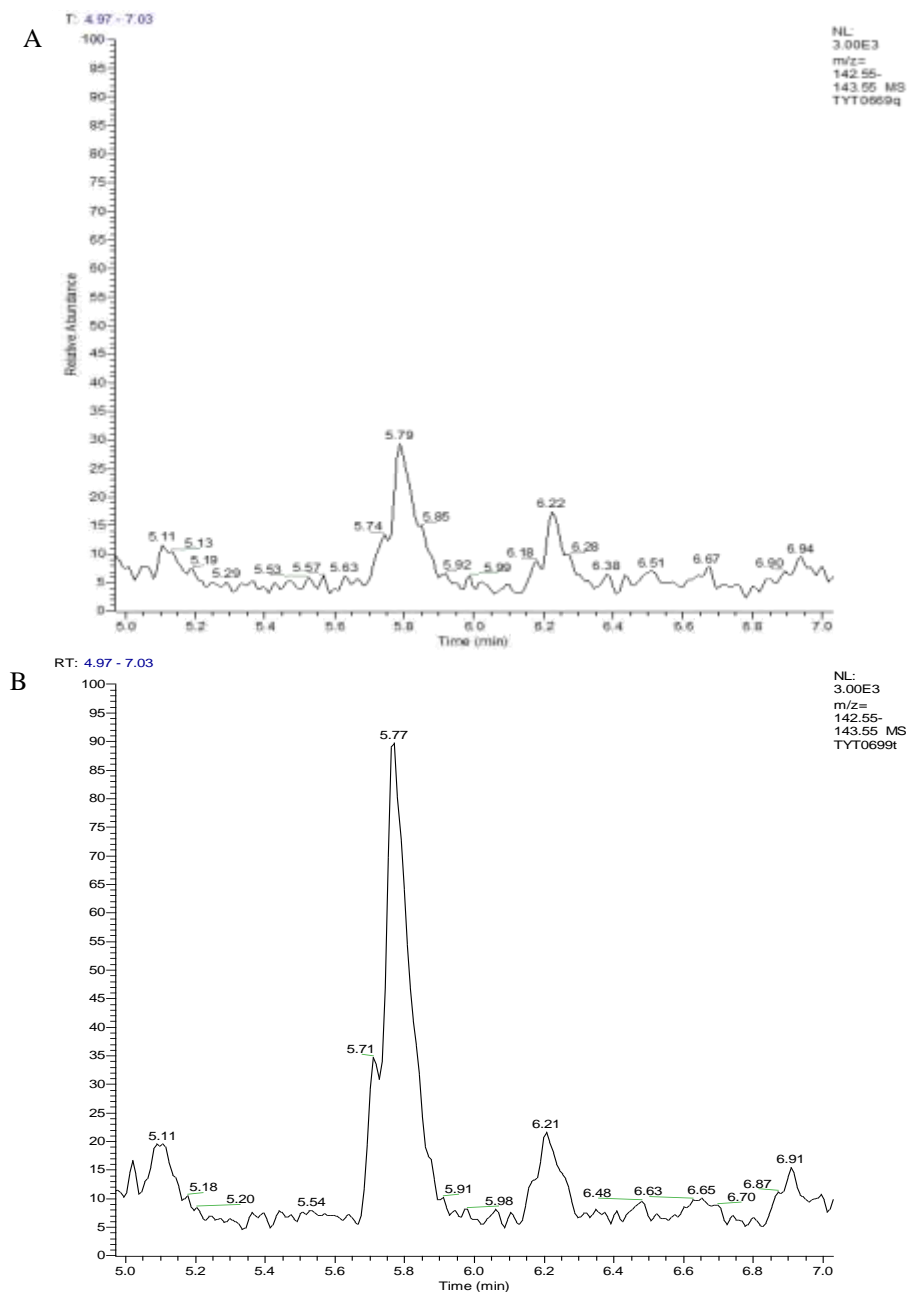


Figure 2.9. EIC for  $m/z$  fragment ion of 143 in AHL spiked-chloroform extract of *P. fluorescens* Pf0-1 supernatant from 4.97 – 7.03 min. (A) Supernatant extract dissolved in HPLC grade MeOH. (B) Supernatant extract dissolved in HPLC grade MeOH spiked with 0.1 ng/μL *N*-butyryl-HSL.

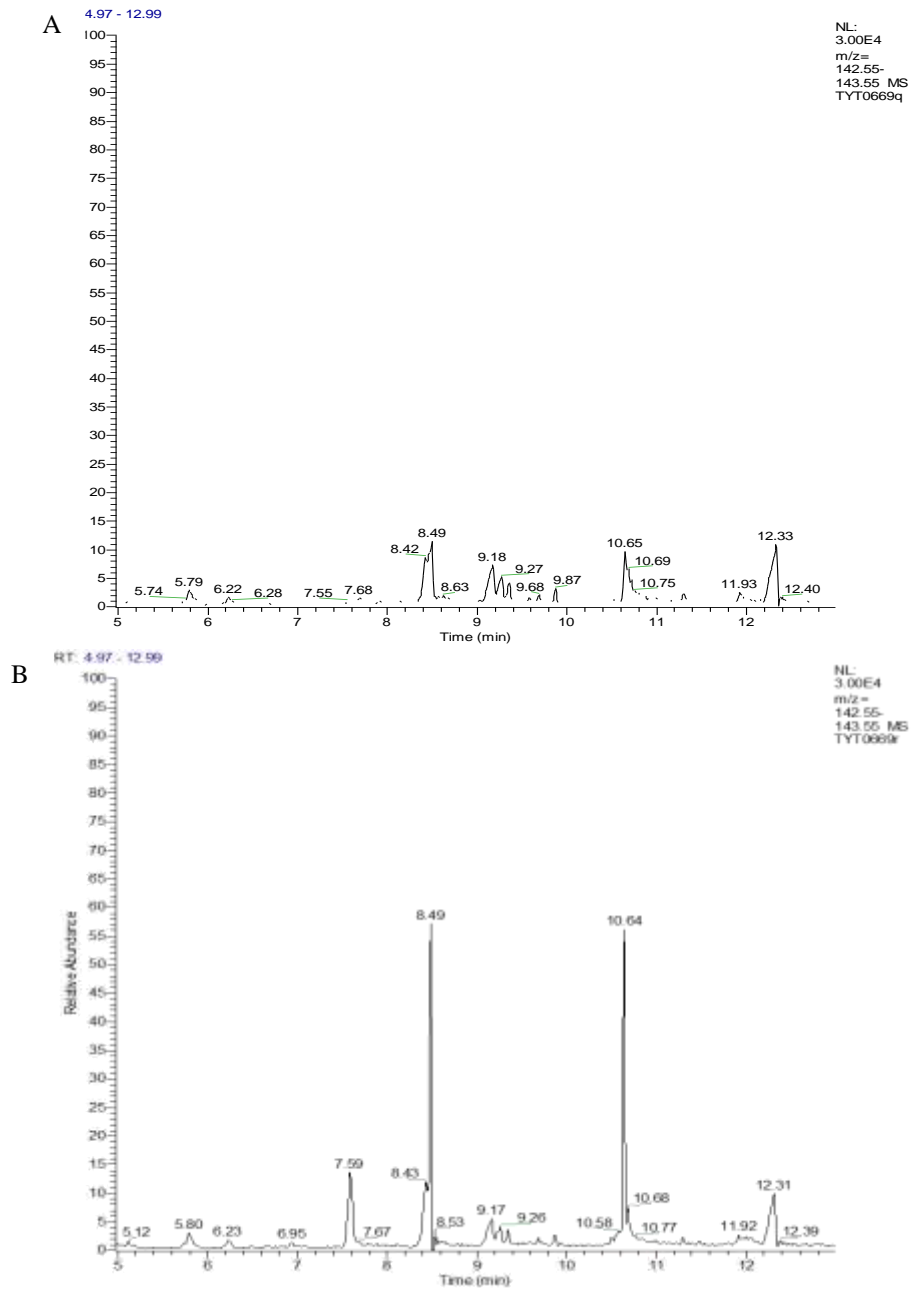


Figure 2.10. EIC for  $m/z$  fragment ion of 143 in AHL-spiked chloroform extract of *P. fluorescens* Pf0-1 supernatant from 4.97 – 12.99 min. (A) Supernatant extract dissolved in HPLC grade MeOH. (B) Supernatant extract dissolved in HPLC grade MeOH spiked with 0.1 ng/ $\mu$ L of the following standards; *N*-hexanoyl-HS, *N*-heptanoyl-HSL, *N*-decanoyl-HSL.

After spiking the supernatant extract with 0.1 ng/ $\mu$ L *N*-butyryl-HSL, an increase in a peak with the retention time of 5.77 min was observed (Figure 2.9), a slight shift in the retention time in comparison to the sample prior to spiking (5.79 min). The high-resolution MID spectra of the

peak in the spiked supernatant extract (Figure 2.11) generated a ratio of fragment ions matching the ratio observed for the standard *N*-butyryl-HSL MID spectra, with the most abundant *m/z* fragment ion of 143. The relatively close retention times between the two samples, with the high-resolution MID spectra provided high confidence in the presence of *N*-butyryl-HSL in the supernatant of *P. fluorescens* Pf0-1.

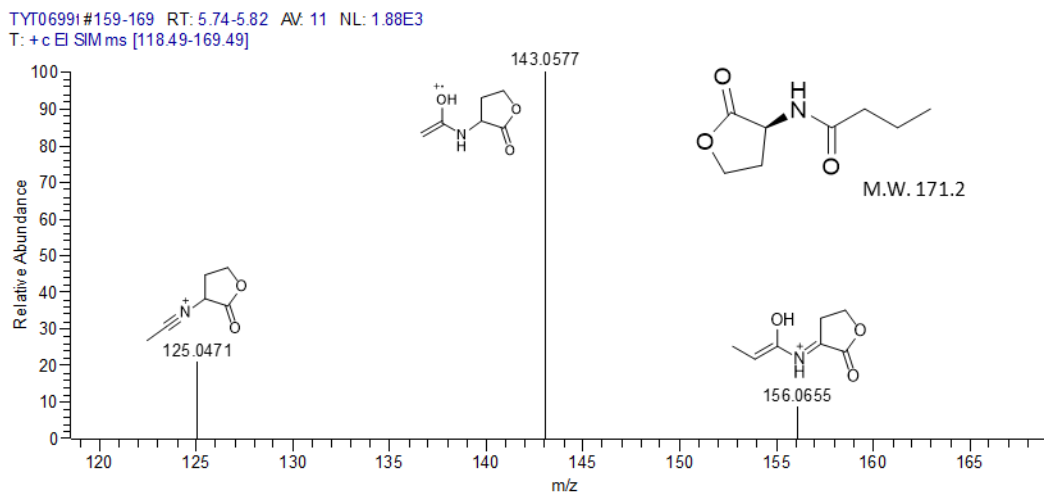


Figure 2.11. High-resolution MID spectra for AHL-spiked chloroform extract of *P. fluorescens* Pf0-1 supernatant at retention time frame of 5.74 – 5.82 min. Sample was spiked with 0.1 ng/ $\mu$ L *N*-butyryl-HSL. EI-SIM mode was performed for *m/z* fragment ions of 125, 143 and 156.

The same spiking experiment was also performed for standard AHLs *N*-hexanoyl-HSL, *N*-heptanoyl-HSL and *N*-decanoyl-HSL. The addition of these standard AHLs to the supernatant extract resulted in an increase in intensity for peaks at retention times 7.59 min, 8.49 min and 10.64 min as highlighted in Figure 2.10B. In the non-spiked supernatant extract, there was no peak observed near 7.59 min (Figure 2.10A) corresponding to the retention time of the *N*-hexanoyl-HSL standard when spiked to a concentration of 0.1 ng/ $\mu$ L in the supernatant extract as shown in Figure 2.10B. This provided further confidence in the absence of this AHL in the supernatant of *P. fluorescens* Pf0-1.

Upon addition of 0.1 ng/ $\mu$ L *N*-decanoyl-HSL to the supernatant extract there was also an increase observed in peak intensity at the retention time of 10.64 min, with only 0.01 min

difference to the peak suspected to belong to this AHL in the non-spiked supernatant extract (Figures 2.10A and 2.4 respectively). The high-resolution MID spectra of this peak further provided confidence in the presence of *N*-decanoyl-HSL, with the ratio of fragment ions matching that of the standard (Figure 2.12).

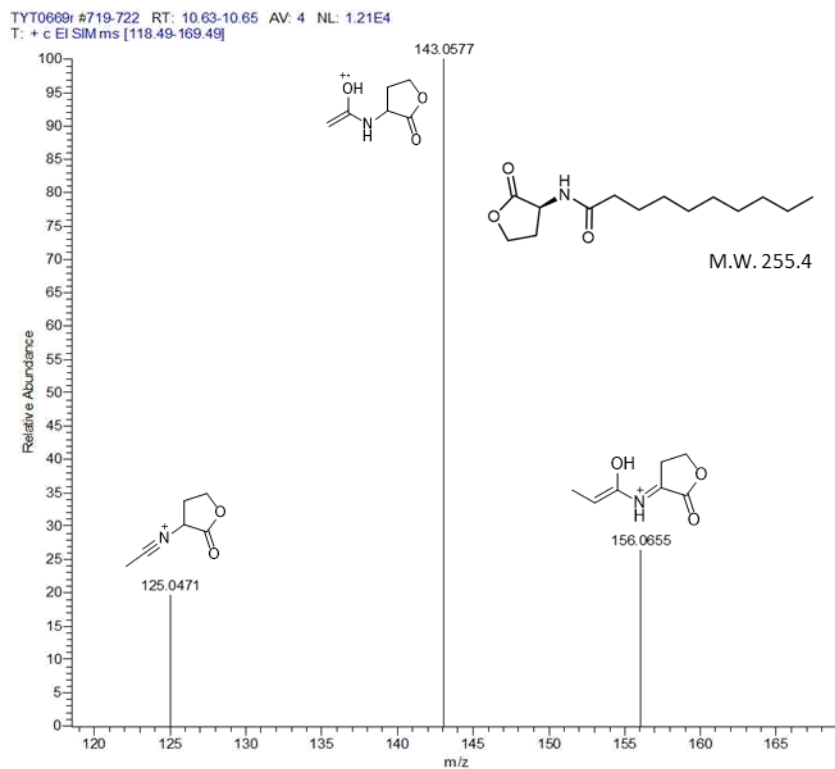


Figure 2.12. High-resolution MID spectra for AHL-spiked chloroform extract of *P. fluorescens* Pf0-1 supernatant at retention time frame of 10.63 – 10.66 min. Sample was spiked with 0.1 ng/ $\mu$ L *N*-decanoyl-HSL. EI-SIM mode was performed for *m/z* fragment ions of 125, 143 and 156.

When the supernatant extract was spiked with 0.1 ng/ $\mu$ L of *N*-heptanoyl-HSL an increase in peak intensity was observed at the retention time of 8.49 min. A subsequent spiking experiment was performed by increasing the concentration of standard to 1 ng/ $\mu$ L, further increasing the peak intensity at 8.49 min (See Appendix Figure A-10). With this information, it can be concluded that the retention time of *N*-heptanoyl-HSL compound was shifted in the supernatant extract. However, analysis of the high-resolution MID spectra near that retention time, shows a different ratio for the

$m/z$  fragment ions 125, 143 and 156. The most abundant  $m/z$  fragment ion was still an  $m/z$  of 125, as seen previously in the non-spiked supernatant extract (Figures 2.13 and 2.8 respectively).

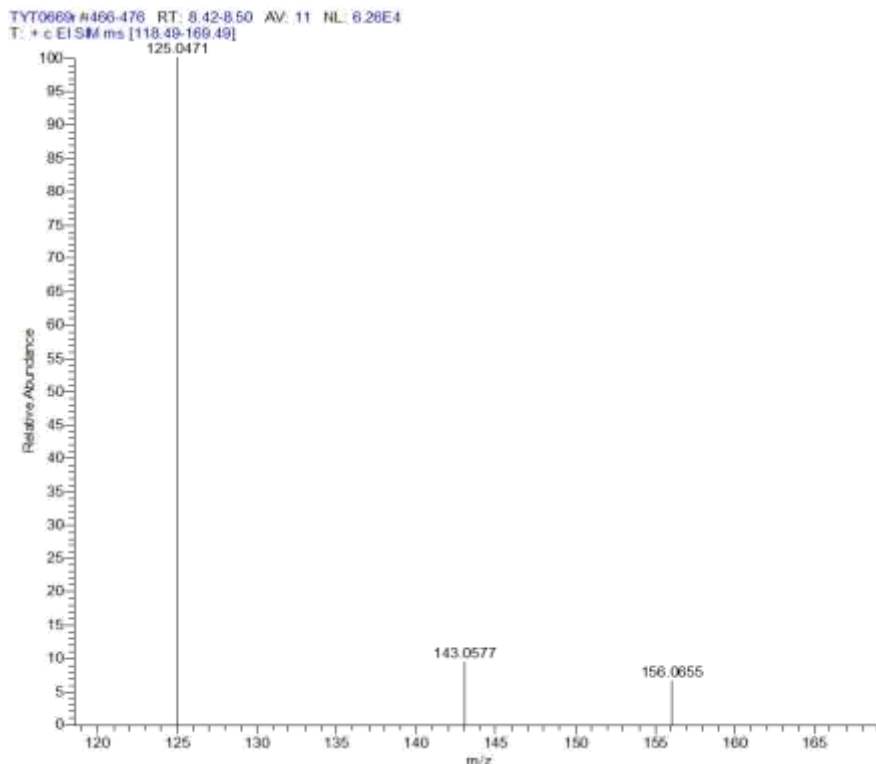
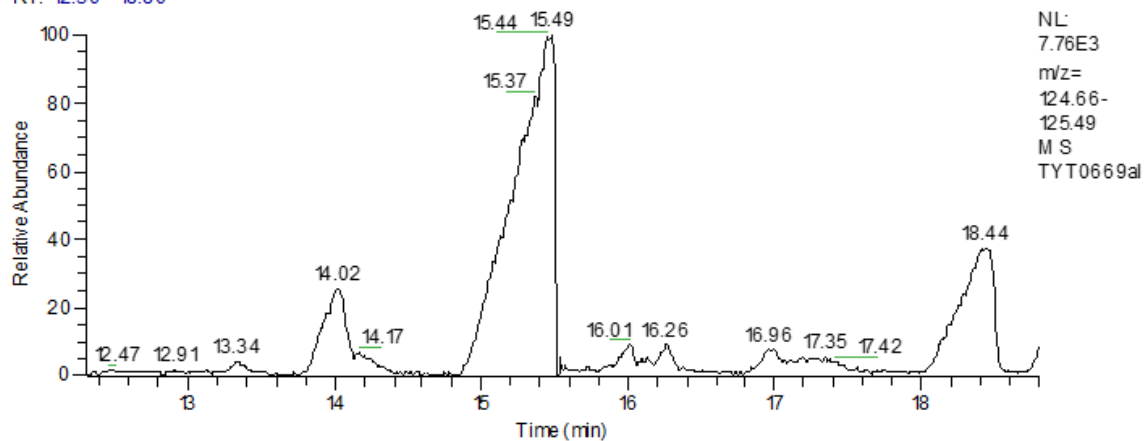


Figure 2.13. High-resolution MID spectra for AHL-spiked chloroform extract of *P. fluorescens* Pf0-1 supernatant at retention time frame of 8.42 – 8.50 min. Sample was spiked with 0.1 ng/ $\mu$ L *N*-heptanoyl-HSL. EI-SIM mode was performed on  $m/z$  fragment ions of 125, 143 and 156.

The suppression of the  $m/z$  fragment ion 143 as well as the increase in retention time can be attributed to a combination of the sample's matrix as well as co-eluting species at 8.42 min. Depending on the chemical nature of the species at 8.42 min, interactions with the standard *N*-heptanoyl-HSL when added to the sample can result in an increased retention within the column. To increase the separation of the peaks at 8.42 min and 8.49 min the oven program was adjusted to a slower rate of temperature increase per minute as noted in Methods Section 2.2.6.

A RT: 12.30 - 18.80



B RT: 12.30 - 18.80

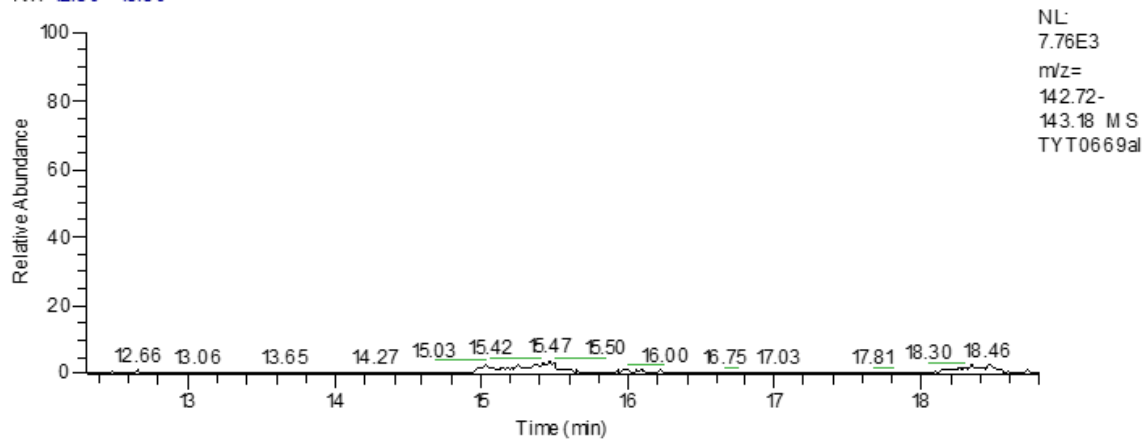
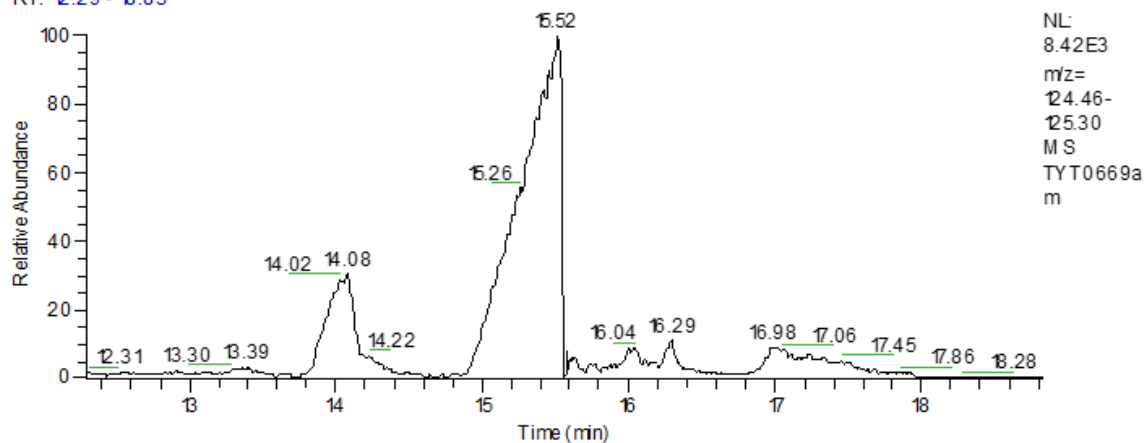


Figure 2.14. EIC for  $m/z$  fragment ion of (A) 125 and (B) 143 in chloroform extract of *P. fluorescens* Pf0-1 supernatant after oven program adjustment. Supernatant extract dissolved in HPLC grade MeOH. Temperature ramp was decreased to 2.5 °C/min

A RT: 12.29 - 18.83



B RT: 12.02 - 18.83

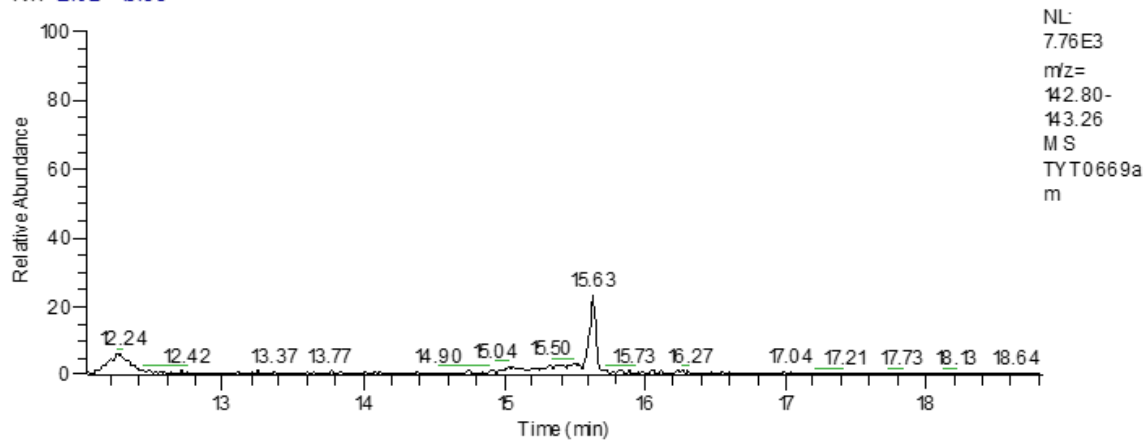


Figure 2.15. EIC for  $m/z$  fragment ion of (A) 125 and (B) 143 in chloroform extract of *P. fluorescens* Pf0-1 supernatant dissolved in HPLC grade MeOH and spiked with 0.1 ng/ $\mu$ L of *N*-heptanoyl-HSL. Temperature ramp was decreased to 2.5  $^{\circ}$ C/min

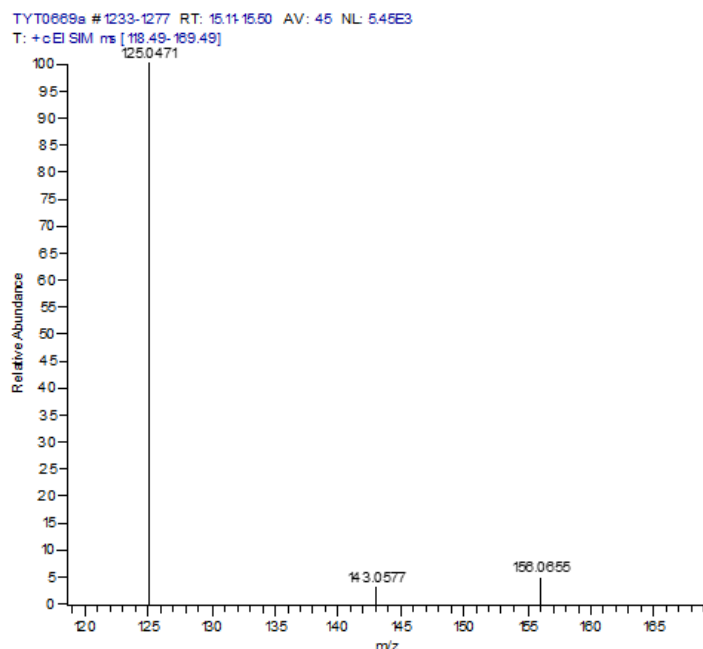


Figure 2.16. High-resolution MID spectrum for chloroform extract of *P. fluorescens* Pf0-1 supernatant at retention time of 15.62 min for the chromatogram in Fig. 2.14A. EI-SIM mode was performed for  $m/z$  fragment ions of 125, 143 and 156.

After decreasing the temperature ramp, the peaks at 8.42 min and 8.49 min in the *P. fluorescens* Pf0-1 supernatant extract were eluted between 15.03 and 15.50 min (Figure 2.14A). The high-resolution MID spectra for this region exhibited a high abundant  $m/z$  fragment ion of 125 as seen prior to the oven program adjustment. (Figure 2.16) The EIC chromatogram for the  $m/z$  fragment ion 143 exhibited no major peaks eluting between 15.03 and 15.50 min (Figure 2.14B).

Spiking the supernatant extract with 0.1 ng/ $\mu$ L of *N*-heptanoyl-HSL standard resulted in a 0.11 min difference in elution time between the previously co-eluting species and the *N*-heptanoyl-HSL standard within the supernatant extract. The *N*-heptanoyl-HSL standard gave rise to a distinct peak eluting at 15.63 min in the EIC chromatogram for the  $m/z$  fragment ion 143 (Figure 2.15B). The ratio of the  $m/z$  fragment ions at 15.63 min corresponded to the ratio observed for the standard *N*-heptanoyl-HSL (Figure 2.17B). As observed in the EIC chromatogram for the  $m/z$  fragment ion 143 in the non-spiked supernatant, there is no major peak at this retention time. The previously co-eluting species was seen eluting at 15.52 min in the

spiked supernatant sample (Figure 2.15A), with a high-resolution MID spectrum that was not characteristic of AHLs, containing a high abundant  $m/z$  fragment ion of 125 (Figure 2.17A).

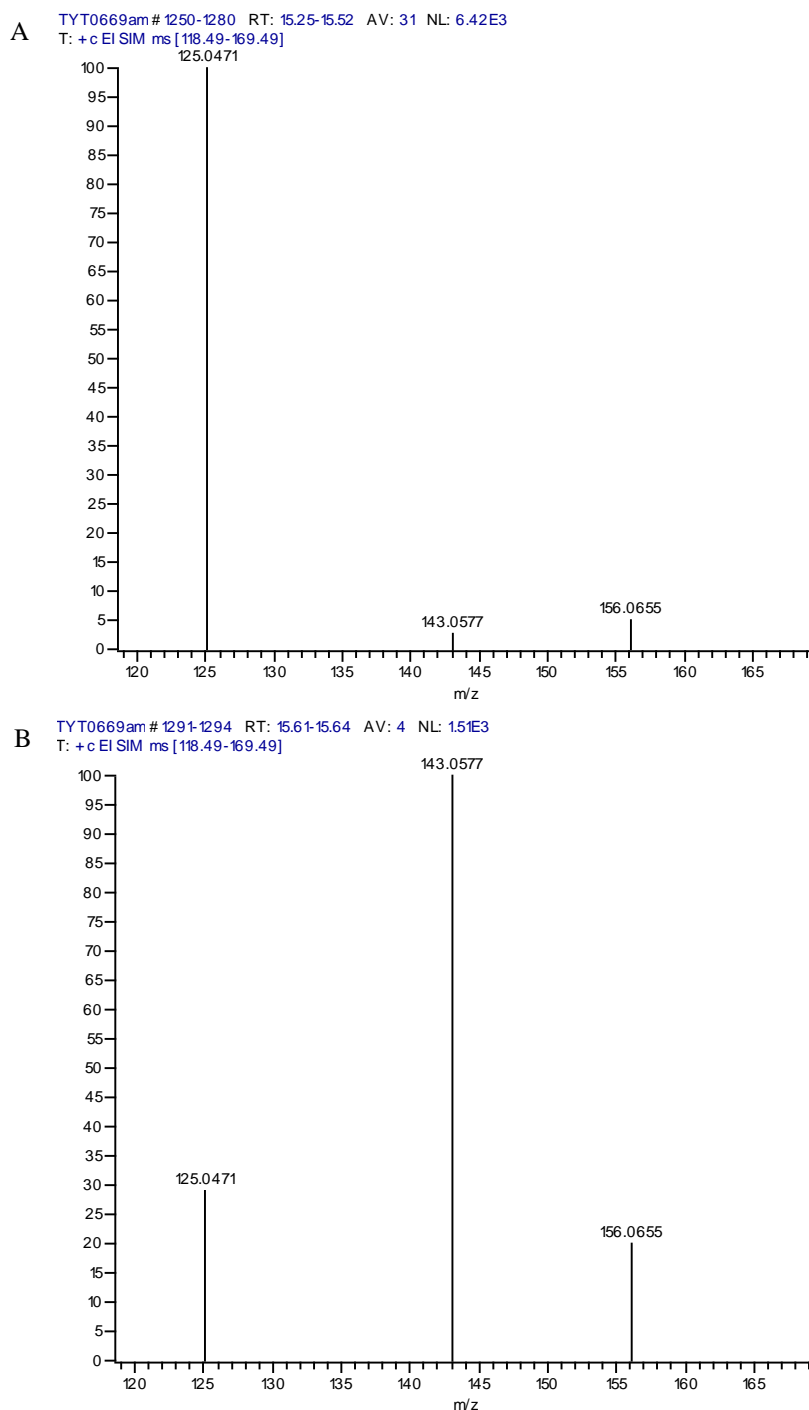


Figure 2.17. High-resolution MID spectra for AHL-spiked chloroform extract of *P. fluorescens* Pf0-1 supernatant. EI-SIM mode was performed for  $m/z$  fragment ions of 125, 143 and 156. (A) Retention time of 15.62 min for the chromatogram in Fig. 2.15A. (B) Retention time of 15.63 min for the chromatogram in Fig. 2.15B.

#### 2.4. Concluding remarks and future works

The identification of *N*-decanoyl-HSL in the supernatant of *P. fluorescens* Pf0-1 is in agreement with the LC-MS/MS findings of a study performed by Zhao *et al.* last year. (Zhao, Zhu, Ye, Ge, & Li, 2016) The data presented in this thesis provides the first evidence of *N*-butyryl-HSL in the supernatant of *P. fluorescens* Pf0-1. The data presented also suggests an absence of the *N*-hexanoyl-HSL and *N*-heptanoyl-HSL in the supernatant of *P. fluorescens* Pf0-1.

Future work will focus on the identification of longer chain AHLs in the supernatant of *P. fluorescens* Pf0-1 cultures grown in LB medium, as well as other environments, to expand on the possible AHLs participating in the quorum sensing network of this microorganism. The identified AHLs will then be added to growing cultures of *P. fluorescens* Pf0-1 to monitor potential changes in the intracellular levels of c-di-GMP by LC-MS/MS. Changes in the concentration for this nucleotide second messenger would provide preliminary evidence for the connection between these two signaling mechanisms in *P. fluorescens* Pf0-1.

## Chapter 3: Troubleshooting biofilm formation in *P. fluorescens* Pf0-1

### 3.1. Introduction and objectives

To initiate the transition from a motile to sessile state of bacterial phenotype, several factors are involved as summarized in Section 1.1. However, when culturing biofilms *in vitro*, replicating biofilm assays from one lab to another can be challenging due to the difference in equipment, materials, as well as protocol execution that can affect the experimental outcome. Inducing the biofilm phenotype can also be difficult due to the lab cultivation of bacteria. (Hufnagel, Depas, & Chapman, 2015) Therefore, small changes that occur within a biofilm assay protocol can result in the reduction of or complete inability of a biofilm to form.

The use of microtiter plates as the platform for static biofilm experiments allows the assessment of microbial attachment onto an abiotic surface. It is a useful method to perform high-throughput screenings of multiple bacterial strains under different growth conditions and analysis of genetic mutants. Although the batch-grown conditions of this platform do not support the formation of mature biofilms obtained in flow cell systems, they are capable of developing properties related to antibiotic tolerance and immune system effector resistance. (O'Toole, 2011)

Prior to this thesis, successful microtiter plate biofilm studies were performed utilizing Fisherbrand™ flat-bottom 96-well polystyrene plates (catalog No. 12-565-501) with *P. fluorescens* Pf0-1 as a model microorganism. Optimal levels of biofilm were reached after an incubation period 8 hrs at 30°C. The biomass of biofilm produced was then quantified by solubilizing the dye in acetic acid to measure the absorbance at 600 nm. *P. fluorescens* Pf0-1 produced solid rings of biofilm at the air-liquid interface, generating an average crystal violet absorbance ranging from an absorbance of 0.380 to as high as 0.800. (Bordeleau, 2014)



Figure 3.1. Crystal violet stained *P. fluorescens* Pf0-1 on a non-treated polystyrene surface. Figure reproduced from Bordeleau, 2014.

After completion of the previous project, subsequent attempts to reproduce the results were unsuccessful and efforts to trigger biofilm formation in *P. fluorescens* Pf0-1 under different conditions failed. (Ameen & da Silva, 2014) Therefore, the initial objective of this work was to investigate the possible factors affecting the consistent development of *P. fluorescens* Pf0-1 biofilm. Throughout experimenting on different surfaces for biofilm development, inconsistencies were observed between plate batches and microtiter plates of the same material but different manufacturers. This effort then led to the investigation of mechanically altering the surface of polystyrene to create a surface that would provide a platform for reproducible and consistent static biofilm assays.

## **3.2. Methods and materials**

### **3.2.1. Bacterial strains and growth conditions**

The strains of *P. fluorescens* used in this study were provided by Professor George O'Toole at Dartmouth College. *P. fluorescens* wild-type strain Pf0-1 were stored as 15-25% v/v glycerol stocks at -80°C. Cultures were revived by streaking onto LB-Miller (LB) agar and subsequent static incubation at 30°C. Overnight pre-cultures were then prepared in LB broth from single colonies of *P. fluorescens* Pf0-1 and incubated at 30°C and 180 RPM until the required optical density for experimentation was reached.

### **3.2.2. LB-Miller (LB) media**

The following reagents were added to 950 mL of distilled water: 10.00 g bacto tryptone, 5.00 g yeast extract, 10.00g NaCl. The pH was adjusted to  $7.00 \pm 0.10$  with NaOH and the final volume of the solution was adjusted to 1 L with distilled water. When preparing solid media 15.00 g of agar was added after pH adjustment. Media was sterilized by autoclaving at 121 °C with a 30 min sterilization cycle, then stored in the dark at room temperature until use.

### **3.2.3. Minimal (M63) media**

The recipes below are adapted from the protocol used in previously successful biofilm experiments.(Bordeleau, 2014)

To 1 L of distilled water 13.60 g  $\text{KH}_2\text{PO}_4$ , 2.00 g  $(\text{NH}_4)_2\text{SO}_4$  and 2.00 g glucose were added. The pH of the solution was adjusted to  $7.00 \pm 0.09$  with KOH. The media was then autoclaved at 121 °C with a 15 min sterilization cycle. After the solution cooled down to room temperature the following components were filter sterilized using a 0.22  $\mu\text{m}$  filter and added to the media broth: 1 mL of a 0.2 g/mL  $\text{MgSO}_4 \cdot 7\text{H}_2\text{O}$  solution and 500  $\mu\text{L}$  of a 1.0 mg/mL solution  $\text{FeSO}_4 \cdot 7\text{H}_2\text{O}$  solution. Media was stored in the dark at room temperature until use.

### **3.2.3.1. Preparation of M63 used for methods sections 3.2.6.1 through to 3.2.6.4**

To 1 L of distilled water 13.60 g  $\text{KH}_2\text{PO}_4$  and 2.00 g  $(\text{NH}_4)_2\text{SO}_4$  were added. The pH of the solution was adjusted to  $7.00 \pm 0.09$  with KOH. The media was then autoclaved at  $121^\circ\text{C}$  with a 30 min sterilization cycle. After the solution cooled down to room temperature the following components were filter sterilized using a  $0.22\ \mu\text{m}$  filter and added to the media broth: 10 mL of a 20 % (w/v) glucose solution, 1 mL of a 0.2 g/mL  $\text{MgSO}_4 \cdot 7\text{H}_2\text{O}$  solution and 500  $\mu\text{L}$  of a 1.0 mg/mL solution  $\text{FeSO}_4 \cdot 7\text{H}_2\text{O}$  solution. Media was stored in the dark at room temperature until use. The bulk media was passed through a  $0.22\ \mu\text{m}$  filter at the beginning of each experiment.

### **3.2.3.2. Preparation of M63 used for methods section 3.2.6.5**

To 1 L of distilled water 13.60 g  $\text{KH}_2\text{PO}_4$ , 2.00 g  $(\text{NH}_4)_2\text{SO}_4$  and 2.00 g glucose were added. The pH of the solution was adjusted to  $7.00 \pm 0.09$  using KOH. The media was then autoclaved at  $121^\circ\text{C}$  with a 30 min sterilization cycle. After the solution cooled down to room temperature the following components were filter sterilized using a  $0.22\ \mu\text{m}$  filter and added to the media broth: 1 mL of a 0.2 g/mL  $\text{MgSO}_4 \cdot 7\text{H}_2\text{O}$  solution and 500  $\mu\text{L}$  of a 1.0 mg/mL solution  $\text{FeSO}_4 \cdot 7\text{H}_2\text{O}$  solution. Media was stored in the dark at room temperature until use.

### **3.2.3.3. Preparation of M63 used for methods section 3.2.6.6**

To 1 L of distilled water 13.60 g  $\text{KH}_2\text{PO}_4$ , 2.00 g  $(\text{NH}_4)_2\text{SO}_4$  and 2.00 g glucose were added. The pH of the solution was adjusted to  $7.00 \pm 0.09$  with KOH. The media was then autoclaved at  $121^\circ\text{C}$  with a 15 min sterilization cycle. After the solution cooled down to room temperature the following components were filter sterilized using a  $0.22\ \mu\text{m}$  filter and added to the media broth: 1 mL of a 0.2 g/mL  $\text{MgSO}_4 \cdot 7\text{H}_2\text{O}$  solution and 500  $\mu\text{L}$  of a 1.0 mg/mL solution  $\text{FeSO}_4 \cdot 7\text{H}_2\text{O}$  solution. Media was stored in the dark at room temperature until use.

### **3.2.4. UV/vis Spectrophotometric measurements**

Bacterial culture growth was monitored through UV spectrophotometric measurements carried out on a ThermoScientific Genesys 10S UV-Vis spectrometer. A Biotek PowerWave XS microtiter plate reader was used to quantify the biomass of biofilm in 96-well microtiter plates by recording absorbance of crystal violet staining at 600 nm. All measurements in the plate reader were made with the lid off the microtiter plate.

### **3.2.5. Statistical analysis**

Using the Excel 2016 program, a 2-tailed *t*-test was used to compare the significances in the quantity of biofilm formed. Experiments with *p* values not greater than 0.05 are considered as statistically significant.

### **3.2.6. Static biofilm assay and quantification**

#### **3.2.6.1. Preliminary analysis of biofilm formation across different brands of microtiter plates**

*P. fluorescens* Pf0-1 was revived from -80°C storage by streaking directly from a glycerol stock onto an LB agar plate for static incubation at 30°C. Upon the generation of single colonies, pre-cultures for experimentation were prepared by inoculating a minimum of 9 mL of LB broth with a pure *P. fluorescens* Pf0-1 single colony. The pre-cultures were incubated at 30°C at 180 RPM until mid-exponential phase was reached after 15 to 16 hrs. Inoculum was prepared by diluting the pre-cultures 1:100 into M63 broth (Methods 3.2.3.1). For each diluted culture, a total of 4 microtiter wells were then inoculated using 100 µL per well with blank media used for control. Plates were then incubated statically at 30 °C for 8 hrs, with the plate covered by either a lid, when provided by the manufacturer, or sterile rayon AeraSeal™ film purchased from Sigma-Aldrich. After incubation, the liquid culture was discarded from the wells by shaking the inverted plate over a waste bucket. The wells were then rinsed with distilled water using an 8-prong wash bottle

shaking contents over waste bucket. Biofilm was then stained with 125  $\mu$ L of a 0.1 % crystal violet solution for 15 min. Post staining, the wells were washed with distilled water and left to dry in the dark.

### **3.2.6.2. Secondary screening of microtiter plates: biofilm formation across different surface treatments of polystyrene**

*P. fluorescens* Pf0-1 pre-cultures were prepared as described in Methods 3.2.6.1. Inoculum was prepared by diluting three individual pre-cultures 1:100 into M63 broth (Methods 3.2.3.1). A total of 12 microtiter plate wells were then inoculated on each plate using 100  $\mu$ L of a diluted pre-culture, with blank media as control. Plates were then incubated statically at 30 °C for 8 hrs, covered by a sterile rayon AeraSeal™ film purchased from Sigma-Aldrich. After incubation, the liquid culture was discarded from the wells by shaking the inverted plate over a waste bucket. The wells were then rinsed with distilled water using an 8-prong wash bottle shaking contents over waste bucket. Biofilm was then stained with 125  $\mu$ L of a 0.1 % crystal violet solution for 15 min. Post staining, the wells were washed with distilled water and left to dry in the dark. The amount of crystal violet bound to biofilm was quantified by solubilizing the dye with a 30 % acetic acid solution. The acetic acid solution was incubated in the wells at room temperature for 15 min prior to being mixed by pipette aspiration and transferred to a new flat well microtitre plate. The absorbance of the crystal violet – acetic acid solution was measured at 600 nm using 30 % acetic acid as a blank.

### **3.2.6.3. Biofilm formation on an untreated Corning (No. 351172) polystyrene microtiter plate**

*P. fluorescens* Pf0-1 pre-cultures were prepared as described in Methods 3.2.6.1. Inoculum was prepared by diluting a pre-culture 1:100 into M63 broth (Methods 3.2.3.1). Prior to inoculation two of the four plates tested were first washed with autoclaved M $\Omega$  water and 70 % ethanol. A

total of 8 microtiter plate wells were then inoculated per plate using 100  $\mu$ L of the diluted culture with blank media as control. Plates were then incubated statically at 30 °C for 8 hrs, covered by a low evaporation lid or a sterile rayon AeraSeal™ film purchased from Sigma-Aldrich. After incubation, the liquid culture was discarded from the wells by shaking the inverted plate over a waste bucket. The wells were then rinsed with distilled water by pipette aspiration. The quantification of biofilm then proceeded as previously described in Section 3.2.6.2.

#### **3.2.6.4. Effect of carbon source on the quantity of biofilm produced on a Corning polystyrene microtiter plates (No. 351172)**

*P. fluorescens* Pf0-1 pre-cultures were prepared as described in Methods 3.2.6.1. To investigate the effects of arginine as the carbon source for biofilm formation, inoculum was prepared by diluting the pre-cultures 1:100 into one of the following media: M63 broth (Methods 3.2.3.1) or M63 broth (Methods 3.2.3.1) supplemented with 0.4 % (w/v) arginine. To investigate the effects of autoclave sterilized or filter sterilized glucose for biofilm formation, the initial solution of  $\text{KH}_2\text{PO}_4$ , and  $(\text{NH}_4)_2\text{SO}_4$  as well as the addition of  $\text{MgSO}_4 \cdot 7\text{H}_2\text{O}$  and  $\text{FeSO}_4 \cdot 7\text{H}_2\text{O}$  was executed as previously described in Methods 3.2.3.1. Each of the diluted cultures were used to inoculate 100  $\mu$ L in a minimum of 4 microtiter plate wells per plate, with blank media as control. Plates were then incubated statically at 30 °C for 8 hrs, covered by a sterile rayon AeraSeal™ film purchased from Sigma-Aldrich. After incubation, the liquid culture was discarded from the wells by shaking the inverted plate over a waste bucket. The wells were then rinsed with distilled water by pipette aspiration. Quantification of biofilm was executed as previously described in Section 3.2.6.2.

### **3.2.6.5. Quantitative analysis of biofilm formed on non-treated polypropylene surface from two different manufacturers**

*P. fluorescens* Pf0-1 pre-cultures were prepared as described in Methods 3.2.6.1. Inoculum was prepared by diluting the pre-cultures 1:100 into M63 broth (Methods 3.2.3.2). Each diluted culture was used to inoculate 100  $\mu$ L in 6 microtiter wells per plate, with blank media as control. Plates were then incubated statically at 30 °C for 8 hrs covered by a sterile rayon AeraSeal™ film purchased from Sigma-Aldrich. Quantification of biofilm was executed as previously described in Section 3.2.6.2.

### **3.2.6.6. Quantitative analysis of biofilm formed on Corning No. 351172 microtiter plates after abrasive treatment**

*P. fluorescens* Pf0-1 pre-cultures were prepared as described in Methods 3.2.6.1. Inoculum was prepared by diluting the pre-culture 1:100 into M63 broth (Methods 3.2.3.2.) or LB broth. A minimum of 6 microtiter plate wells were inoculated with 100  $\mu$ L per culture with blank media used for control. Plates were then incubated statically at 30 °C for 8 hrs covered by a low evaporation lid. Quantification of biofilm was executed as previously described in Section 3.2.6.2.

### **3.2.8. Abrasive treatment of microtiter plates**

Microtiter plates were purchased from VWR, Corning brand Product No. 351172, lot No. 6045119 and 6243006. A uni-blaster was used to bombard the microtiter plates with 80 grit, brown aluminum oxide to modify the polystyrene surface. Plates were held 6 inches away from the uni-blaster and the brown aluminum oxide was sprayed at the surface with a pressure of 80 psi. The uni-blaster was moved across each row, working left to right at a constant speed to ensure equal coverage. The plates were treated 5 times, each in a different position; first so that sand was sprayed onto the bottom of the wells directly, then angled so that each of the 4 sides of the microtitre well-walls were exposed. For experiments where only treated half of the microtiter plate

was treated, the untreated control side was covered by a metal plate to prevent contamination. To prevent treatment of the well-bottoms, polytetrafluoroethylene (PTFE) discs were inserted into each well. After treatment, the wells on both the treated and untreated sides, were rinsed thoroughly with distilled water in the same fashion as they were treated with the sand. Plates were then rinsed twice with 70% ethanol and then rinsed twice more with distilled water. Prior to use in a static biofilm assay the plates were sterilized under UV for 20 min.

### **3.2.9. Drill press modification of microtiter plates**

Microtiter plates were purchased from VWR, Corning brand Product No. 351172, lot No. 6243006. A drill press was used as a substitute for the uni-blaster to modify the polystyrene surface.



Figure 3.2. Drill bit used to modify microtiter plate wells

The drill press was used to insert the drill bit, shown in Figure 3.2, in and out of the microtiter plate wells once to create uniform crevases on the surface. Following modification, plates were rinsed and sterilized following the same protocol used in Section 3.2.8.

### **3.2.10. Scanning electron microscopy (SEM)**

Microtiter plate well-surfaces were investigated through scanning electron microscopy (SEM) performed on a JEOL JSM-7000F (McMaster University, Canada). Two wells obtained from a Corning (No. 351172) microtiter plate for analysis. A single well was from the unmodified side of the polystyrene plate and the other well was obtained from the other side of the polystyrene plate post-abrasive media treatment. Each well was originally positioned in the middle of their

respective side of the microtiter plate to eliminate edge-well discrepancies. To obtain information on the surface composition images were taken in COMPO mode using backscattered electrons (BSE). Images pertaining to surface topography were obtained by operating the instrument in secondary electron mode (SEI). The instrument was operated at 2.0 kV and 15.0 kV for both BSE-SEM and SEI-SEM analysis and images were taken at 200x, 500x and 1000x magnification.

### 3.3 Results

#### 3.3.1. Preliminary analysis of biofilm formation across different brands of microtiter plates

As described previously, this part of the thesis was driven by the efforts to reproduce the biofilm formation assay results demonstrated in our previous work (Bordeleau, 2014), but failed when polystyrene microtiter plates from a different batch were used. It was hypothesized that there was either (1) a change in the production process of the polystyrene plates resulting in different adsorption properties or (2) the original batch of Fisherbrand™ plates were produced with a deformity altering the adsorption properties that were not produced in the new batch. A third batch of plates was purchased, however, *P. fluorescens* Pf0-1 biofilm formation was inconsistent and was not reproducible across multiple plates. (Ameen & da Silva, 2014) If the levels of biofilms in previous work was unique to the first batch of Fisherbrand™ (No. 12-565-501) then a surface that supported reproducible levels of biofilm formation would need to be identified. Thus, other brands of microtiter plates were tested to compare the levels of biofilm formed in search of a surface that could support reproducible *P. fluorescens* Pf0-1 biofilm formation.

While microtiter plates of other brands were tested, it was also important to investigate other factors that could be potentially inhibiting the maturation of biofilm. Firstly, the viability of the glycerol stocks had decreased and it was hypothesized that the glycerol stocks may have lost key biofilm traits. (Stepanović *et al.*, 2007) To eliminate the bacterial glycerol stock integrity as the source of the problem, a new stab culture of *P. fluorescens* Pf0-1 was obtained from Dr. George O'Toole's lab at Dartmouth College. To be consistent with the biofilm-inducing conditions utilized in the laboratory at Dartmouth College, the protocol for minimal M63 broth preparation was altered for these initial experiments as well. When preparing the M63 broth, the component glucose was filter sterilized instead of being autoclaved as apart of the initial KH<sub>2</sub>PO<sub>4</sub> and

(NH<sub>4</sub>)<sub>2</sub>SO<sub>4</sub> solution. New stocks of media components were also purchased to exclude any contaminants that could be inhibiting the development of biofilm. (Donlan, 2002)

Another potential factor for the decrease in biofilm formation was protein contamination. The presence of proteins could interfere with interactions between the bacterial cells and the plastic during the initial phases of surface attachment. (Fletcher, 1976; Pringle & Fletcher, 1986) Therefore, new glassware was obtained for media storage. Both the M63 broth as well as LB broth were also passed through a sterile 0.22 µm syringe filter prior to use to prevent contamination by large particulates that could interfere with bacteria-surface interactions. (Müsken, Di Fiore, Römling, & Häussler, 2010)

Four microtiter plates, as summarized in Table 3.1, were initially surveyed for their ability to support *P. fluorescens* Pf0-1 biofilm.

Table 3.1. Product information for preliminary screening of microtiter plates

<b>Microtiter Plate Brand Name</b>	<b>Product Number</b>	<b>Material</b>	<b>Surface Treatment</b>	<b>Well-Bottom Shape</b>
Fisherbrand™	12-565-501	Polystyrene	None	Flat-bottom
Sarstedt	83.1835 <sup>a</sup>	Polystyrene	Tissue culture	Flat-bottom
Nunc™	N/A	Polystyrene	MaxiSorp™	Flat-bottom
Norgen	24310 <sup>b</sup>	Polypropylene	None	C-bottom

<sup>a</sup>. Order number is now currently 83.3924 for this product, 83.1835 represents the former product number at time of purchase.

<sup>b</sup>. This is the product number for the Norgen RNA extraction kit that contains this plate. The product number from the manufacturer Axygen is P-96-450R-C-S

After performing a qualitative static biofilm assay, each of the plates exhibited crystal violet staining to different degrees. No difference was observed between wells inoculated with cultures previously grown in filtered LB broth and non-filtered LB broth. With this observation, the M63 broth was filtered in subsequent experiments since this medium would be the largest source of particulate contamination. It was found that the Norgen polypropylene plate (Figure 3.3A) and a Nunc™ polystyrene plate (Figure 3.3B) gave the highest intensities and consistencies

of crystal violet biofilm staining across the inoculated wells in comparison to the Sarstedt (Figure 3.3C) and Fisherbrand™ plate (Figure 3.3D).

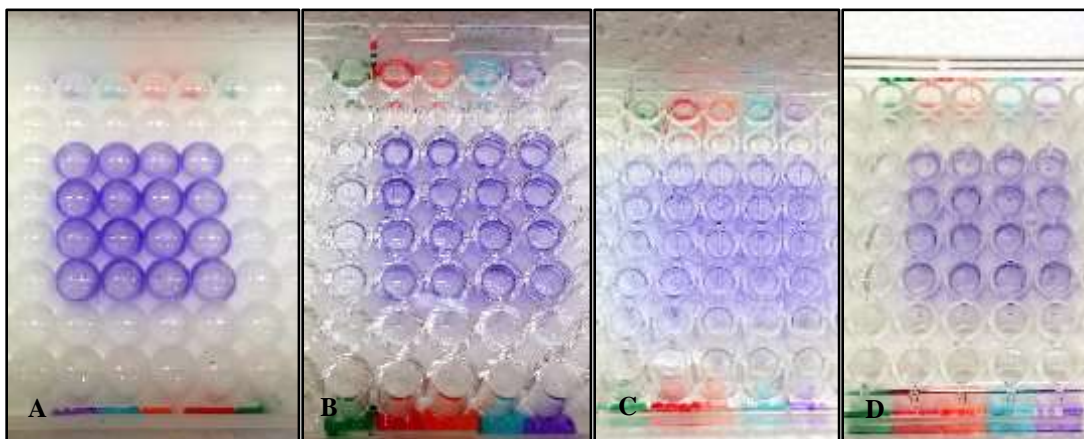


Figure 3.3. Initial qualitative analysis of microtiter plates that support *P. fluorescens* Pf0-1 biofilm formation. Each photograph is a bottom-view of the following microtiter plates post staining of biofilm with 0.1 % crystal violet. (A) Norgen (B) Nunc™ (C) Sarstedt (D) Fisherbrand™  
Green wells – media blank control. Orange and purple wells – filtered LB broth used for pre-culture. Red and cyan wells – non-filtered LB broth used for pre-culture.

To be consistent with biofilm work done previously with polystyrene microtiter plates, it was decided to proceed using the Nunc™ polystyrene microtiter plate. A subsequent experiment was performed utilizing the wild-type strain of *P. fluorescens* Pf0-1 on the Nunc™ microtiter plate generating an average crystal violet absorbance of 0.380 at 600 nm, thus generating biofilm on the lower end of the range of biofilm levels obtained in previous work. (Bordeleau, 2014) Unfortunately, there was only a couple of these plates available in the neighbouring lab and ordering information was not available. After consultation with the manufacturer, it was deduced that the Nunc™ plate had a MaxiSorp™ surface treatment.

### 3.3.2. Secondary screening of microtiter plates: biofilm formation across different surface treatments of polystyrene

Untreated polystyrene is a hydrophobic surface that can be modified to increase its binding capacity based on the experimental needs. There are four types of surface treatments supplied by Nunc™ that allow for the passive adsorption of a variety of biomolecules; PolySorp™,

MediSorp™, MaxiSorp™ and MultiSorp™. The range of hydrophilicity among each of the surfaces is generated through an undisclosed process introducing hydroxyl and carboxyl functional groups to varying degrees on the polystyrene. The MaxiSorp™ surface has a midrange hydrophilicity allowing it to bind the greatest range of biomolecules. (ThermoFisher Scientific, 2014)

As the Nunc™ plate tested was unavailable, free samples were obtained from ThermoFisher Scientific that contained the MaxiSorp™ surface treatment (Table 3.2). A polyvinyl chloride plate was also tested as a positive control, as it has been shown to lead to successful biofilm formation in O’Toole’s lab where the *P. fluorescens* Pf0-1 isolate was obtained.

Table 3.2. Product information for secondary screening of microtiter plates

<b>Product Number</b>	<b>Material</b>	<b>Surface Treatment</b>	<b>Well-Bottom Shape</b>
446612	Polystyrene	MaxiSorp™	C-bottom
446469	Polystyrene	MaxiSorp™	C-bottom
468667	Polystyrene	MaxiSorp™	Flat-bottom
2797	Polyvinyl chloride	None	U-bottom
12-565-501	Polystyrene	None	Flat-bottom

Microtiter plates No. 446612, No. 2797 and No. 12-565-501 were the only plates that produced crystal violet stained biofilm with a high enough intensity and consistent staining pattern for quantification (Figure 3.4). The highest amount of biofilm formed was in the wells of plate No. 446612 and was consistent with levels of biofilm obtained in past experiments. The microtiter plate No. 12-565-501 produced levels of biofilm consistent with minimal levels obtained in previous studies. (Bordeleau, 2014) However, the inconsistencies observed between plates of No. 12-565-501 did not make it a reliable candidate for biofilm assays moving forward. Unfortunately, subsequent attempts to replicate these results in plates of No. 446612 generated levels of biofilm that were too low for quantification or absent completely.

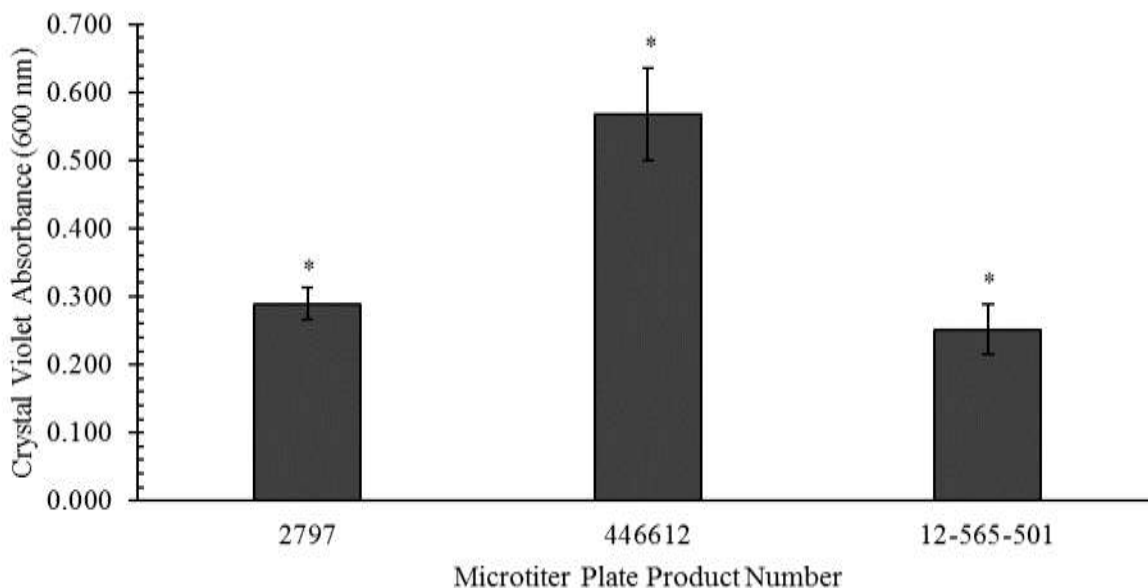


Figure 3.4. Quantitative analysis of *P. fluorescens* Pf0-1 biofilm formation during secondary screening of microtiter plates. The bars represent the average amount of biofilm formed by the same culture replicated on each microtiter plate. Quantities of biofilm were determined by measuring the absorbance at 600 nm after crystal violet bound to the biofilm was solubilized in 30 % acetic acid. Error bars represent the mean  $\pm$  standard deviation. (n=12) Star represents significant difference in biofilm formed between each microtiter plate tested. \* $p \leq 0.01$

### 3.3.3. Biofilm formation on a Corning (No. 351172) microtiter plate untreated polystyrene surface

Due to the inconsistencies observed with plate No. 446612, as well as No. 12-565-501, microtiter plates from a different manufacturer were obtained to test their ability to support biofilm formation. Two plates from Corning were investigated for their potential as a new platform for static microtiter plate assays in this laboratory, No. 3590 and No. 351172, whose properties are summarized in Table 3.3. The high binding plate No. 3590 is similar surface chemistry to the ThermoFisher Scientific's MaxiSorp™ plate No. 446612, containing negatively charged moieties. (Gibbs & Kennebunk, 2001; Corning Life Sciences, 2015) The process for which the surface is treated is also not publicly available and thus the extent of negatively charged groups attached to the polystyrene surface cannot be confirmed. Without this knowledge, the microtiter plate No. 3590 was not an appropriate platform for biofilm studies as the surface chemistry cannot be compared against other surfaces. The No. 351172 plate is a sterile, non-tissue culture treated

polystyrene surface whose hydrophobic nature is comparable to the Fisherbrand™ (No. 12-565-501) plate. The plate also comes with a unique low evaporation lid to help prevent moisture loss during biofilm incubation periods as well as condensation rings above each well to prevent cross contamination. (Corning Life Sciences, 2013) These properties made Corning microtiter plate No. 351172 the most ideal candidate microtiter plate to proceed with in biofilm assays in comparison to Fisherbrand™ microtiter plate No. 12-565-501.

Table 3.3. Product information for microtiter plates purchased from Corning

Product Number	Material	Surface Treatment	Well-Bottom Shape	Sterile?
351172	Polystyrene	Non-tissue culture treated medium binding	Flat-bottom	Yes
3590	Polystyrene	High-binding	Flat-bottom	No

Although levels of biofilm were lower than what was previously obtained, across the first two plates tested, there was a consistent level of crystal violet staining as shown in Figure 3.5.

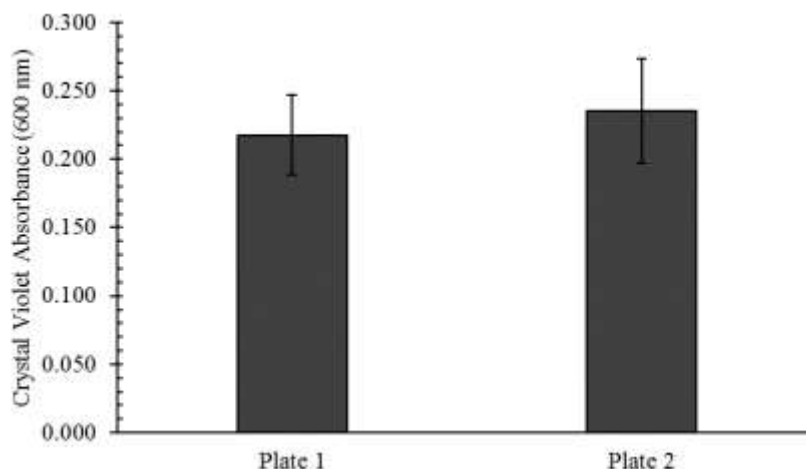


Figure 3.5. Biofilm formation in two individual Corning microtiter plates No. 351172. The bars represent the average amount of biofilm formed in each microtiter plate. Quantities of biofilm were determined by measuring the absorbance at 600 nm after crystal violet bound to the biofilm was solubilized in 30 % acetic acid. Error bars represent the mean  $\pm$  standard deviation. (n=8)  $p > 0.05$

With lower levels of biofilm formation observed for microtiter plates No. 351172 and inconsistencies with No. 446612, it was conceivable that there could be other interfering factors from the surface. During the production process additives are used to catalyze polymerization and

stabilize the product. Manufacturers also may use a “slipping agent” during the moulding process to facilitate easier and faster removal from the moulds. (McDonald *et al.*, 2008; Olivieri *et al.*, 2012; Gerke & Grzeskowiak, 2015) A coating such as a releasing agent, could result in unfavourable surface properties for the bacterial cells to adhere to. To account for this, biofilm assays were performed where plates were rinsed first with 70% ethanol and then autoclaved MQ water to remove any remaining substances from production. The plates were then sterilized by UV radiation prior to use. Unfortunately, this modification did not improve upon levels of biofilm formed in plates of No. 351172 and for a No. 446612 plate there was no level of biofilm formed.

#### **3.3.4. Effect of carbon source on the quantity of biofilm produced on a medium binding crystal grade polystyrene surface**

As discussed previously, the formation of biofilm can be triggered through several pathways that are species specific and reliant on environmental factors. The substitution of amino acid for glucose can trigger the production of a more robust biofilm. (O'Toole, 2011; O'Toole & Kolter, 1998; Palmer, Aye, & Whiteley, 2007) The amino acid arginine was chosen for this part of the study to investigate the ability of this carbon source in triggering higher quantities of biofilm. (Osorno *et al.*, 2012)

As observed in Figure 3.6, the levels of biofilm formed by the wild-type in glucose based M63 broth were consistent with those seen previously in Corning microtiter plates No. 351172. When cultures were grown on the same microtiter plate but in M63 broth supplemented with arginine, the levels of biofilm increased almost two-fold.

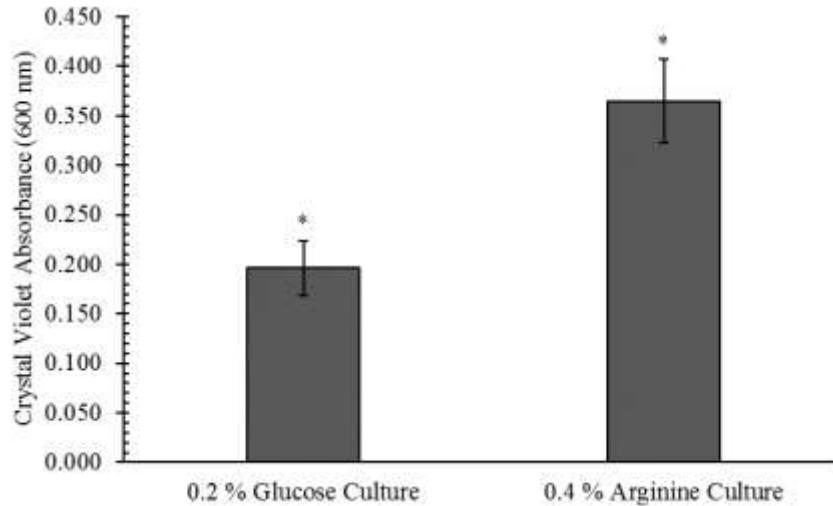


Figure 3.6. Quantitative analysis of the effects the carbon source has on biofilm formation in *P. fluorescens* Pf0-1 No. 1. The bars represent the average amount of biofilm formed by each culture on the same microtiter plate. Quantities of biofilm were determined by measuring the absorbance at 600 nm after crystal violet bound to the biofilm was solubilized in 30 % acetic acid. Error bars represent the mean  $\pm$  standard deviation. (n=8) Star represents significance between cultures fed different carbon sources  $*p \leq 5.7 \times 10^{-7}$

The increase in both quantity and quality of biofilm can also be observed upon close inspection of the crystal violet stained biofilm. As shown in Figure 3.7, the arginine fed culture resulted in a solid ring of biofilm forming at the air-surface interface in comparison to the glucose fed culture.

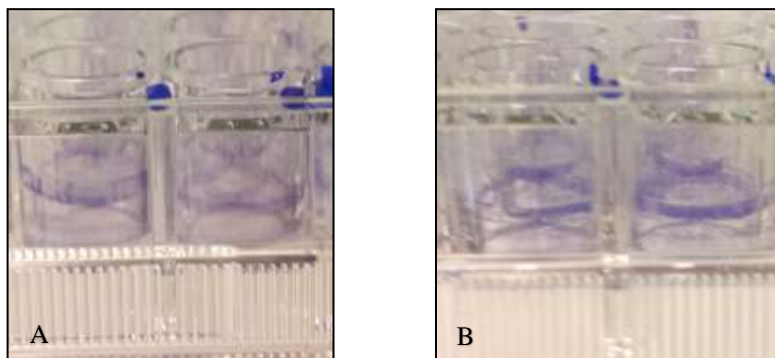


Figure 3.7. Qualitative analysis of the effects the carbon source has on biofilm formation in *P. fluorescens* Pf0-1. Photographs of Corning (Product No. 351172) microtiter plate wells containing crystal violet stained Pf0-1 biofilm. (A) Photograph of Pf0-1 biofilm stained with 0.1 % crystal violet. Cultures grown in 0.2 % glucose supplemented M63 media. (B) Photograph of Pf0-1 biofilm stained with 0.1% crystal violet. Cultures grown in 0.4 % arginine supplemented M63 media.

Upon repeating the experiment on two separate Corning microtiter plates, the same trends were observed in that the arginine fed cultures grew a significantly higher amount of biofilm than the glucose fed cultures (Figure 3.8). Despite the higher levels of biofilm generated by arginine, the

remaining experiments utilized glucose as a carbon source to maintain consistency with the protocol used in previous work. (Bordeleau, 2014)

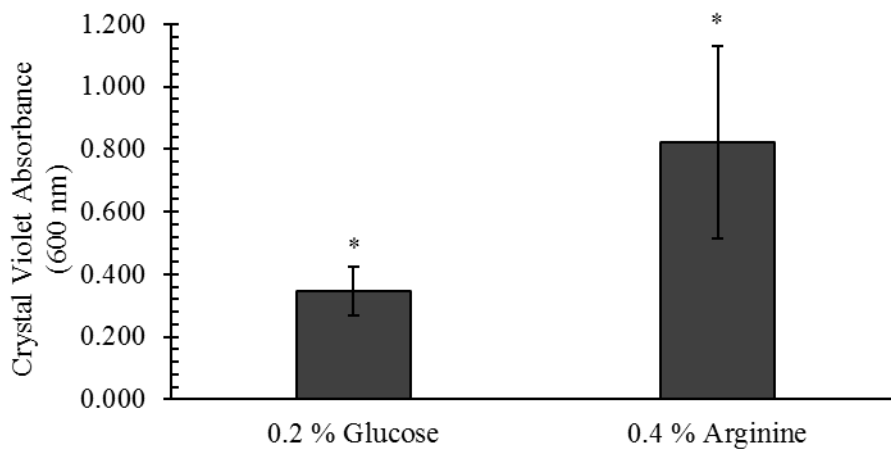


Figure 3.8. Quantitative analysis of the effects the carbon source has on biofilm formation in *P. fluorescens* Pf0-1 No. 2. The bars represent the average amount of biofilm formed across the two microtiter plates. Quantities of biofilm were determined by measuring the absorbance at 600 nm after crystal violet bound to the biofilm was solubilized in 30 % acetic acid. Error bars represent the mean  $\pm$  standard deviation. (n=2) Star represents significance between cultures fed different carbon sources. \* $p \leq 0.001$

In subsequent experiments, two methods to sterilize glucose were compared for their impact on the formation of *P. fluorescens* Pf0-1 biofilm, that is, filter sterilization and autoclaving. As noted in the beginning of Methods Section 3.2.3, previous work in this laboratory performed static biofilm assays with M63 broth supplemented with 0.2 % glucose that had been autoclaved in the bulk medium. (Bordeleau, 2014) The autoclave-sterilization of glucose for different lengths of time while in the presence of other media components generate multiple side products. (Byrd, Cheville, Bose, & Kaspar, 1999; Finkelstein & Lankford, 1957; Forssk, Popoff, & Theander, 1976; Yoneyama, Hara-Kudo, & Kumagai, 2007) These side products could potentially alter interactions between bacterial cells and the surface and/or alter pathways involved in the initial phases of biofilm formation. (Donlan, 2002; Nielsen, Tolker-Nielsen, Barken, & Molin, 2000) It would therefore be of importance to investigate if the quantity of biofilm generated in previous studies could be induced on the surface of the Corning (No. 351172) plates due to the presence, or lack there of, these side products.

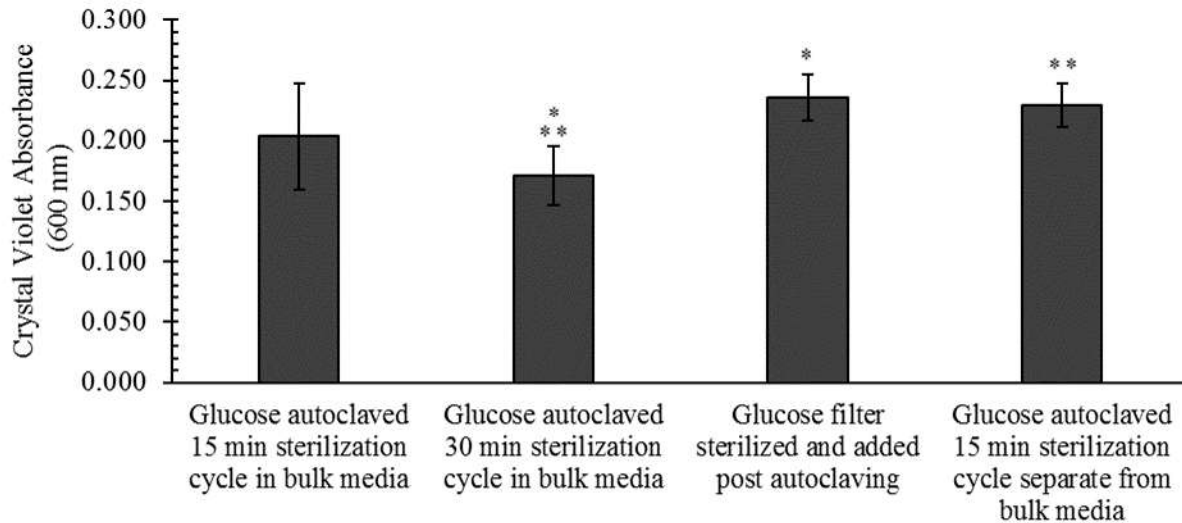


Figure 3.9. Comparison of biofilm formed by *P. fluorescens* Pf0-1 cultures using glucose as the carbon source, either filter- or autoclave sterilized. The bars represent the average amount of biofilm formed by the same culture diluted into the different media formulations. Quantities of biofilm were determined by measuring the absorbance at 600 nm after crystal violet bound to the biofilm was solubilized in 30 % acetic acid. Error bars represent the mean  $\pm$  standard deviation (n=6) for each column except for glucose autoclaved 15 min cycle in bulk media (n=12) Stars represent significant difference between conditions. \* $p \leq 0.002$  \*\* $p \leq 0.004$ .

The different preparations of M63 broth with respect to the glucose component did not restore levels of biofilm to levels seen in previous work (average absorbance of crystal violet ranging from 0.380 – 0.800) (Bordeleau, 2014) Highest levels of biofilm formation were seen in the cultures when glucose was filter sterilized post autoclaving (Figure 3.9), however the difference in biofilm formation as shown in Figure 3.10 is marginal. Therefore, glucose was autoclave-sterilized in subsequent experiments in order to maintain consistency with previous protocols in this laboratory. (Bordeleau, 2014)

### 3.3.5. Quantitative analysis of biofilm formed on non-treated polypropylene surface from two different manufacturers

After testing several microtiter plate surfaces for their ability to support biofilm formation, Corning plates (No. 351172) were found to produce the most consistent results for a non-treated polystyrene surface. Successful assays were also performed on a microtiter plate obtained on a non-treated polypropylene plate obtained from Norgen (No. 24310). The increased levels of biofilm formed on the polypropylene surface warranted further investigation of this material as a

platform for future biofilm studies. Due to the higher costs of purchasing the Norgen microtiter plates, non-treated polypropylene plates from ThermoFisher Scientific (No. 267334, manufactured by Nunc) were investigated.

Table 3.4. Product information for polypropylene plates tested

<b>Distributor</b>	<b>Lot Number</b>	<b>Product Number</b>	<b>Manufacturer</b>	<b>Sterile</b>
ThermoFisher Scientific	144871	267334	Nunc	Yes
Norgen	25914113	24310 <sup>a</sup>	Corning	Yes

<sup>a</sup>. This is the product number indicated for the Norgen RNA extraction kit that contains this plate. The product number from the manufacturer Corning (Axygen® brand) is P-96-450R-C-S.

The first experiment performed on a Nunc polypropylene microtiter plate from ThermoFisher Scientific was found to form less biofilm than the previously tested polypropylene plates purchased from Norgen (data not shown). With these observations, a comparison was performed to determine if the differences in biofilm quantities between plates from these two manufacturers were statistically significant.

The initial comparison assay used two sets of inocula for the Norgen and ThermoFisher Scientific plate, each originating from an individual pre-culture. Both cultures led to statistically significant increases of biofilm forming on the Norgen; with 2.3 folds more biofilm produced overall. (Figure 3.10)

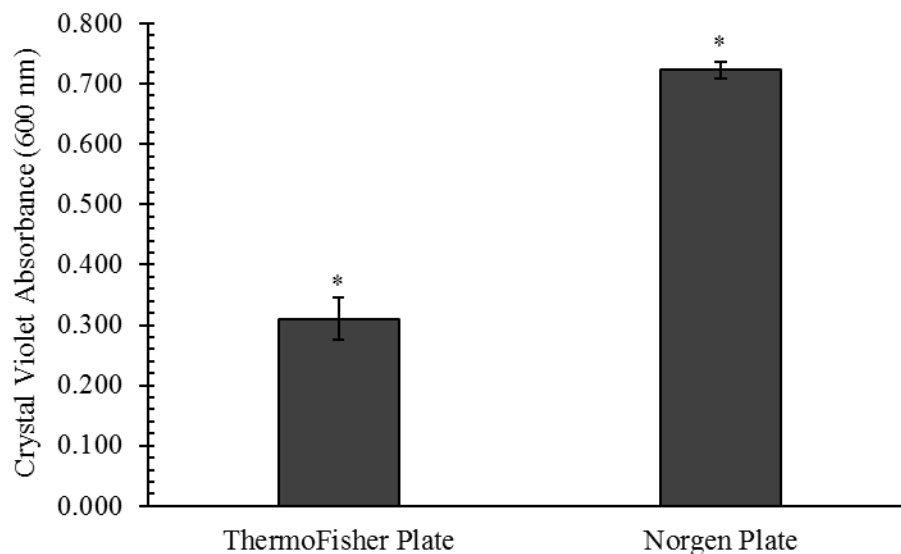


Figure 3.10. Initial comparison of Norgen polypropylene plate and ThermoFisher Scientific Plate for quantity of *P. fluorescens* Pf0-1 biofilm formed. The bars represent the average amount of biofilm formed across two cultures. Quantities of biofilm were determined by measuring the absorbance at 600 nm after crystal violet bound to the biofilm was solubilized in 30 % acetic acid. Error bars represent the mean  $\pm$  standard deviation ( $n=2$ ). Star represents significant difference in biofilm formed across microtiter plates tested.  $*p \leq 2.0 \times 10^{-12}$

The comparison was then repeated across two sets of Norgen and ThermoFisher Scientific plates. Each set of plates were inoculated approximately an hour and a half apart, using three individual cultures of *P. fluorescens* Pf0-1 (Figure 3.11A and 3.12A). The differences in the intensity of crystal violet staining at the air-liquid interface can be observed in the wells of both plates (Figure 3.11B-E and 3.12B-E).

Overall, the cultures produced an average quantity of biofilm that was statistically significantly higher on the Norgen microtiter plates. The three cultures used to inoculate the first set of plates produced on average 1.3 folds more biofilm on the Norgen plates. The three cultures used to inoculate the second set of plates produced on average 1.1 folds more biofilm on the Norgen plates. All the cultures displayed higher biofilm ring integrity at the air-surface interface on the Norgen plates (Figure Figure 3.11 and 3.12B-E). The biofilm rings formed on the ThermoFisher Scientific plates are blotchy in appearance in comparison to the more defined and continuous ring of biofilm formed in the Norgen plates.

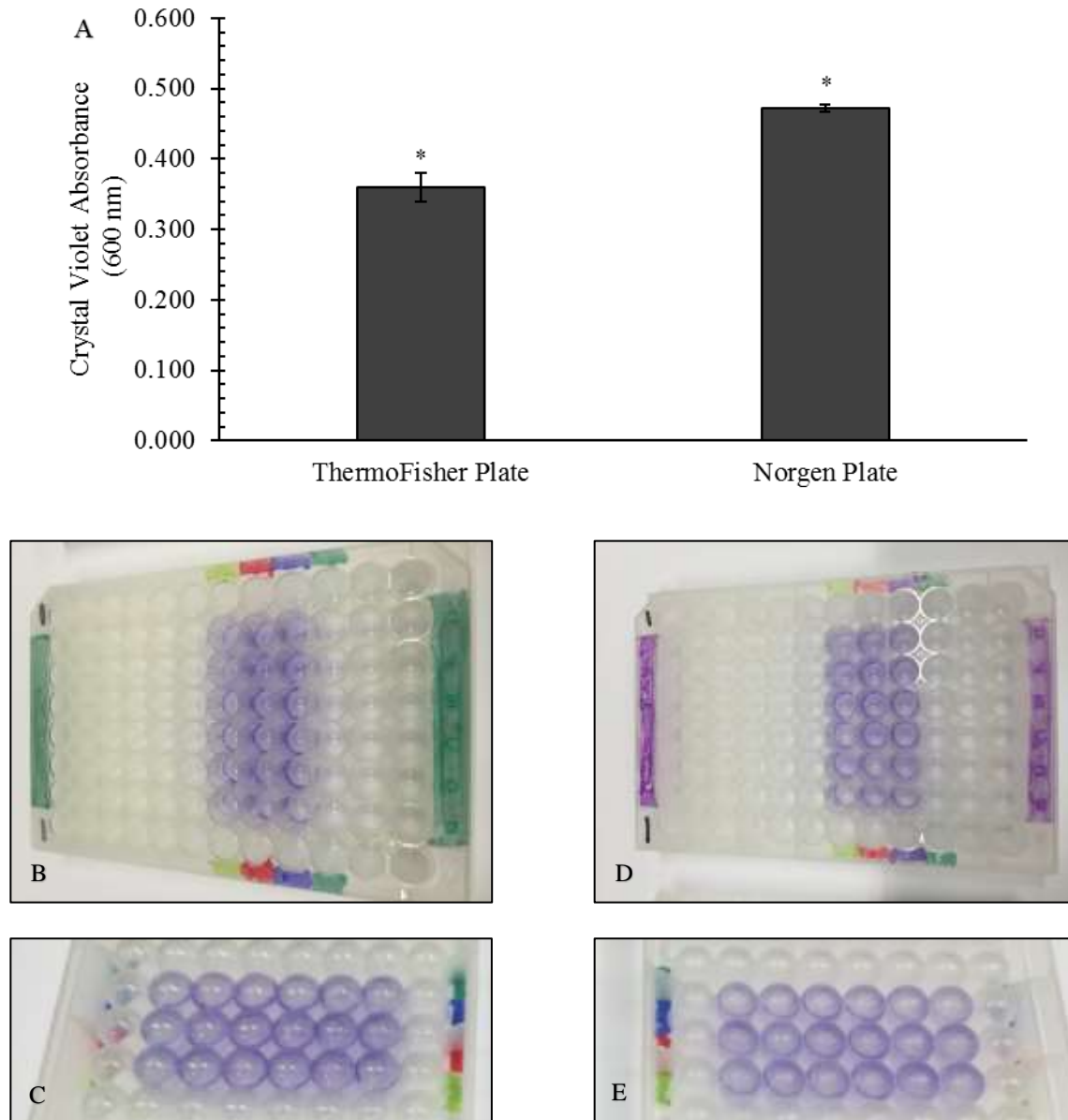


Figure 3.11. Norgen and ThermoFisher Scientific microtiter plate comparison biofilm assay No. 1.

(A) The bars represent the average amount of biofilm formed across three cultures. Quantities of biofilm were determined by measuring the absorbance at 600 nm after crystal violet bound to the biofilm was solubilized in 30 % acetic acid. Error bars represent the mean  $\pm$  standard deviation (n=3). Star represents significant difference in biofilm formed between the microtiter plates tested.  $*p \leq 5.1 \times 10^{-12}$  Top-view photograph of microtiter plate from (B) Norgen and (D) ThermoFisher Scientific post staining biofilm with 0.1% crystal violet. Bottom-view photograph of microtiter plate from (C) Norgen and (E) ThermoFisher Scientific post staining biofilm with 0.1% crystal violet. Green column – blank media control. Each of the other column colours (lime green, red, blue) represents inoculum originating from a different culture.

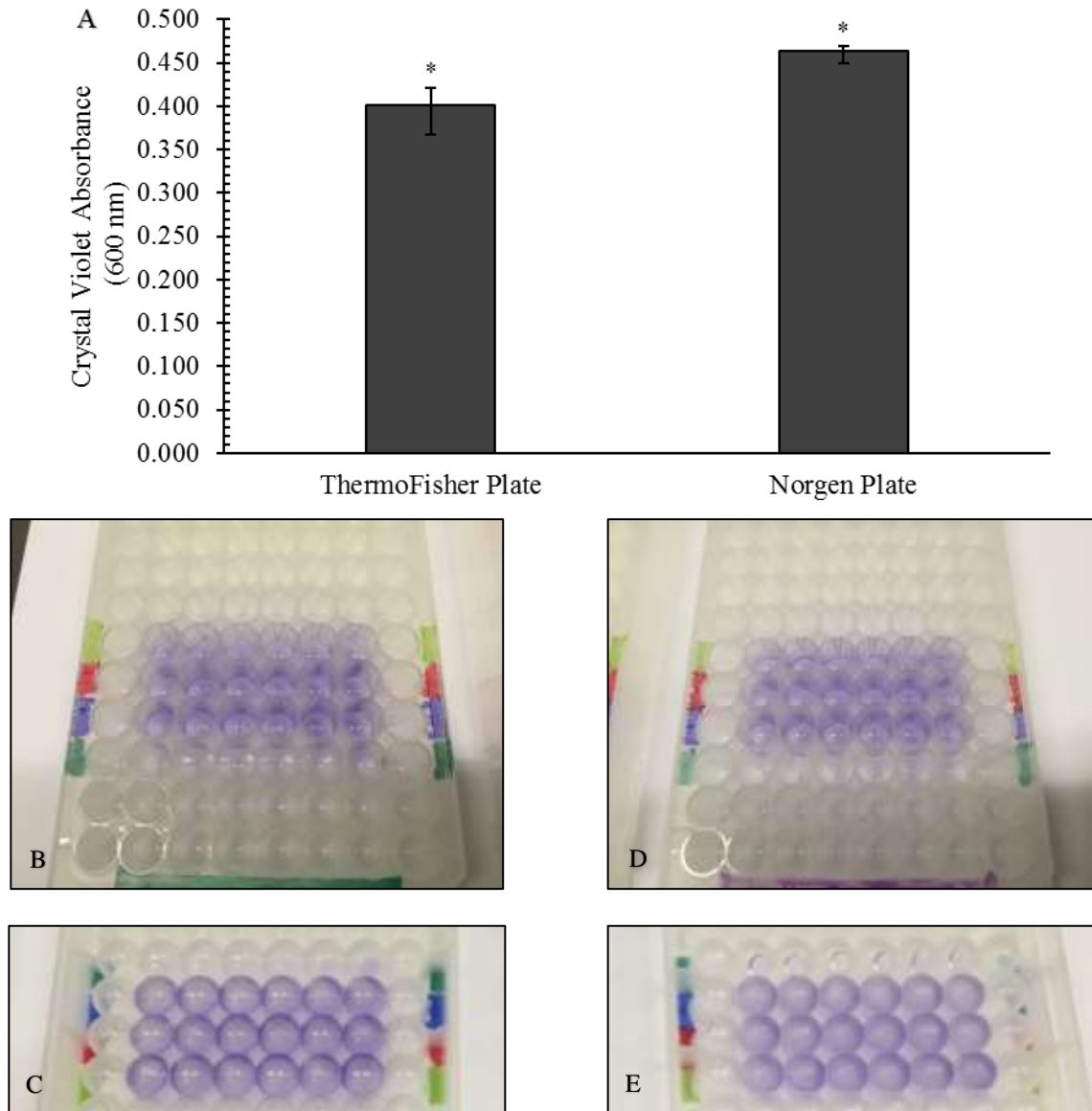


Figure 3.12. Norgen and ThermoFisher Scientific microtiter plate comparison biofilm assay No. 2.

(A) The bars represent the average amount of biofilm formed across three cultures. Quantities of biofilm were determined by measuring the absorbance at 600 nm after crystal violet bound to the biofilm was solubilized in 30 % acetic acid. Error bars represent the mean  $\pm$  standard deviation (n=3). Star represents significant difference in biofilm formed between the microtiter plates tested.  $*p \leq 0.0006$  Top-view photograph of microtiter plate from (B) Norgen and (D) ThermoFisher Scientific post staining biofilm with 0.1% crystal violet. Bottom-view photograph of microtiter plate from (C) Norgen and (E) ThermoFisher Scientific post staining biofilm with 0.1% crystal violet. Green column – blank media control. Each of the other column colours (lime green, red, blue) represents inoculum originating from a different culture.

A third comparison assay was performed on one set of microtiter plates (one Norgen plate and one ThermoFisher Scientific plate) however there was no statistically significant difference observed in the quantity of biofilm formed across each of the independent cultures used for inoculation (Figure 3.13).

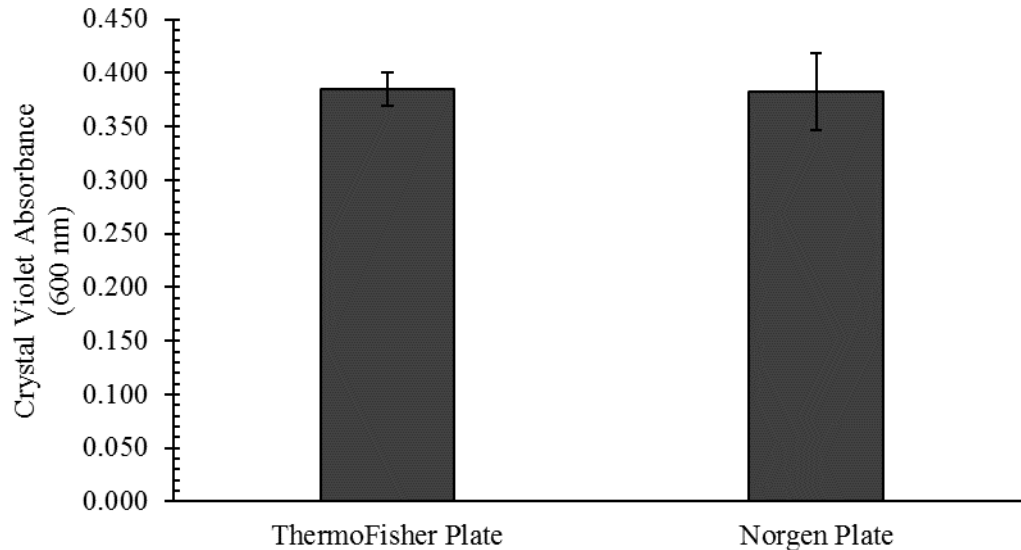


Figure 3.13. Norgen and ThermoFisher Scientific microtiter plate comparison biofilm assay No. 3. The bars represent the average amount of biofilm formed across three cultures. Quantities of biofilm were determined by measuring the absorbance at 600 nm after crystal violet bound to the biofilm was solubilized in 30 % acetic acid. Error bars represent the mean  $\pm$  standard deviation (n=3).  $p > 0.05$

The variations in the quantities of biofilms formed between these two plates can be attributed, in part, to the differences in plate manufacturing, giving rise to different physical and chemical stresses on the plate material. (Crowther, 2000; Robinson, Sadick, Deming, Estdale, & Bergelson, 2014; Zaitsev *et al.*, 2011) As a result, folds of varying height and direction can be introduced, which can greatly affect the adsorption properties of the microtiter plate wells. The variability in these structures can lead to either increases or decreases in the bacterial cell adhesion depending on the type of interactions it creates with the bacteria cell surface, in conjunction with other adhesion factors in the environment of the microtiter plate well. (Crawford *et al.*, 2012; Zaitsev *et al.*, 2011)

### **3.3.6. Qualitative analysis of topographical changes in polystyrene surfaces post abrasive treatment with 80-grit aluminum oxide**

As observed in the previous sections, the results of a biofilm assay can be effected by a number of factors. Plates from different suppliers or even different lots can lead to difference in the level of biofilm formation. (An & Friedman, 2000) With the inconsistent results from different batches of Fisherbrand™ (No. 12-565-501) plates and the lower levels of biofilm observed with Corning (No. 351172) plates, a polystyrene surface with a topography that could support higher, reproducible levels of biofilm would be desirable. To this end, microtiter plates were bombarded with 80-grit aluminum oxide (sand) particles to alter the surface topography and provide a greater surface area for the bacterial cells to adhere to. This form of modification is referred to as an abrasive treatment and was performed on the Corning (No. 351172) polystyrene microtiter plates. This type of modification has been shown to increase the adhesion of *S. epidermidis* on titanium surfaces (Wu *et al.*, 2011) as well as silicone (Tang *et al.*, 2009).

Scanning electron microscopy was performed at McMaster University at the Canadian Centre for Electron Microscopy to characterize the topographical differences between polystyrene plates with or without abrasive treatment. The area of the well near the center of the microtiter plate well wall was analyzed to provide the most accurate representation of the topography encountered by the bacterial cells once reaching the air-liquid interface.

Using backscattered electrons (BSE), contrast in images is generated due to the differences in the average atomic number of the material where electron scattering occurs. Areas where heavier elements are present create brighter images as electrons are more effectively scattered out of the sample to the detector. (Crewe & Lin, 1976; Kaczmarek, 1997; Welton, 1984) The BSE-SEM image for the polystyrene post abrasive treatment, displayed a high amount of heavier element particles of varying sizes scattered throughout the surface (Figure 3.14A). These particles are most

likely the aluminum oxide particles that remained impregnated on the surface after washing. The BSE-SEM image for the untreated polystyrene surface also displayed unknown heavier elements scattered over the polystyrene surface, but in much lower quantities (Figure 3.14C).

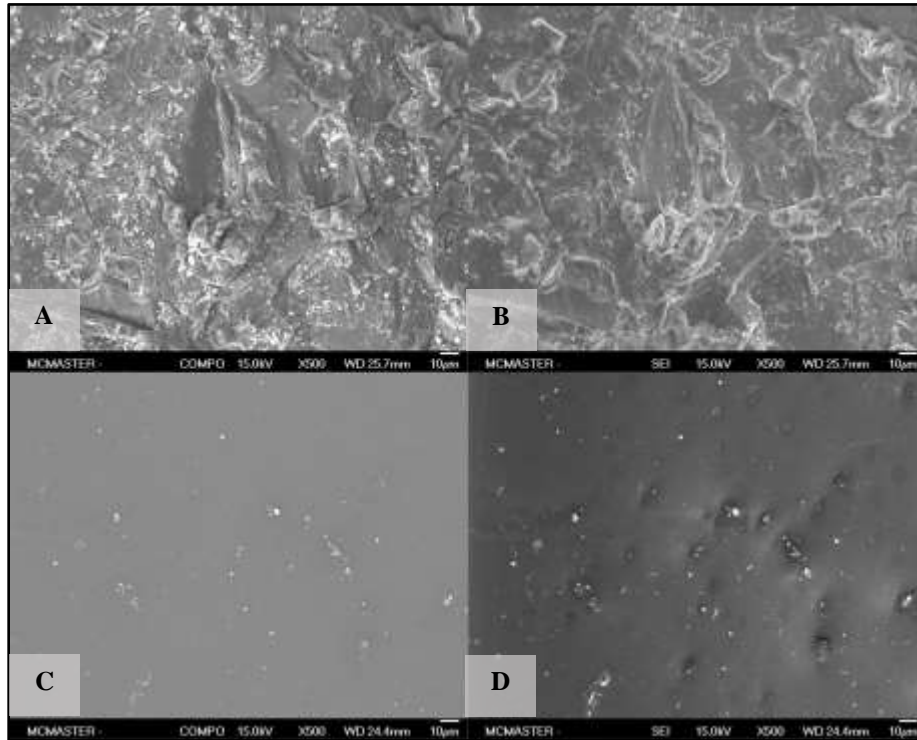


Figure 3.14. Comparison of polystyrene surface post abrasive treatment to the unmodified polystyrene surface using SEM. 15.0 kV used for SEM analysis at a magnification of 500x. Polystyrene post abrasive treatment (A) BSE-SEM (B) SEI-SEM. Unmodified polystyrene (C) BSE-SEM (D) SEI-SEM

When the same surface area was then scanned with low energy secondary electrons (SE), images of higher resolution were obtained to provide details about the surface topography. Structures protruding from the surface will scatter more electrons to be collected by the detector and thus appear brighter. Areas of the surface which are hidden from topographical features, do not obtain sufficient energy for the electrons to escape and thus appear darker. (Seiler, 1983; Welton, 1984)

Various structures of random spatial orientation were seen for the polystyrene post bombardment with aluminum oxide particles (Figure 3.14B). To increase the surface detail observed for the modified polystyrene surface, the beam energy was then reduced from 15.0 kV

to 2.0 kV, generating the secondary electron image (SEI) in Figure 3.15. This image is also a 1000x magnification of the same surface area observed in Figure 3.14B.

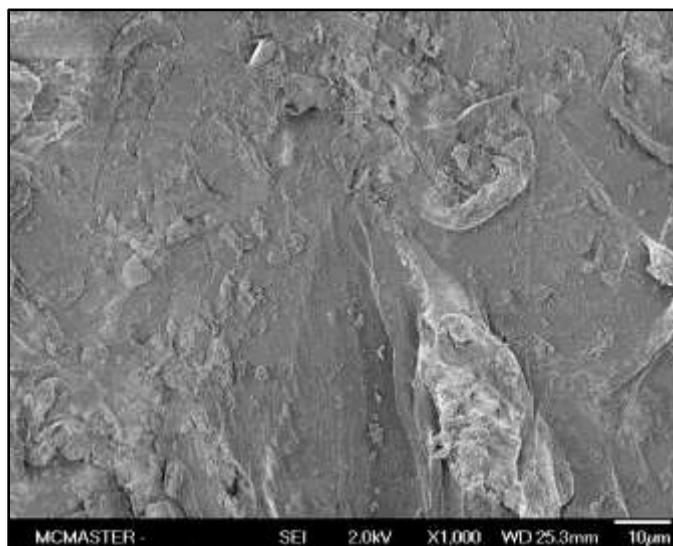


Figure 3.15. SEM analysis of polystyrene post abrasive treatment at 2.0 kV and 1000x magnification

As shown through both BSE and SE imaging, each surface provides a unique topographical profile for the formation of *P. fluorescens* Pf0-1 biofilm. The structures on the surface of the modified polystyrene can provide increased points of attachment during the initial phases of biofilm formation. The depressions and surface contaminants observed on the untreated polystyrene surface also have the potential to affect biofilm.

### **3.3.7. Quantitative analysis of biofilm formed on sandblasted Corning No. 351172 microtiter plates**

Biofilm formation assay was carried out on two individual microtiter plates, one treated by sandblasting as described in 3.2.8, and another untreated as a control. As shown in Figure 3.16A, the level of biofilm formed on the treated plates was more than double. Visual examination of the plate wells with biofilm stained with crystal violet showed continuous ring formation at the air-liquid interface (Figure 3.16C).

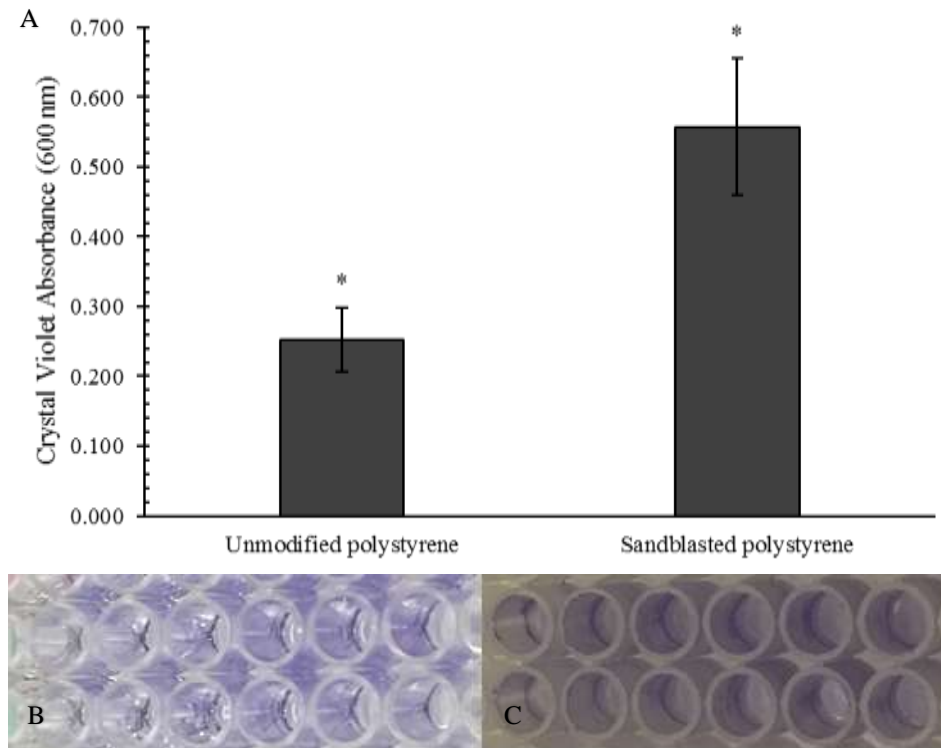


Figure 3.16. Comparison of *P. fluorescens* Pf0-1 biofilm formed on an unmodified polystyrene plate and a polystyrene plate post abrasive treatment. (A) Quantitative results from biofilm assay. The bars represent the average amount of biofilm formed. Quantities of biofilm were determined by measuring the absorbance at 600 nm after crystal violet bound to the biofilm was solubilized in 30 % acetic acid. Error bars represent the mean  $\pm$  standard deviation (n=12) Star represents significant difference in biofilm formed across microtiter plates tested  $*p \leq 4.7 \times 10^{-8}$  (B) *P. fluorescens* Pf0-1 biofilm post staining biofilm with 0.1% crystal violet in unmodified polystyrene wells. (C) *P. fluorescens* Pf0-1 biofilm post staining biofilm with 0.1% crystal violet in polystyrene wells that have undergone abrasive treatment.

In order to eliminate plate-to-plate variation in the comparison, subsequent biofilm assay experiments were carried out on a microtiter plate where half of the plate wells were sandblasted while the other half were not. This plate was produced by covering half of the plate during the sandblasting process. To eliminate edge-effects of microtiter plates, the perimeter of the treated and non-treated areas was not used to cultivate biofilm cultures (See Figure 3.17B). (SeraCare Life Sciences, 2013)

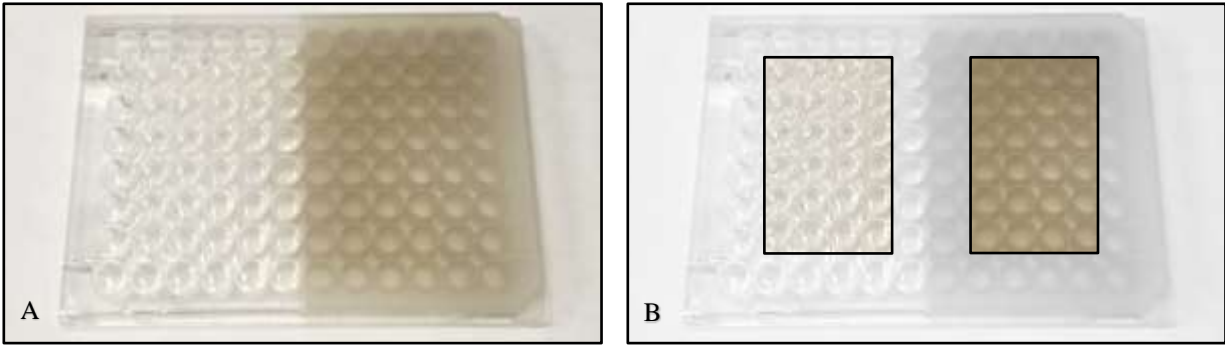


Figure 3.17. Photograph of sand-treated microtiter plate. (A) Photograph of Corning (Product No. 351172) microtiter plate after half of the plate has undergone sand-blast treatment. (B) The same photograph is Figure 3.18A however the highlighted portions represent the only wells used for inoculation.

Two replicate experiments were carried out on the “50/50” sand-treated microtiter plates. In both assays, the level of biofilm formation in treated wells was statistically significantly higher than that found in untreated wells (Figures 3.18 and 3.19). Each experiment, although performed at two different times and thus two separate cultures, produced quantities of biofilm on the modified polystyrene surface that were not statistically significant different from one another. The amount of biofilm formed in the unmodified polystyrene surface in the two replicates showed greater variation, however, both in statistically significantly lower quantity.

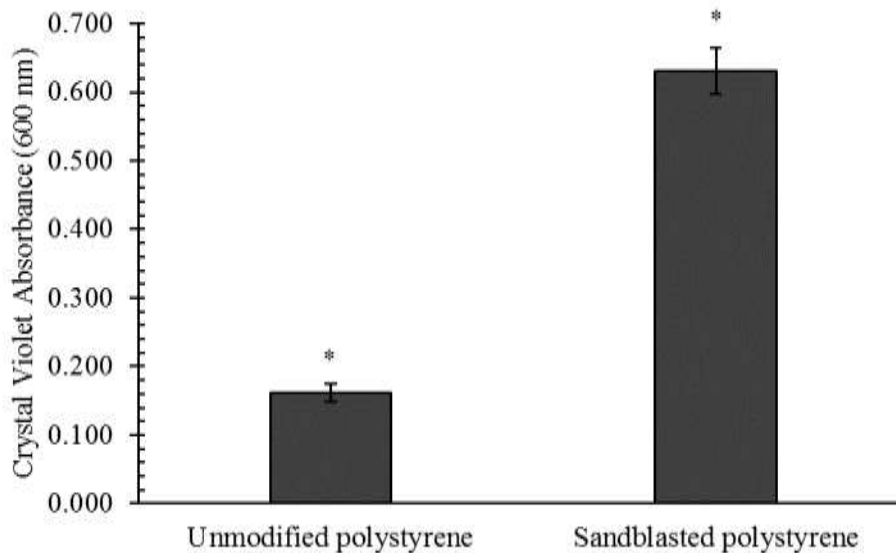


Figure 3.18. Quantitative comparison No. 1 of *P. fluorescens* Pf0-1 biofilm formed on unmodified and sandblasted polystyrene on the same plate. The bars represent the average amount of biofilm formed. Quantities of biofilm were determined by measuring the absorbance at 600 nm after crystal violet bound to the biofilm was solubilized in 30 % acetic acid. Error bars represent the mean  $\pm$  standard deviation (n=6) Star represents significant difference in biofilm formed between the two surface treatments on the same microtiter plate  $*p \leq 2.9 \times 10^{-8}$ .

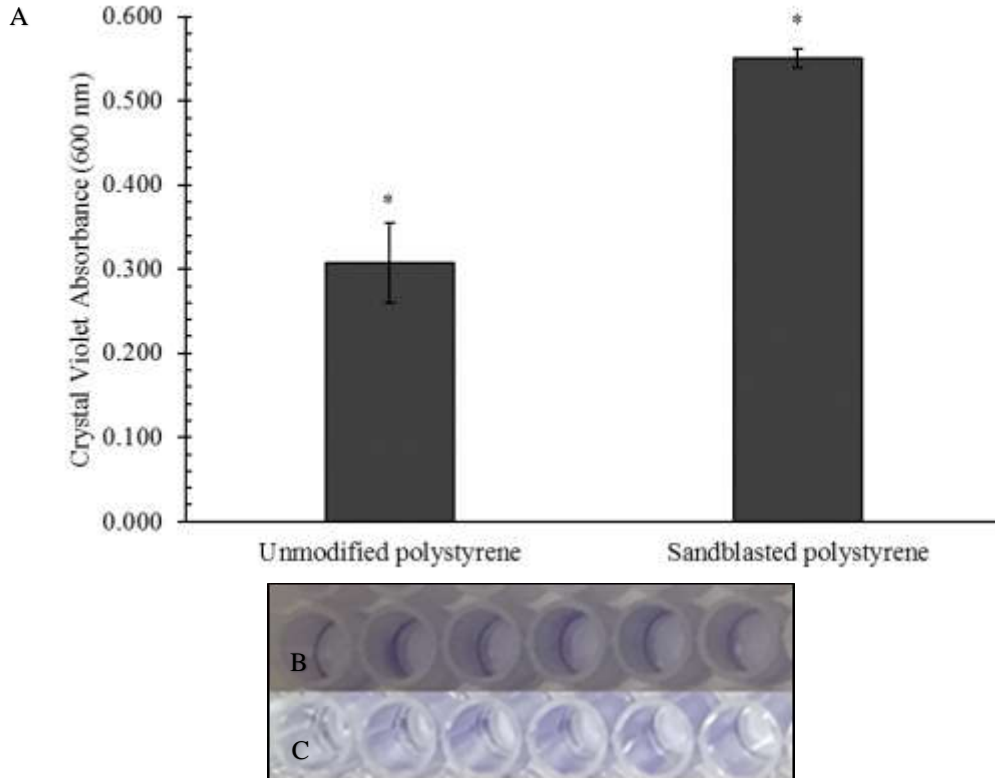


Figure 3.19. Quantitative comparison No. 2 of *P. fluorescens Pf0-1* biofilm formed on unmodified and sandblasted polystyrene. (A) Static biofilm assay results. The bars represent the average amount of biofilm formed. Quantities of biofilm were determined by measuring the absorbance at 600 nm after crystal violet bound to the biofilm was solubilized in 30 % acetic acid. Error bars represent the mean  $\pm$  standard deviation (n=6) Star represents significant difference in biofilm formed between the two surface treatments on the same microtiter plate  $*p \leq 3.2 \times 10^{-5}$ . (B) *P. fluorescens Pf0-1* biofilm post staining biofilm with 0.1% crystal violet in polystyrene wells that have undergone abrasive treatment. (C) *P. fluorescens Pf0-1* biofilm post staining biofilm with 0.1% crystal violet in unmodified polystyrene wells.

For each of the experiments a consistent biofilm ring is formed across the wells inoculated (Figure 3.16C and 3.19B), however, future studies should investigate potential differences in structural components between the biofilms formed on treated and untreated surfaces. Since the crystal violet staining is representative of the total biomass of biofilm, the increased quantities can be a result of more effective cell recruitment during initial attachment phases, increased reproductive activity or increase in structural components to hold the cells together on the different topography.

The abrasive treatment by sandblasting described above generates rough surfaces both in the well walls and the bottom of wells making it challenging to monitor culture growth spectrophotometrically. Therefore, small PTFE discs were inserted to the bottoms of the plate wells prior to the abrasive treatment process, preventing the bottom of the wells from being modified.

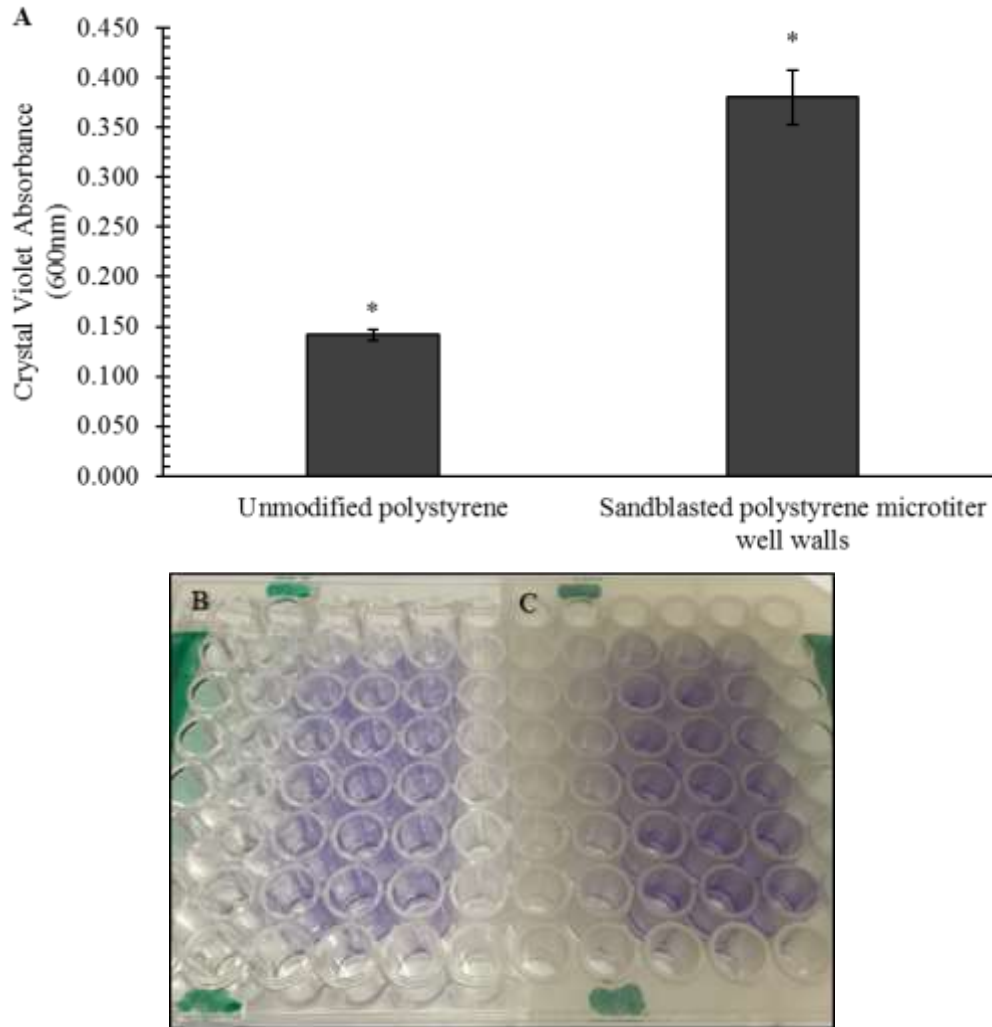


Figure 3.20. Quantitative comparison No. 3 of *P. fluorescens* Pf0-1 biofilm formed on unmodified and sandblasted polystyrene. (A) Static biofilm assay results. The bars represent the average amount of biofilm formed across three cultures. Quantities of biofilm were determined by measuring the absorbance at 600 nm after crystal violet bound to the biofilm was solubilized in 30 % acetic acid. Error bars represent the mean  $\pm$  standard deviation (n=3) Star represents significant difference in biofilm formed between the two surface treatments on the same microtiter plate.  $*p \leq 2.0 \times 10^{-3}$  (B) *P. fluorescens* Pf0-1 biofilm post staining biofilm with 0.1% crystal violet in unmodified polystyrene wells. (C) *P. fluorescens* Pf0-1 biofilm post staining biofilm with 0.1% crystal violet in polystyrene wells that have undergone sandblasting treatment only on the sides of the well. Green column represents the media blank control wells for both sides of the microtiter plates. Each culture was inoculated in an individual column to the right of the media control column (6 wells per culture)

Results in Figure 3.20 show a statistically significantly higher quantity of biofilm formed on the modified polystyrene surface overall across the three cultures tested, with more distinctive rings of biofilm present at the air liquid interface in the treated wells (Figure 3.20C).

The increase in biofilm formation observed could be attributed to not only the topography of the surface but also the presence of the aluminum oxide particulates impregnated on the surface post treatment (See SEM Results Section 3.3.4). To eliminate the potential effects from the aluminum oxide impregnation, another set of microtiter plates were modified using a drill press. The drill bit used to modify the polystyrene would not have left behind residue and thus changes in biofilm formation would be attributed solely to differences in topography. This treated surface should also be examined by SEM in future works to identify the extent in topography differences in comparison to the abrasive-treatment.

The final experiment involved the inoculation of four microtiter plates, two plates where only half of the wells were sandblasted, and the other two plates where only half of the wells were treated by the drill press. *P. fluorescens* Pf0-1 biofilms were cultured in M63 as well as LB broth to compare the effects of topography on biofilm development under different nutritional conditions.

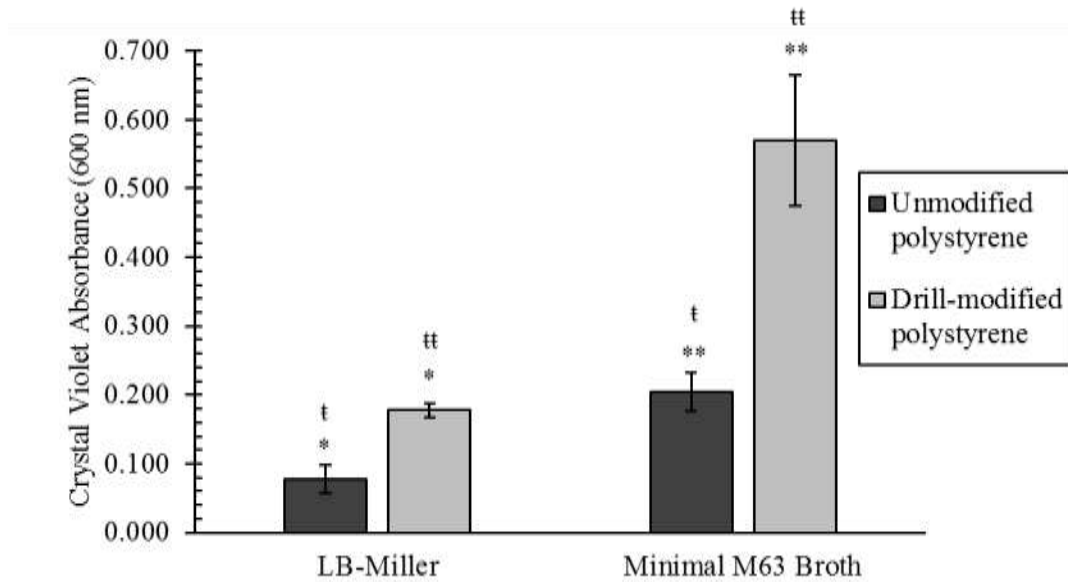


Figure 3.21. Quantitative comparison No. 4: *P. fluorescens* Pf0-1 biofilm formed on unmodified and drill-modified polystyrene plate No.1. The bars represent the average amount of biofilm formed. Quantities of biofilm were determined by measuring the absorbance at 600 nm after crystal violet bound to the biofilm was solubilized in 30 % acetic acid. Error bars represent the mean  $\pm$  standard deviation (n=6) Symbol represents significant difference in biofilm formed between the two surface treatments on the same microtiter plate \* $p \leq 1.3 \times 10^{-5}$  \*\* $p \leq 1.2 \times 10^{-4}$  † $p \leq 7.5 \times 10^{-6}$  †† $p \leq 1.5 \times 10^{-4}$

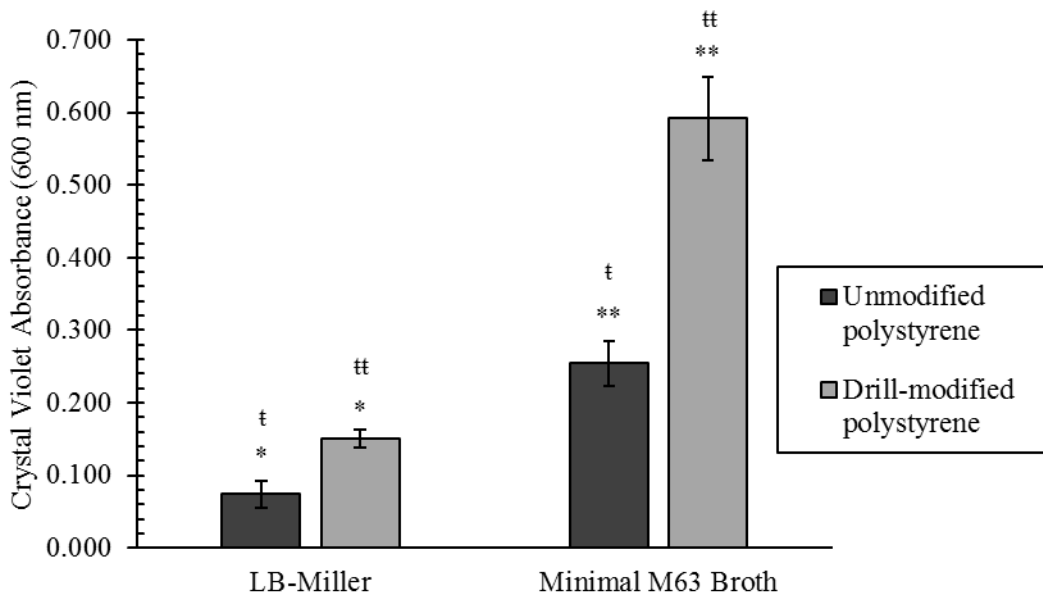


Figure 3.22. Quantitative comparison No. 4: *P. fluorescens* Pf0-1 biofilm formed on unmodified and drill-modified polystyrene plate No.2. The bars represent the average amount of biofilm formed. Quantities of biofilm were determined by measuring the absorbance at 600 nm after crystal violet bound to the biofilm was solubilized in 30 % acetic acid. Error bars represent the mean  $\pm$  standard deviation (n=6) Symbol represents significant difference in biofilm formed between the two surface treatments on the same microtiter plate \* $p \leq 2.0 \times 10^{-5}$  \*\* $p \leq 2.0 \times 10^{-6}$  † $p \leq 1.4 \times 10^{-6}$  †† $p \leq 4.0 \times 10^{-6}$

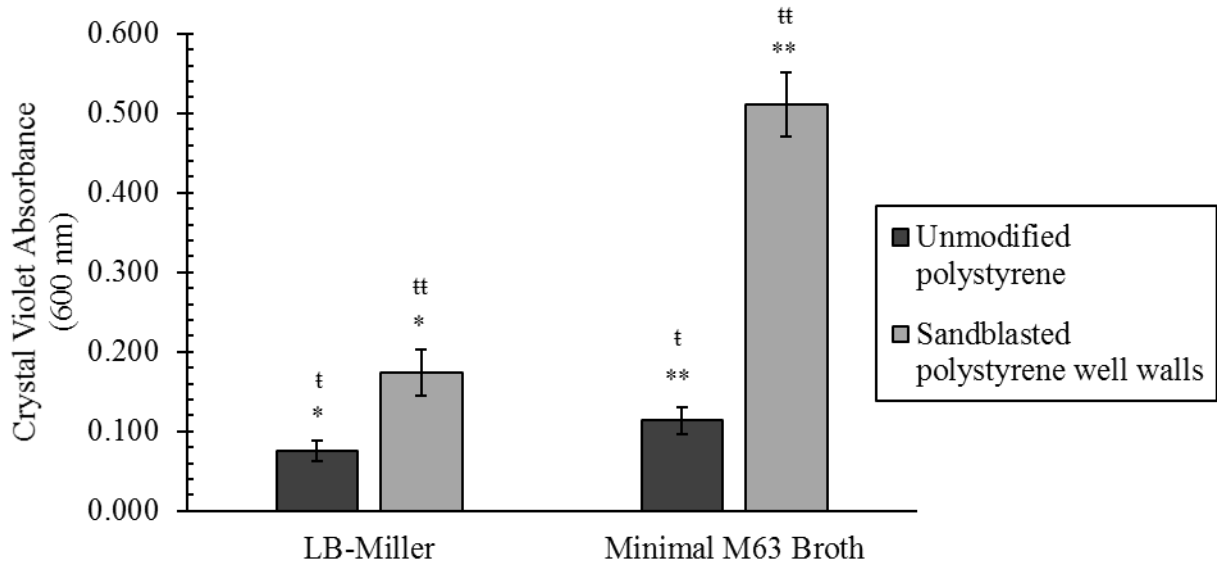


Figure 3.23. Quantitative comparison No. 4: *P. fluorescens* Pf0-1 biofilm formed on unmodified and sandblasted polystyrene plate No.1. The bars represent the average amount of biofilm formed. Quantities of biofilm were determined by measuring the absorbance at 600 nm after crystal violet bound to the biofilm was solubilized in 30 % acetic acid. Error bars represent the mean  $\pm$  standard deviation (n=6) Symbol represents significant difference in biofilm formed between the two surface treatments on the same microtiter plate \* $p \leq 0.002$  \*\* $p \leq 8.6 \times 10^{-8}$  † $p \leq 0.0003$  †† $p \leq 3.0 \times 10^{-7}$

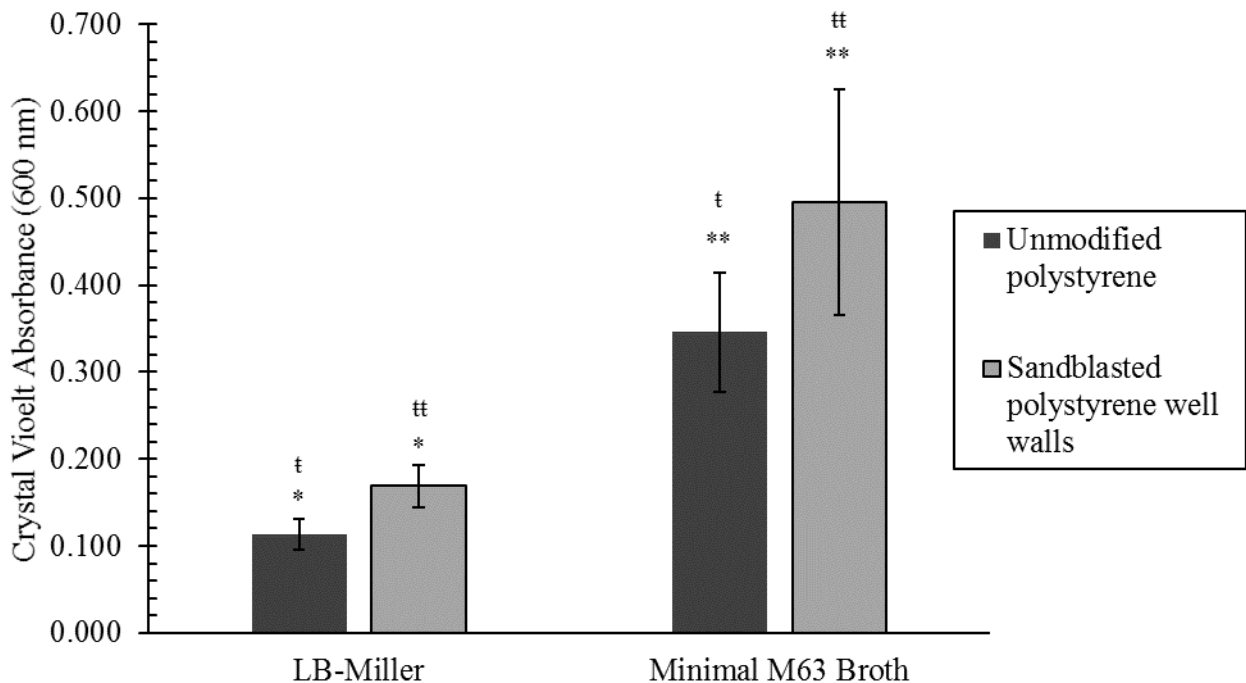


Figure 3.24. Quantitative comparison No. 4: *P. fluorescens* Pf0-1 biofilm formed on unmodified and sandblasted polystyrene plate No.2. The bars represent the average amount of biofilm formed. Quantities of biofilm were determined by measuring the absorbance at 600 nm after crystal violet bound to the biofilm was solubilized in 30 % acetic acid. Error bars represent the mean  $\pm$  standard deviation (n=6) Symbol represents significant difference in biofilm formed between the two surface treatments on the same microtiter plate \* $p \leq 0.001$  \*\* $p \leq 0.04$  † $p \leq 0.0003$  †† $p \leq 0.001$

In each set of plates, both sandblast and drill pressed treated surface modifications resulted in the significant increase in biofilm formed (Figure 3.21 – 3.24). The quantity of biofilm formed in M63 medium across the two drill-press modified polystyrene plates was highly reproducible, generating average crystal violet absorbance values of 0.569 for plate 1 and 0.592 for plate 2. In the case of the sandblasted polystyrene, the M63-grown culture reflected a slight decrease in the biofilm formed from plate 1 to plate 2 ( $p \leq 0.001$ ).

The quantity of biofilms cultivated in LB medium was also observed to increase a statistically significant amount across plates for the modified surface compared with the unmodified polystyrene control. However, the increases observed were not of the same extent as biofilm assay carried out in the M63 broth. The biofilm formation in the M63 broth in drill-press modified wells was at least 3 folds higher than that found in LB media. A similar trend was found in the sandblasted wells.

Future work will characterize the biofilms by, SEM, atomic force microscopy (AFM) and/or confocal laser scanning microscopy (CSLM), which would allow for the comparison of the attachment patterns on each surface and structural differences during microcolony development.

### **3.4. Concluding remarks and future works**

The initial goal of the work described in this chapter was to identify the potential factors that contribute to inconsistency found in the microtiter plate-based biofilm assay. The study began by exploring the quantity of biofilm formed across different brands of polystyrene microtiter plates to investigate the effects of different surface chemistries and manufacturing processes. Quantities of biofilm were found to vary on the surface of microtiter wells dependent on the lot used or the supplier. A non-tissue culture treated, hydrophobic, microtiter plate from Corning (No. 351172) was found to consistently form biofilm, however, at lower levels than that obtained in previous

work. (Bordeleau, 2014) Through the treatment of the Corning microtiter plates by sandblasting and a drill-press, statistically significant increases in biofilm quantities were observed that was reproducible across multiple plates of two different lots. It is suggested in the future to develop a holder for the microtiter plates that is set at a fixed distance from the uni-blaster, which is also mounted in place at a fixed angle to the plate. This will help to increase consistent treatment across sandblasted microtiter plates.

The use of these surfaces will expand the type of biofilm studies that can be conducted in this laboratory. A recent study in *V. cholerae* and *S. aureus* has shown quorum sensing expression to be affected by fluid flow as well as different topographies such as crevices or pores. (Kim, Ingremeau, Zhao, Bassler, & Stone, 2016) Thus, the modified surfaces produced in microtiter plates can be utilized in quorum sensing studies of *P. fluorescens* Pf0-1; to investigate connections between c-di-GMP mediated biofilm formation on these surfaces and quorum sensing networks.

## Chapter 4: Literature cited

- Agilent Technologies. (2009). *Metabolomics: Approaches Using Mass Spectrometry* (5990-4314EN).
- Alhede, M., Bjarnsholt, T., Jensen, P. Ø., Phipps, R. K., Moser, C., Christophersen, L., . . . Høiby, N. (2009). *Pseudomonas aeruginosa* recognizes and responds aggressively to the presence of polymorphonuclear leukocytes. *Microbiology*, *155*(11), 3500-3508.
- Allesen-Holm, M., Barken, K. B., Yang, L., Klausen, M., Webb, J. S., Kjelleberg, S., . . . Tolker-Nielsen, T. (2006). A characterization of DNA release in *Pseudomonas aeruginosa* cultures and biofilms. *Molecular microbiology*, *59*(4), 1114-1128.
- Ameen, E., & da Silva, A. M. (2014). Undergraduate Research. Brock University.
- Amikam, D., & Galperin, M. Y. (2006). PilZ domain is part of the bacterial c-di-GMP binding protein. *Bioinformatics*, *22*(1), 3-6.
- An, Y. H., & Friedman, R. J. (2000). *Handbook of bacterial adhesion: principles, methods, and applications* (Vol. 204): Springer Science & Business Media.
- Anetzberger, C., Pirch, T., & Jung, K. (2009). Heterogeneity in quorum sensing-regulated bioluminescence of *Vibrio harveyi*. *Molecular microbiology*, *73*(2), 267-277.
- Barraud, N., Kjelleberg, S., & Rice, S. A. (2015). Dispersal from Microbial Biofilms. *Microbiology spectrum*, *3*(6).
- Bell, M. (2014). Identification of acyl-homoserine lactones in *Pseudomonas fluorescens* using LCMS/MS. Bachelor of Science Honour's Thesis. Brock University.
- Berne, C., Ducret, A., Hardy, G. G., & Brun, Y. V. (2015). Adhesins involved in attachment to abiotic surfaces by Gram-Negative bacteria. *Microbiology spectrum*, *3*(4).
- Beškosi, V., Gojgić-Cvijović, G., Jovančićević, B., & Vrvic, M. (2012). In Salih B., & Çelikbıçak Ö., (Eds.) Gas Chromatograph in Environmental Sciences and Evaluation of Bioremediation. *Gas Chromatography–Biochemicals, Narcotics and Essential Oils*, pp. 3-28.
- Bigger, J. (1944). Treatment of staphylococcal infections with penicillin by intermittent sterilisation. *The Lancet*, *244*(6320), 497-500.
- Bjarnsholt, T., Jensen, P. Ø., Burmølle, M., Hentzer, M., Haagensen, J. A., Hougen, H. P., . . . Molin, S. (2005). *Pseudomonas aeruginosa* tolerance to tobramycin, hydrogen peroxide and polymorphonuclear leukocytes is quorum-sensing dependent. *Microbiology*, *151*(2), 373-383.
- Bjarnsholt, T., Jensen, P. Ø., Moser, C. E., & Høiby, N. (2010). *Biofilm infections*. Springer Publishing Company.
- Bordeleau, E. (2014). The effect of c-di-GMP and analogues on biofilm formation in *Pseudomonas fluorescens* and *Escherichia coli*. Bachelor of Science Honour's Thesis. Brock University.
- Brameyer, S., Bode, H. B., & Heermann, R. (2015). Languages and dialects: bacterial communication beyond homoserine lactones. *Trends in microbiology*, *23*(9), 521-523.
- Byrd, J. J., Cheville, A. M., Bose, J. L., & Kaspar, C. W. (1999). Lethality of a heat-and phosphate-catalyzed glucose by-product to *Escherichia coli* O157: H7 and partial protection conferred by the rpoSRegulon. *Applied and environmental microbiology*, *65*(6), 2396-2401.
- Cataldi, T., Bianco, G., Frommberger, M., & Schmitt-Kopplin, P. (2004). Direct analysis of selected N-acyl-L-homoserine lactones by gas chromatography/mass spectrometry. *Rapid communications in mass spectrometry*, *18*(12), 1341-1344.
- Cathcart, G. R., Quinn, D., Greer, B., Harriott, P., Lynas, J. F., Gilmore, B. F., & Walker, B. (2011). Novel inhibitors of the *Pseudomonas aeruginosa* virulence factor LasB: a potential therapeutic approach for the attenuation of virulence mechanisms in pseudomonal infection. *Antimicrobial agents and chemotherapy*, *55*(6), 2670-2678.
- Corning Life Sciences. (2013). Customer Technical Data Sheet - Microtest TC Plates - 96 Well - Flat Bottom.
- Corning Life Sciences. (2015). Corning and Falcon Microplate Selection Guide For Assays and Drug Discovery. (CLS-C-DL-MP-014 REV3 ed.).
- Costerton, J. W. (2007). *The biofilm primer* (Vol. 1): Springer Science & Business Media.

- Costerton, J. W., Stewart, P. S., & Greenberg, E. P. (1999). Bacterial biofilms: a common cause of persistent infections. *Science*, 284(5418), 1318-1322.
- Crawford, R. J., Webb, H. K., Truong, V. K., Hasan, J., & Ivanova, E. P. (2012). Surface topographical factors influencing bacterial attachment. *Advances in colloid and interface science*, 179, 142-149.
- Crewe, A., & Lin, P. (1976). The use of backscattered electrons for imaging purposes in a scanning electron microscope. *Ultramicroscopy*, 1(3), 231-238.
- Crowther, J. R. (2000). *The ELISA guidebook* (Vol. 149): Springer Science & Business Media.
- Cullum, N., Meng, C. K., & Zavitsanos, P. (2004). Effect of Sample Matrix on Suppression of Ionization in Water Samples Using LC-ESI-MS. *Agilent Technologies*: Santa Clara, CA, 1-10.
- De Kievit, T. R., Gillis, R., Marx, S., Brown, C., & Iglewski, B. H. (2001). Quorum-sensing genes in *Pseudomonas aeruginosa* biofilms: their role and expression patterns. *Applied and environmental microbiology*, 67(4), 1865-1873.
- Deng, Y., Schmid, N., Wang, C., Wang, J., Pessi, G., Wu, D., . . . Chang, C. (2012). Cis-2-dodecenoic acid receptor RpfR links quorum-sensing signal perception with regulation of virulence through cyclic dimeric guanosine monophosphate turnover. *Proceedings of the National Academy of Sciences*, 109(38), 15479-15484.
- Donlan, R. M. (2002). Biofilms: microbial life on surfaces. *Emerg Infect Dis*, 8(9), 881-890
- El-Sayed, A. K., Hothersall, J., Cooper, S. M., Stephens, E., Simpson, T. J., & Thomas, C. M. (2003). Characterization of the mupirocin biosynthesis gene cluster from *Pseudomonas fluorescens* NCIMB 10586. *Chemistry & biology*, 10(5), 419-430.
- El-Sayed, A. K., Hothersall, J., & Thomas, C. M. (2001). Quorum-sensing-dependent regulation of biosynthesis of the polyketide antibiotic mupirocin in *Pseudomonas fluorescens* NCIMB 10586. *Microbiology*, 147(8), 2127-2139.
- Engebrecht, J., Neelson, K., & Silverman, M. (1983). Bacterial bioluminescence: isolation and genetic analysis of functions from *Vibrio fischeri*. *Cell*, 32(3), 773-781.
- Fazli, M., Almblad, H., Rybtke, M. L., Givskov, M., Eberl, L., & Tolker-Nielsen, T. (2014). Regulation of biofilm formation in *Pseudomonas* and *Burkholderia* species. *Environmental microbiology*, 16(7), 1961-1981.
- Finkelstein, R. A., & Lankford, C. E. (1957). A bacteriotoxic substance in autoclaved culture media containing glucose and phosphate. *Applied microbiology*, 5(2), 74-79.
- Fletcher, M. (1976). The effects of proteins on bacterial attachment to polystyrene. *Microbiology*, 94(2), 400-404.
- Forssk, I., Popoff, T., & Theander, O. (1976). Reactions of D-xylose and D-glucose in alkaline, aqueous solutions. *Carbohydrate Research*, 48(1), 13-21.
- Franklin, M. J., Chang, C., Akiyama, T., & Bothner, B. (2015). New Technologies for Studying Biofilms. *Microbiology spectrum*, 3(4).
- Fuqua, C., & Greenberg, E. P. (2002). Listening in on bacteria: acyl-homoserine lactone signalling. *Nature Reviews Molecular Cell Biology*, 3(9), 685-695.
- Fuqua, C., Parsek, M. R., & Greenberg, E. P. (2001). Regulation of gene expression by cell-to-cell communication: acyl-homoserine lactone quorum sensing. *Annual review of genetics*, 35(1), 439-468.
- Gambello, M. J., & Iglewski, B. H. (1991). Cloning and characterization of the *Pseudomonas aeruginosa* lasR gene, a transcriptional activator of elastase expression. *Journal of bacteriology*, 173(9), 3000-3009.
- Gambello, M. J., Kaye, S., & Iglewski, B. H. (1993). LasR of *Pseudomonas aeruginosa* is a transcriptional activator of the alkaline protease gene (apr) and an enhancer of exotoxin A expression. *Infection and immunity*, 61(4), 1180-1184.
- Gerke, N., & Grzeskowiak R., (2015). *Leachables: Minimizing the Influence of Plastic Consumables on the Laboratory Workflows*. Retrieved from Eppendorf White Paper 026
- Gibbs, J., & Kennebunk, M. (2001). Immobilization Principles—Selecting the Surface. *ELISA Technical Bulletin*(1), 1-8.

- Gomelsky, M., & Klug, G. (2002). BLUF: a novel FAD-binding domain involved in sensory transduction in microorganisms. *Trends in biochemical sciences*, 27(10), 497-500.
- Ha, D.-G., & O'Toole, G. A. (2015). c-di-GMP and its effects on biofilm formation and dispersion: a *Pseudomonas aeruginosa* review. *Microbiology spectrum*, 3(2), 5-20
- Hagen, S. J. (2015). *The Physical Basis of Bacterial Quorum Communication*: Springer.
- Hartmann, A., Rothballer, M., Hense, B. A., & Schröder, P. (2015). Bacterial quorum sensing compounds are important modulators of microbe-plant interactions. *The plant microbiome and its importance for plant and human health*, 41.
- Hecht, G. B., & Newton, A. (1995). Identification of a novel response regulator required for the swarmer-to-stalked-cell transition in *Caulobacter crescentus*. *Journal of bacteriology*, 177(21), 6223-6229.
- Hense, B. A., Müller, J., Kuttler, C., & Hartmann, A. (2012). Spatial heterogeneity of autoinducer regulation systems. *Sensors*, 12(4), 4156-4171.
- Hentzer, M., Riedel, K., Rasmussen, T. B., Heydorn, A., Andersen, J. B., Parsek, M. R., . . . Høiby, N. (2002). Inhibition of quorum sensing in *Pseudomonas aeruginosa* biofilm bacteria by a halogenated furanone compound. *Microbiology*, 148(1), 87-102.
- Hinsa, S. M., & O'Toole, G. A. (2006). Biofilm formation by *Pseudomonas fluorescens* WCS365: a role for LapD. *Microbiology*, 152(5), 1375-1383.
- Hoffman, L. R., Kulasekara, H. D., Emerson, J., Houston, L. S., Burns, J. L., Ramsey, B. W., & Miller, S. I. (2009). *Pseudomonas aeruginosa* lasR mutants are associated with cystic fibrosis lung disease progression. *Journal of Cystic Fibrosis*, 8(1), 66-70.
- Hothersall, J., Murphy, A. C., Iqbal, Z., Campbell, G., Stephens, E. R., Wu, J. e., . . . Crosby, J. (2011). Manipulation of quorum sensing regulation in *Pseudomonas fluorescens* NCIMB 10586 to increase mupirocin production. *Applied microbiology and biotechnology*, 90(3), 1017-1026.
- Høyland-Kroghsbo, N. M., Paczkowski, J., Mukherjee, S., Broniewski, J., Westra, E., Bondy-Denomy, J., & Bassler, B. L. (2016). Quorum sensing controls the *Pseudomonas aeruginosa* CRISPR-Cas adaptive immune system. *Proceedings of the National Academy of Sciences*, 201617415.
- Hsu, L. C., Fang, J., Borca-Tasciuc, D. A., Worobo, R. W., & Moraru, C. I. (2013). Effect of micro-and nanoscale topography on the adhesion of bacterial cells to solid surfaces. *Applied and environmental microbiology*, 79(8), 2703-2712.
- Hufnagel, D. A., Depas, W. H., & Chapman, M. R. (2015). The Biology of the *Escherichia coli* Extracellular Matrix. *Microbiology spectrum*, 3(3).
- Jensen, P. Ø., Bjarnsholt, T., Phipps, R., Rasmussen, T. B., Calum, H., Christoffersen, L., . . . Givskov, M. (2007). Rapid necrotic killing of polymorphonuclear leukocytes is caused by quorum-sensing-controlled production of rhamnolipid by *Pseudomonas aeruginosa*. *Microbiology*, 153(5), 1329-1338.
- Jimenez, P. N., Koch, G., Thompson, J. A., Xavier, K. B., Cool, R. H., & Quax, W. J. (2012). The multiple signaling systems regulating virulence in *Pseudomonas aeruginosa*. *Microbiology and Molecular Biology Reviews*, 76(1), 46-65.
- Kaczmarek, D. (1997). The method of increasing COMPO contrast by linearization of backscattering characteristic  $\eta = f(Z)$ . *Scanning*, 19(4), 310-315.
- Kalia, D., Merey, G., Nakayama, S., Zheng, Y., Zhou, J., Luo, Y., . . . Sintim, H. O. (2013). Nucleotide, c-di-GMP, c-di-AMP, cGMP, cAMP(p) ppGpp signaling in bacteria and implications in pathogenesis. *Chemical Society Reviews*, 42(1), 305-341.
- Kalia, V. C. (Ed.). (2015). *Quorum sensing vs quorum quenching: a battle with no end in sight*. Springer India.
- Kaplan, J. á. (2010). Biofilm dispersal: mechanisms, clinical implications, and potential therapeutic uses. *Journal of dental research*, 89(3), 205-218.
- Kim, M. K., Ingremeau, F., Zhao, A., Bassler, B. L., & Stone, H. A. (2016). Local and global consequences of flow on bacterial quorum sensing. *Nature Microbiology*, 1, 15005.
- Kwak, Y.-S., & Weller, D. M. (2013). Take-all of wheat and natural disease suppression: a review. *The plant pathology journal*, 29(2), 125.

- Laue, B. E., Jiang, Y., Chhabra, S. R., Jacob, S., Stewart, G. S., Hardman, A., . . . Williams, P. (2000). The biocontrol strain *Pseudomonas fluorescens* F113 produces the Rhizobium small bacteriocin, N-(3-hydroxy-7-cis-tetradecenoyl) homoserine lactone, via HdtS, a putative novel N-acylhomoserine lactone synthase. *Microbiology*, *146*(10), 2469-2480.
- Lee, J., & Zhang, L. (2015). The hierarchy quorum sensing network in *Pseudomonas aeruginosa*. *Protein & cell*, *6*(1), 26-41.
- Leid, J. G., Willson, C. J., Shirliff, M. E., Hassett, D. J., Parsek, M. R., & Jeffers, A. K. (2005). The exopolysaccharide alginate protects *Pseudomonas aeruginosa* biofilm bacteria from IFN- $\gamma$ -mediated macrophage killing. *The Journal of Immunology*, *175*(11), 7512-7518.
- McDonald, G. R., Hudson, A. L., Dunn, S. M., You, H., Baker, G. B., Whittall, R. M., . . . Holt, A. (2008). Bioactive contaminants leach from disposable laboratory plasticware. *Science*, *322*(5903), 917-917.
- McLafferty, F. W. (1959). Mass spectrometric analysis. Molecular rearrangements. *Analytical Chemistry*, *31*(1), 82-87.
- Mei, L., Busscher, H. J., van der Mei, H. C., & Ren, Y. (2011). Influence of surface roughness on streptococcal adhesion forces to composite resins. *Dental materials*, *27*(8), 770-778.
- Mitik-Dineva, N., Wang, J., Truong, V. K., Stoddart, P., Malherbe, F., Crawford, R. J., & Ivanova, E. P. (2009). *Escherichia coli*, *Pseudomonas aeruginosa*, and *Staphylococcus aureus* Attachment Patterns on Glass Surfaces with Nanoscale Roughness. *Current Microbiology*, *58*(3), 268-273.
- Müsken, M., Di Fiore, S., Römling, U., & Häussler, S. (2010). A 96-well-plate-based optical method for the quantitative and qualitative evaluation of *Pseudomonas aeruginosa* biofilm formation and its application to susceptibility testing. *Nature protocols*, *5*(8), 1460-1469.
- Newell, P. D., Boyd, C. D., Sondermann, H., & O'Toole, G. A. (2011). A c-di-GMP effector system controls cell adhesion by inside-out signaling and surface protein cleavage. *PLoS Biol*, *9*(2), e1000587.
- Newell, P. D., Monds, R. D., & O'Toole, G. A. (2009). LapD is a bis-(3', 5')-cyclic dimeric GMP-binding protein that regulates surface attachment by *Pseudomonas fluorescens* Pf0-1. *Proceedings of the National Academy of Sciences*, *106*(9), 3461-3466.
- Nielsen, A. T., Tolker-Nielsen, T., Barken, K. B., & Molin, S. (2000). Role of commensal relationships on the spatial structure of a surface-attached microbial consortium. *Environmental microbiology*, *2*(1), 59-68.
- O'Toole, G. A. (2011). Microtiter dish biofilm formation assay. *JoVE (Journal of Visualized Experiments)*(47), e2437-e2437.
- O'Toole, G. A., & Kolter, R. (1998). Initiation of biofilm formation in *Pseudomonas fluorescens* WCS365 proceeds via multiple, convergent signalling pathways: a genetic analysis. *Molecular microbiology*, *28*(3), 449-461.
- Ochsner, U. A., & Reiser, J. (1995). Autoinducer-mediated regulation of rhamnolipid biosurfactant synthesis in *Pseudomonas aeruginosa*. *Proceedings of the National Academy of Sciences*, *92*(14), 6424-6428.
- Olivieri, A., Degenhardt, O. S., McDonald, G. R., Narang, D., Paulsen, I. M., Kozuska, J. L., & Holt, A. (2012). On the disruption of biochemical and biological assays by chemicals leaching from disposable laboratory plasticware. *Canadian journal of physiology and pharmacology*, *90*(6), 697-703.
- Osorno, O., Castellanos, L., Ramos, F. A., & Arévalo, C. (2012). Gas chromatography as a tool in quorum sensing studies. *Gas Chromatography-Biochemicals, Narcotics and Essential Oils. Intech, Croatia*, 67-96.
- Palmer, K. L., Aye, L. M., & Whiteley, M. (2007). Nutritional cues control *Pseudomonas aeruginosa* multicellular behavior in cystic fibrosis sputum. *Journal of bacteriology*, *189*(22), 8079-8087.
- Pamp, S. J., Gjermansen, M., Johansen, H. K., & Tolker-Nielsen, T. (2008). Tolerance to the antimicrobial peptide colistin in *Pseudomonas aeruginosa* biofilms is linked to metabolically

- active cells, and depends on the pmr and mexAB-oprM genes. *Molecular microbiology*, 68(1), 223-240.
- Papenfort, K., & Bassler, B. L. (2016). Quorum sensing signal-response systems in Gram-negative bacteria. *Nature Reviews Microbiology*, 14(9), 576-588.
- Passador, L., Cook, J. M., Gambello, M. J., Rust, L., & Iglewski, B. H. (1993). Expression of *Pseudomonas aeruginosa* virulence genes requires cell-to-cell communication. *Science*, 260(5111), 1127-1130.
- Patel, H. K., Suárez-Moreno, Z. R., Degrassi, G., Subramoni, S., González, J. F., & Venturi, V. (2013). Bacterial LuxR solos have evolved to respond to different molecules including signals from plants. *Frontiers in plant science*, 4, 447.
- Patterson, A. G., Jackson, S. A., Taylor, C., Evans, G. B., Salmond, G. P., Przybilski, R., . . . Fineran, P. C. (2016). Quorum Sensing Controls Adaptive Immunity through the Regulation of Multiple CRISPR-Cas Systems. *Molecular Cell*.
- Pearson, J. P., Van Delden, C., & Iglewski, B. H. (1999). Active efflux and diffusion are involved in transport of *Pseudomonas aeruginosa* cell-to-cell signals. *Journal of bacteriology*, 181(4), 1203-1210.
- Penesyan, A., Gillings, M., & Paulsen, I. T. (2015). Antibiotic discovery: combatting bacterial resistance in cells and in biofilm communities. *Molecules*, 20(4), 5286-5298.
- Pringle, J., & Fletcher, M. (1986). Influence of substratum hydration and adsorbed macromolecules on bacterial attachment to surfaces. *Applied and environmental microbiology*, 51(6), 1321-1325.
- Rani, S., Kumar, A., Malik, A. K., & Schmitt-Kopplin, P. (2011). Occurrence of N-Acyl homoserine lactones in extracts of bacterial strain of *Pseudomonas aeruginosa* and in sputum sample evaluated by gas chromatography–mass spectrometry. *American Journal of Analytical Chemistry*, 2(02), 294.
- Robinson, C. J., Sadick, M., Deming, S. N., Estdale, S., & Bergelson, S. (2014). Assay Acceptance Criteria for Multiwell-Plate–Based Biological Potency Assays. *BioProcess Int*, 12(1).
- Roilides, E., Simitopoulou, M., Katragkou, A., & Walsh, T. J. (2015). How biofilms evade host defenses. *Microbiology spectrum*, 3(3).
- Römling, U., Galperin, M. Y., & Gomelsky, M. (2013). Cyclic di-GMP: the first 25 years of a universal bacterial second messenger. *Microbiology and Molecular Biology Reviews*, 77(1), 1-52.
- Ross, P., Weinhouse, H., Aloni, Y., Michaeli, D., Weinberger-Ohana, P., Mayer, R., . . . Van Boom, J. (1987). Regulation of cellulose synthesis in *Acetobacter xylinum* by cyclic diguanylic acid.
- Ryan, R. P., Fouhy, Y., Lucey, J. F., Crossman, L. C., Spiro, S., He, Y.-W., . . . Williams, P. (2006). Cell–cell signaling in *Xanthomonas campestris* involves an HD-GYP domain protein that functions in cyclic di-GMP turnover. *Proceedings of the National Academy of Sciences*, 103(17), 6712-6717.
- Ryjenkov, D. A., Simm, R., Römling, U., & Gomelsky, M. (2006). The PilZ domain is a receptor for the second messenger c-di-GMP: the PilZ domain protein YcgR controls motility in Enterobacteria. *Journal of Biological Chemistry*, 281(41), 30310-30314.
- Sauer, K., Camper, A. K., Ehrlich, G. D., Costerton, J. W., & Davies, D. G. (2002). *Pseudomonas aeruginosa* displays multiple phenotypes during development as a biofilm. *Journal of bacteriology*, 184(4), 1140-1154.
- Scales, B. S., Dickson, R. P., LiPuma, J. J., & Huffnagle, G. B. (2014). Microbiology, genomics, and clinical significance of the *Pseudomonas fluorescens* species complex, an unappreciated colonizer of humans. *Clinical microbiology reviews*, 27(4), 927-948.
- Schikora, A., Schenk, S. T., & Hartmann, A. (2016). Beneficial effects of bacteria-plant communication based on quorum sensing molecules of the N-acyl homoserine lactone group. *Plant molecular biology*, 90(6), 605-612.
- Seiler, H. (1983). Secondary electron emission in the scanning electron microscope. *Journal of Applied Physics*, 54(11), R1-R18.

- SeraCare Life Sciences. (2013) *Technical Guide for ELISA*. Retrieved from <https://www.seracare.com/globalassets/resources/technical-guides/guide-kpl-elisa-technical-guide.pdf>
- Silby, M. W., Winstanley, C., Godfrey, S. A., Levy, S. B., & Jackson, R. W. (2011). *Pseudomonas* genomes: diverse and adaptable. *FEMS microbiology reviews*, 35(4), 652-680.
- Silvestro, L., Tarcomnicu, I., & Savu, S. R. (2013). Matrix effects in mass spectrometry combined with separation methods—comparison HPLC, GC and discussion on methods to control these effects. *Tandem mass spectrometry—molecular characterization. InTech Publisher, Rijeka*, 3-37.
- Song, F., Koo, H., & Ren, D. (2015). Effects of material properties on bacterial adhesion and biofilm formation. *Journal of dental research*, 94(8), 1027-1034.
- Srivastava, D., & Waters, C. M. (2012). A tangled web: regulatory connections between quorum sensing and cyclic di-GMP. *Journal of bacteriology*, 194(17), 4485-4493.
- Stepanović, S., Vuković, D., Hola, V., Bonaventura, G. D., Djukić, S., Ćirković, I., & Ruzicka, F. (2007). Quantification of biofilm in microtiter plates: overview of testing conditions and practical recommendations for assessment of biofilm production by staphylococci. *Apmis*, 115(8), 891-899.
- Stewart, P. S. (2015). Antimicrobial tolerance in biofilms. *Microbiology spectrum*, 3(3).
- Stewart, P. S., & Franklin, M. J. (2008). Physiological heterogeneity in biofilms. *Nature Reviews Microbiology*, 6(3), 199-210.
- Tal, R., Wong, H. C., Calhoon, R., Gelfand, D., Fear, A. L., Volman, G., . . . Weinhouse, H. (1998). Three *cdg* operons control cellular turnover of cyclic di-GMP in *Acetobacter xylinum*: genetic organization and occurrence of conserved domains in isoenzymes. *Journal of bacteriology*, 180(17), 4416-4425.
- Tang, H., Cao, T., Liang, X., Wang, A., Salley, S. O., McAllister, J., & Ng, K. (2009). Influence of silicone surface roughness and hydrophobicity on adhesion and colonization of *Staphylococcus epidermidis*. *Journal of Biomedical Materials Research Part A*, 88(2), 454-463.
- Taylor, B. L., & Zhulin, I. B. (1999). PAS domains: internal sensors of oxygen, redox potential, and light. *Microbiology and Molecular Biology Reviews*, 63(2), 479-506.
- Taylor, M. W., Schupp, P. J., Baillie, H. J., Charlton, T. S., De Nys, R., Kjelleberg, S., & Steinberg, P. D. (2004). Evidence for acyl homoserine lactone signal production in bacteria associated with marine sponges. *Applied and environmental microbiology*, 70(7), 4387-4389.
- ThermoFisher Scientific. (2014). Thermo Scientific Microplates Guide *Nunc Plate Selection Guide*.
- Tischler, A. D., & Camilli, A. (2004). Cyclic diguanylate (c-di-GMP) regulates *Vibrio cholerae* biofilm formation. *Molecular microbiology*, 53(3), 857-869.
- Toder, D., Gambello, M., & Iglewski, B. (1991). *Pseudomonas aeruginosa* LasA: a second elastase under the transcriptional control of lasR. *Molecular microbiology*, 5(8), 2003-2010.
- Tolker-Nielsen, T. (2015). Biofilm Development. *Microbiology spectrum*, 3(2).
- Tuson, H. H., & Weibel, D. B. (2013). Bacteria–surface interactions. *Soft matter*, 9(17), 4368-4380.
- Van Houdt, R., & Michiels, C. W. (2010). Biofilm formation and the food industry, a focus on the bacterial outer surface. *Journal of applied microbiology*, 109(4), 1117-1131.
- Venturi, V., & Ahmer, B. M. (2015). Editorial: LuxR Solos are Becoming Major Players in Cell–Cell Communication in Bacteria. *Frontiers in cellular and infection microbiology*, 5.
- Verran, J., Jackson, S., Coulthwaite, L., Scallan, A., Loewy, Z., & Whitehead, K. (2014). The effect of dentifrice abrasion on denture topography and the subsequent retention of microorganisms on abraded surfaces. *The Journal of prosthetic dentistry*, 112(6), 1513-1522.
- Waters, C. M., Lu, W., Rabinowitz, J. D., & Bassler, B. L. (2008). Quorum sensing controls biofilm formation in *Vibrio cholerae* through modulation of cyclic di-GMP levels and repression of *vpsT*. *Journal of bacteriology*, 190(7), 2527-2536.
- Wei, H.-L., & Zhang, L.-Q. (2006). Quorum-sensing system influences root colonization and biological control ability in *Pseudomonas fluorescens* 2P24. *Antonie van Leeuwenhoek*, 89(2), 267-280.

- Welton, J. E., and SEM Petrology Atlas. "The American Association of Petroleum Geologists." Tulsa, Oklahoma, USA (1984): 237.
- Whiteley, M., Lee, K. M., & Greenberg, E. (1999). Identification of genes controlled by quorum sensing in *Pseudomonas aeruginosa*. *Proceedings of the National Academy of Sciences*, 96(24), 13904-13909.
- Winson, M. K., Camara, M., Latifi, A., Foglino, M., Chhabra, S. R., Daykin, M., . . . Bycroft, B. W. (1995). Multiple N-acyl-L-homoserine lactone signal molecules regulate production of virulence determinants and secondary metabolites in *Pseudomonas aeruginosa*. *Proceedings of the National Academy of Sciences*, 92(20), 9427-9431.
- Wood, T. K., Knabel, S. J., & Kwan, B. W. (2013). Bacterial persister cell formation and dormancy. *Applied and environmental microbiology*, 79(23), 7116-7121.
- Wu, Y., Zitelli, J. P., TenHuisen, K. S., Yu, X., & Libera, M. R. (2011). Differential response of Staphylococci and osteoblasts to varying titanium surface roughness. *Biomaterials*, 32(4), 951-960.
- Yoneyama, N., Hara-Kudo, Y., & Kumagai, S. (2007). Effects of heat-degraded sugars on survival and growth of *Vibrio parahaemolyticus* and other bacteria. *Journal of Food Protection*®, 70(2), 373-377.
- Zaitsev, B., Yudina, I., Cherepanova, N., Bakirov, T., Rukavishnikov, M. Y., & Kanev, A. (2011). An atomic force microscopy study in the detection of hepatitis B surface antigen by enzyme linked immunosorbent assay. *Journal of Immunoassay and Immunochemistry*, 32(3), 191-206.
- Zhai, C., Zhang, P., Shen, F., Zhou, C., & Liu, C. (2012). Does *Microcystis aeruginosa* have quorum sensing? *FEMS microbiology letters*, 336(1), 38-44.
- Zhao, A., Zhu, J., Ye, X., Ge, Y., & Li, J. (2016). Inhibition of biofilm development and spoilage potential of *Shewanella baltica* by quorum sensing signal in cell-free supernatant from *Pseudomonas fluorescens*. *International journal of food microbiology*, 230, 73-80.

## Appendix

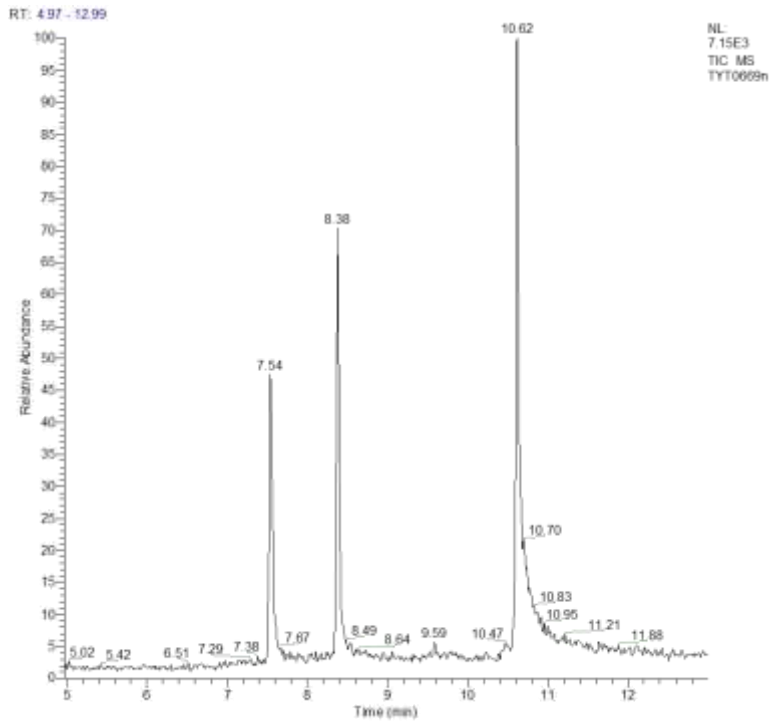


Figure A-1. TIC for standard AHLs; *N*-hexanoyl-HSL, *N*-heptanoyl-HSL and *N*-decanoyl-HSL. Standards spiked to a concentration of 0.1 ng/ $\mu$ L in HPLC grade MeOH

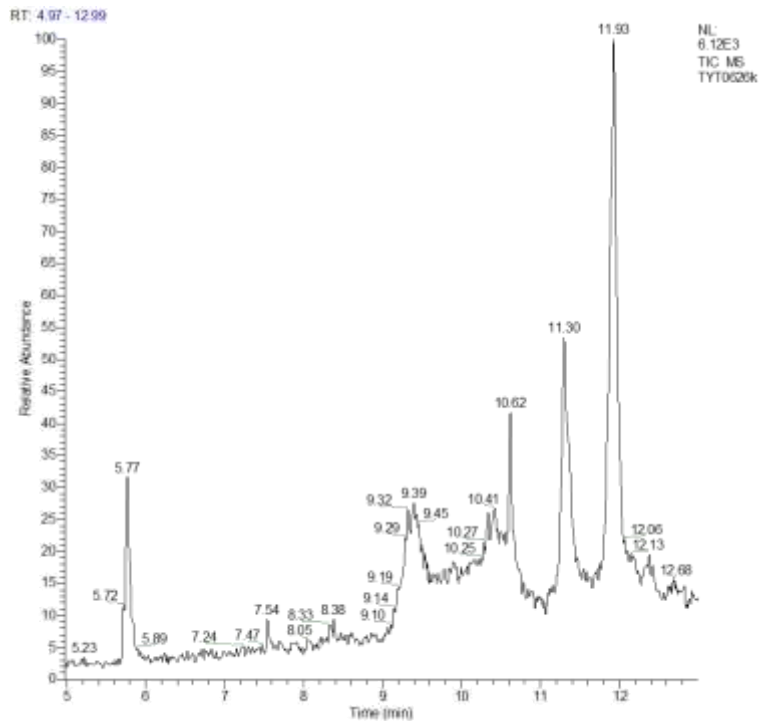


Figure A-2. TIC for standard AHL *N*-butyryl-HSL. Standard spiked to a concentration of 0.1 ng/ $\mu$ L in HPLC grade MeOH

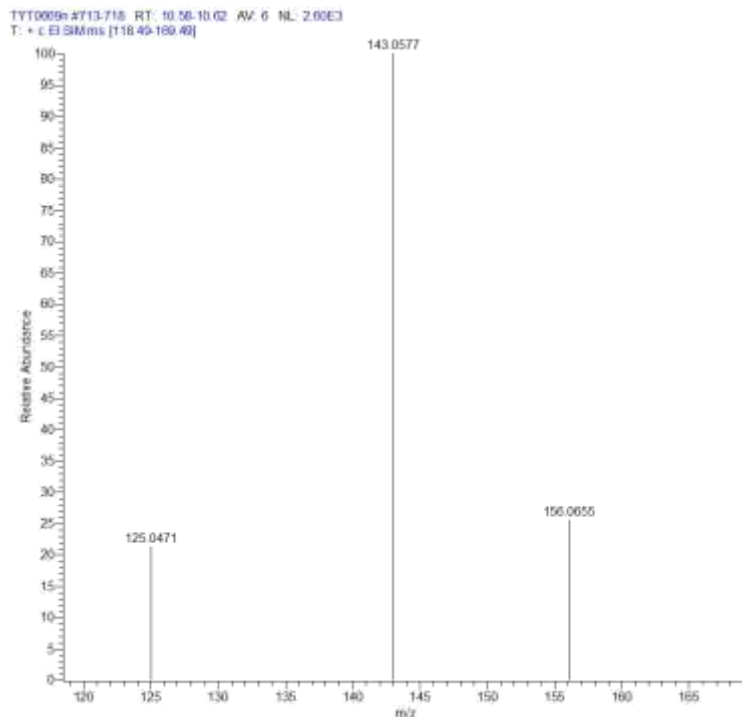


Figure A-3. High-resolution MID spectra of *N*-heptanoyl-HSL standard. EI-SIM mode was performed on *m/z* fragment ions of 125, 143 and 156.

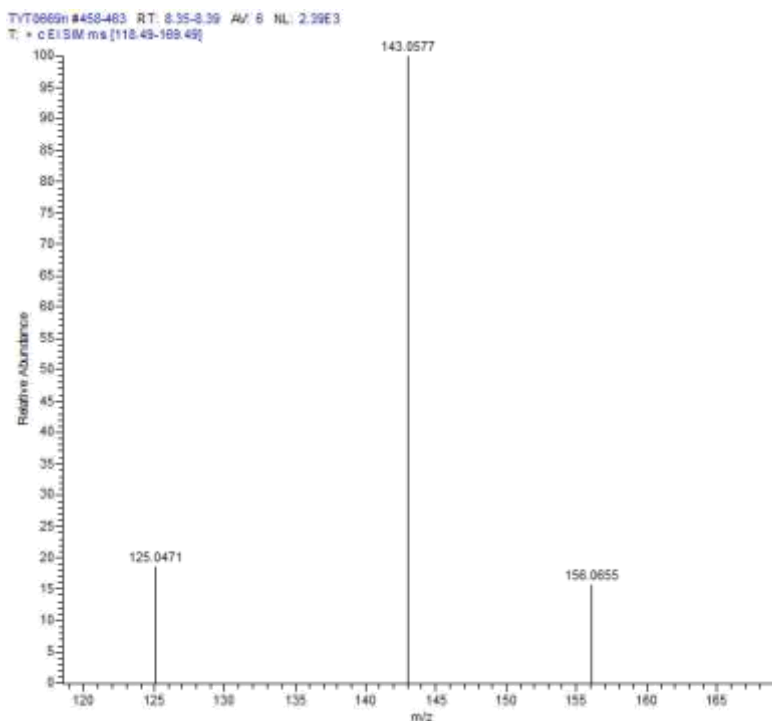


Figure A-4. High-resolution MID spectra of *N*-decanoyl-HSL standard. EI-SIM mode was performed on *m/z* fragment ions of 125, 143 and 156.

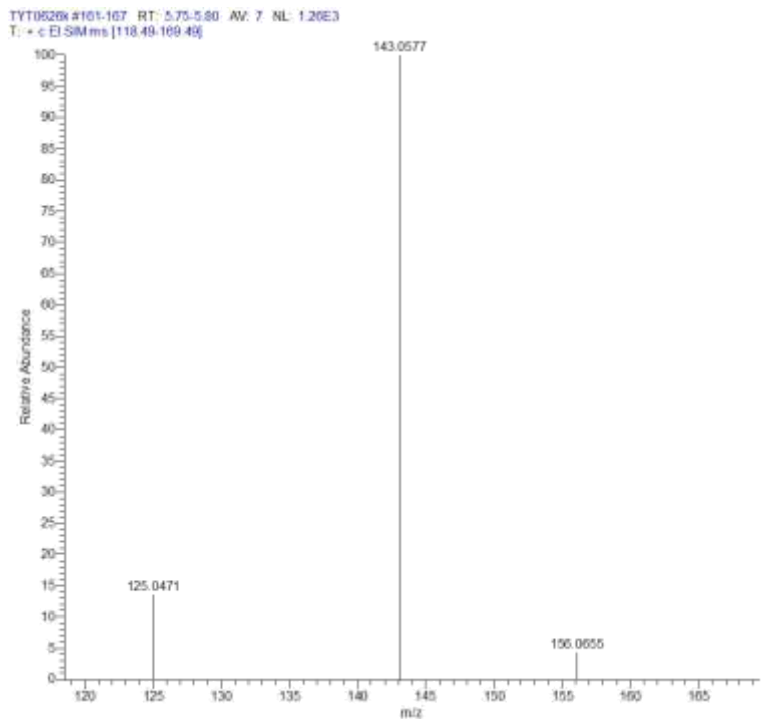


Figure A-5. High-resolution MID spectra of *N*-butyryl-HSL standard. EI-SIM mode was performed on *m/z* fragment ions of 125, 143 and 156.

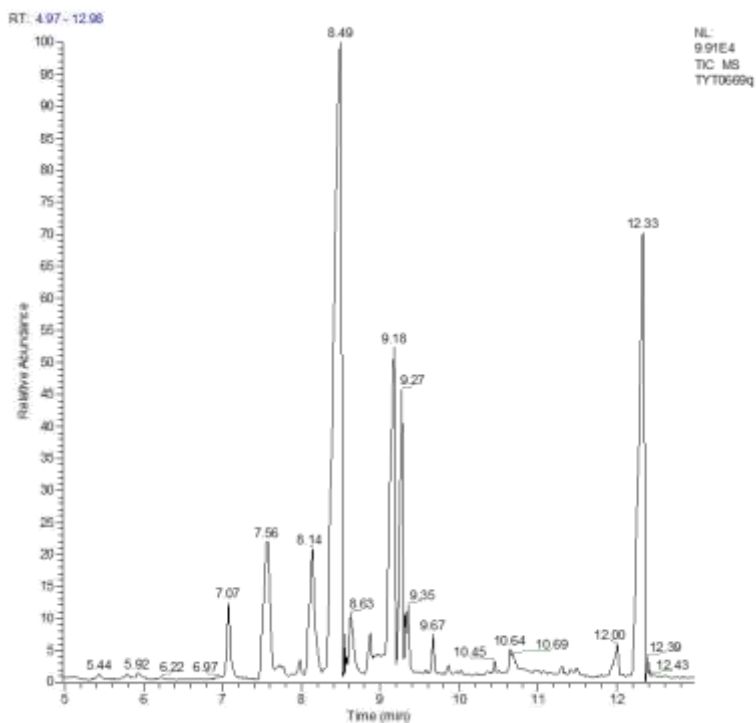


Figure A-6. TIC for chloroform extract of *P. fluorescens* Pf0-1 supernatant in HPLC grade MeOH

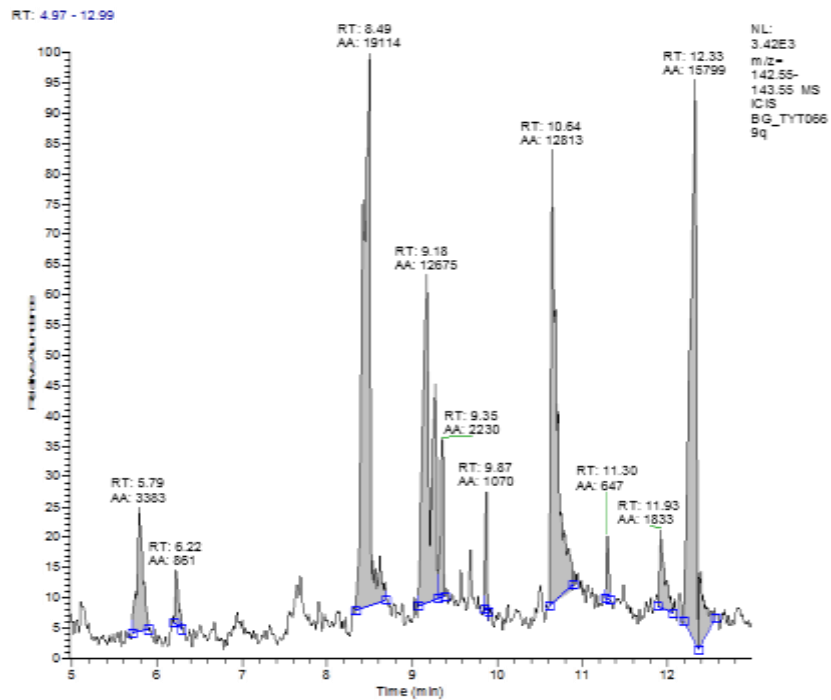


Figure A-7. EIC for  $m/z$  fragment ion of 143 in chloroform extract of *P. fluorescens* Pf0-1 supernatant. Supernatant extract dissolved in HPLC grade MeOH

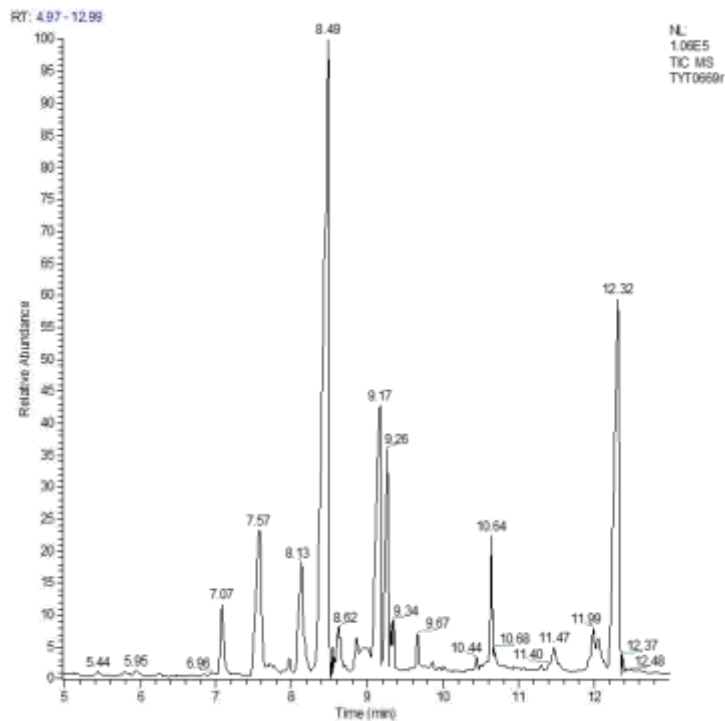


Figure A-8. TIC for 0.1 ng/ $\mu$ L standard spiked-chloroform extract of *P. fluorescens* Pf0-1 supernatant. Sample dissolved in HPLC grade MeOH spiked with 0.1 ng/ $\mu$ L of the following AHL standards; *N*-hexanoyl-HSL, *N*-heptanoyl-HSL and *N*-decanoyl-HSL

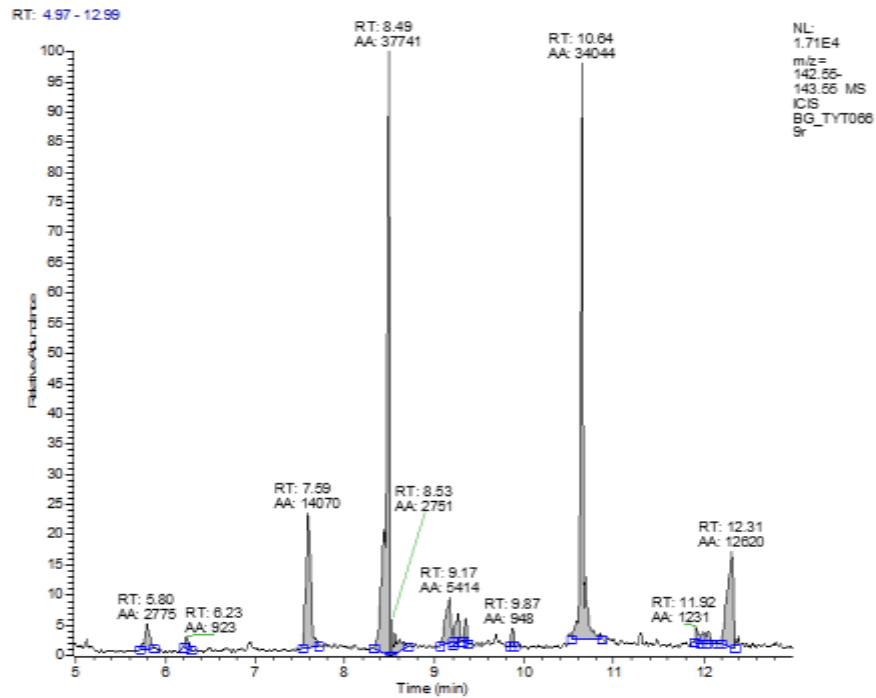


Figure A-9. EIC for  $m/z$  fragment ion of 143 in 0.1 ng/ $\mu$ L standard spiked-chloroform extract of *P. fluorescens* Pf0-1 supernatant. Supernatant extract dissolved in HPLC grade MeOH spiked with 0.1 ng/ $\mu$ L of the following standards; *N*-hexanoyl-HSL, *N*-heptanoyl-HSL, *N*-decanoyl-HSL.

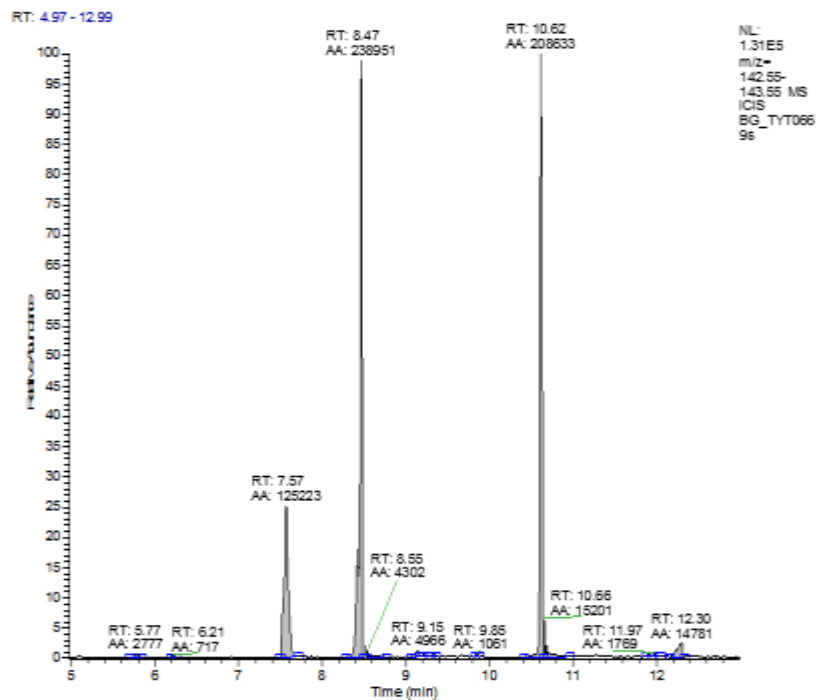


Figure A-10. EIC for  $m/z$  fragment ion of 143 in 1 ng/ $\mu$ L standard spiked-chloroform extract of *P. fluorescens* Pf0-1 supernatant. Supernatant extract dissolved in HPLC grade MeOH spiked with 1 ng/ $\mu$ L of the following standards; *N*-hexanoyl-HSL, *N*-heptanoyl-HSL, *N*-decanoyl-HSL.